# THÈSE

**En vue de l'obtention du**

# DOCTORAT DE L'UNIVERSITÉ DE TOULOUSE

**Délivré par :**

Université Toulouse III Paul Sabatier (UT3 Paul Sabatier)

**Discipline ou spécialité :**

Océanographie Physique

---

**Présentée et soutenue par :**

Audrey HASSON

**le :** 15 Octobre 2013

**Titre :**

Etude diagnostique de la variabilité de la salinité de surface de l'Océan Pacifique. Apport des données SMOS.

---

**Ecole doctorale :**
Sciences de l'Univers, de l'Environnement et de l'Espace (SDU2E)

**Unité de recherche :**
UMR5566 LEGOS

**Directeur(s) de Thèse :**

Thierry Delcroix

**Rapporteurs :**

M. Gilles REVERDIN, Rapporteur, LOCEAN
M. Jerome VIALARD, Rapporteur, LOCEAN

**Membre(s) du jury :**

Mme Jacqueline BOUTIN, Examinateur, LOCEAN
M. Thierry DELCROIX, Directeur de thèse, LEGOS
M. Jordi FONT, Examinateur, Institut de Ciències del Mar CMIMA-CSIC
Mme Fabienne GAILLARD, Examinateur, LPO Ifremer
M. Nick HALL, Examinateur, UPS
M. Nicolas REUL. Examinateur. LOS Ifremer

# Résumé

La salinité est un paramètre clé de l'océan car elle impacte la dynamique océanique par la densité. Elle est considérée comme une Variable Climatique Essentielle. La distribution du sel dans l'océan est le résultat d'un équilibre subtile entre le forçage de surface (Evaporation moins Précipitation), l'advection horizontale de sel (aux basses et hautes fréquences) et le forçage vertical de sub-surface (entrainement et mélange), chacun de ces termes étant d'égale importance. Même si ces processus sont bien connus de façon qualitative, quantifier l'effet de chacun d'entres eux est un challenge et toujours une question ouverte. Mon travail de thèse a pour but de : a) quantifier les mécanismes responsables de la variabilité de la salinité de surface dans l'Océan Pacifique tropical (principalement aux échelles saisonnières et interannuelles), b) décrire et évaluer les processus à l'origine des variations de salinité de surface pendant l'évènement La Nina de 2010-2011 et c) analyser la formation et la variabilité du noyau de maximum de sel de l'Océan Pacifique subtropical (aux mêmes échelles de temps). Pour se faire, différents jeux de données sont utilisés conjointement : des observations de salinité in situ principalement des bateaux marchands et des profileurs Argo, des données de salinité de surface dérivées du nouveau satellite SMOS ainsi que d'autres produits issus de mesures satellitaires tels que les précipitations, l'évaporation et les courants de surface. Une simulation spécifique d'un modèle forcé est aussi employée. Les principaux résultats de ce travail sont publiés, « in press » et soumis dans des journaux à comités de lecture.

# Abstract

Salinity is one of the key parameters of the ocean impacting its dynamics through density. It is considered as an Essential Climate Variable. The salinity patterns result from a subtle balance between surface forcing (E-P, Evaporation minus Precipitation), horizontal salt advection (at low and high frequencies) and subsurface forcing (entrainment and mixing), all terms being of analogous importance. While processes responsible for sea surface salinity (SSS) changes are qualitatively well known, quantifying those mechanisms is very challenging and hence still under debate. My Ph.D. research work aims at: a) quantifying mechanisms responsible for the tropical Pacific Ocean SSS variability (mainly at seasonal and ENSO time scale), b) describing and assessing mechanisms behind the 2010-2011 La Niña SSS changes, and c) analysing the formation and variability of the south Pacific subtropical high SSS core (at the same time scales). In order to do so, various datasets are used conjointly: in-situ salinity observations mainly from voluntary observing ships and Argo profilers, satellite based surface salinity (from SMOS), precipitation, evaporation and near-surface currents as well as a specific forced model simulation. The main results of my work are published, in press and submitted in peer review research articles.

# Table of Contents

4

6

# Chapter 1. Introduction

The three key physical variables in the ocean are its temperature, salinity and pressure, which are linked together by density via the seawater equation of state (e.g., see, Gill, 1982; Millero, 2010). Density is of particular importance since small spatial gradients can drive the ocean circulation, which redistributes heat meridionally and therefore contributes to the global climate system. Historically, studies of the ocean temperature have been abundant because of the relative high numbers of in situ temperature profiles and remotely-sensed surface measurements and its major influence on density. In contrast, the role of salinity in the ocean remains under-explored, mainly because of the lack of data.

The present thesis analyses salinity mean patterns in the tropical Pacific Ocean and their temporal and spatial variability. In the following introductory Chapter, the reader will be first introduced to the different evolving definitions of salinity (Section I), then to the importance of salinity in oceanography (Section II). We will subsequently describe the in situ salinity data presently available to scientists (Section III). A description of the mean SSS in the Global Ocean and in particular in the tropical Pacific Ocean will be given (Section IV) as well as a brief literature review of its variability at different time/space scales (Section V). Finally, we will underline three major issues insufficiently addressed in literature (Section VI), which will be the base of this thesis.

## I. Salinity

Our knowledge of salinity has been growing since the late 19$^{th}$ century and its definition has evolved in parallel. This complex evolution, detailed in Millero et al. (2008) and the references therein, is briefly described in this section. In the first sub-section, we will present the conceptual definition of salinity, followed by the evolution of salinity measurements leading to practical definitions. The last sub-section will focus on the salinity geological cycle, which explains the salt contents of seawater.

### I.1. Standard Definition

Salinity is the "Total amount of dissolved material in grams in one kilogram of sea water" (Sverdrup et al, 1942). Salinity is therefore the ratio of the weight of drought matter

over the weight of water sample. Salinity is dimensionless and has consequently no unit but a scale: the practical salinity scale (pss) corresponding to g/kg. Salinity was first measured in the 19th century by weighing what was left after complete evaporation. However, this method was highly inaccurate as some components were lost during the process.

The Principle of Constant Proportions states that "*regardless of the absolute concentration, the relative proportions of the different major constituents are virtually constant*"(Dittmar, 1884), except in regions of high dilution (low salinity), where minor deviations may occur. Table 1 presents the average composition of these major constituents in 1 litre of seawater with a salinity of 35.000 pss. The different constituents' concentrations for lower or higher salinity can be obtained by scaling by the same factor. From this table, we note that chloride and sodium are the principal constituents of the dissolved matter in seawater, respectively accounting for 55 and 31%, and are the main component of what is commonly called "table salt".

| Component | Formula | Concentration (g/kg) | Percentage of salt |
|---|---|---|---|
| Chloride | $Cl^-$ | 19.35g | 55 % |
| Sodium | $Na^{2+}$ | 10.78g | 31 % |
| Sulphate | $SO_4^{2-}$ | 2,71g | 8% |
| Magnesium | $Mg^{2+}$ | 1.28g | 4% |
| Calcium | $Ca^{2+}$ | 0.41g | 1% |
| Potassium | $K^{2+}$ | 0.39g | 1% |
| Other | | 0.00…g | 0.0…% |

Table I.1 Salt composition of an average sample of one litre of seawater with $S_P$=35.000 pss (Pawlowicz, 2013)

## I.2. Practical Definitions

Because of the (quasi) unvarying composition of salt ions in seawater, salinity can theoretically be deduced by measuring one of them and using a simple scaling. Chloride, one of the dominant components, can be measured by a simple chemical analysis. Using Copenhagen "Normal water" standards, Salinity is defined by Knudsen (1903) based on chlorinity (*Cl*) as:

$S_1$=0.03+1.805*$Cl$

In turn, establishing a strict definition of chlorinity took some time. As Bromides and Iodides also precipitate with Chlorides during the silver nitrate titration, chlorinity was first defined in 1902 as "*the total amount of chlorine, bromine, and iodine in grams contained in one kilogram of sea water, assuming that the bromine and the iodine had been replaced by chlorine* » (Sverdrup et al. 1942).

Salinity can also be obtained by measuring density and temperature of a water sample. However, this method relies on empirical tables and/or delicate optical instruments (LeMenn et al., 2011) and it is time-consuming to reach accuracies obtained from the silver nitrate titration method.

Measuring salinity via conductivity has also been developed as early as the 1930s (Thomas et al., 1934). This method was much more convenient than the silver nitrate titration and has been used regularly by oceanographers since the 1960s. The conductivity gives a different equation for salinity by Cox et al. (1967):

$$S = -0.04980 + 15.66367 \cdot R_{15} + 7.08993 \cdot R_{15}^2$$
$$-5.91110 \cdot R_{15}^3 + 3.31363 \cdot R_{15}^4 - 0.73240 \cdot R_{15}^5$$

and

$$R_{15} = \frac{C(s,15,0)}{C(35,15,0)}$$

where C(s,15,0) is the conductivity of the sea water sample and C(35,15,0) of the Copenhagen "Normal Water", both measured at 15ºC and at 1 atm pressure.

This equation has been revised in order to obtain the conductivity ratio based on [*KCl*] only and not other components of the seawater (i.e. chlorinity).

$$S = -0.0080 - 0.1692 \cdot K_{15}^{1/2} + 25.3851 \cdot K_{15}$$
$$+14.0941 \cdot K_{15}^{3/2} - 7.0261 \cdot K_{15}^2 + 2.7081 \cdot K_{15}^{5/2}$$

and

$$K_{15} = \frac{C(s,15,0)}{C(KCl,15,0)}$$

where C(*KCl*,15,0) is the conductivity of the standard Potassium-Chloride solution containing a mass of 32.435 6 grams of *KCl* in a mass of 1.000 000kg of solution. This definition is the official « Practical Salinity Scale 1978 » (Unesco, 1981).

In recent years, studies have shown the importance of the weak changes in the seawater dissolved-matter composition on salinity. A new standard called TEOS-10 (Thermodynamic Equation of Seawater, 2010) was adopted by the International Oceanographic Commission (IOC) at its 25th assembly in June 2009; see http://www.teos-10.org/. The « Normal Water » or « Standard Seawater » have a known composition and its "Absolute Salinity" ($S_A$) (i.e. mass fraction of dissolved material) is 35.1650 g.kg$^{-1}$, which is different from its "Practical Salinity"($S_P$) (35 pss). It is used to scale the $S_P$ to get the « Reference Salinity » ($S_R$) of a sample. The "Standard Seawater" or "Normal Water" is based on North Atlantic surface waters, which contain no nutrients. Other parts of the global ocean show a high nutrient concentration, such as the deep Southern ocean, deep North Pacific and regions off large river mouths. As nutrients do not conduct electricity very well, estimates based on conductivity underestimate $S_A$.

$$S_R = \frac{35.16504}{35} \times S_P$$
$$S_A = S_R + \delta S_A$$

where $\delta S_A$ is the salinity correction factor due to nutrients, usually positive. There is a global atlas of the correction factor part of TEOS-10 for computing $S_A$.

In the present manuscript, we will consider "Practical Salinity" only as the greatest discrepancies are found outside of our study domain: North and South of 30ºN/S and at depth below the mixed layer. Moreover, all the in situ salinity data we use in the following studies are stored under the pss-78 format in data banks, in agreement with IOC recommendations: "Importantly, while Absolute Salinity (g/kg) is the salinity variable that is needed in order to calculate density and other seawater properties, the salinity which should be archived in national data bases continues to be the measured salinity variable, Practical Salinity (PSS-78)"

The last but not least, a final method to estimate salinity has emerged in the recent decade: measurements from space by the SMOS (Figure I.1; Kerr et al., 2010; Font et al., 2010) and Aquarius/SAC-D (Lagerloef et al., 2008) satellites. In this manuscript, we will focus on SMOS data mainly.

Figure I.1 Artist's rendering of SMOS in orbit. Credits: ESA.

The SMOS satellite was launched on December 29, 2009 to a sun-synchronous orbit with a 758 km altitude. The mission is a joint ESA/CNES/CDTI Earth Observation Program and was selected as the 2nd Earth Explorer Opportunity Mission (Kerr, 1998). SMOS instruments measure microwave radiation emitted from Earth's surface within the L-band (1.4 GHz) using an interferometric radiometer. The ocean surface emissivity is modified by the ion content of the water from which salinity can be deduced. In turn the emissivity affects the microwave radiations the interferometer measures. SMOS's Microwave Imaging Radiometer using Aperture Synthesis (MIRAS) contains 69 small receivers dispatched on three antennas (Figure I.1) measuring the phase difference of incident radiation over an area of almost 3000 km in diameter. However, only a hexagon-like shape of about 1000 km of diameter called "the alias-free zone" can be used to determine salinity due to the interferometry principle and the Y-shaped antenna. Details on technical issues can be obtained from Waldteufel et al. (2003). SMOS data will be furthered described in section 2.

### I.3. Salinity geological cycle

"Why are the oceans salty?" is one of the most frequent questions both children and grown ups have been asking me during the three years of my Ph.D. Albarède and Thomas

(Ecole Normal Supérieure de Lyon) have published two remarkable blog posts from which I gathered the information presented below.

Salt in the ocean comes from the silicates' erosion from surface and underground rivers run-offs. Rivers are 1000 times less concentrated in ions than the ocean as observed when comparing the ionic composition of fresh water (e.g., found on water bottles) and Table 1. Atmospheric circulation also transports salt ions from the land surface and volcanos. Salt ions concentration builds up once in the ocean as they do not react with marine minerals and they are left behind after evaporation. However, it has been shown from sediments analyses that ocean salinity has been (almost) stable for millions of year. The sources of ions (runoff) must be in equilibrium with sinks of ions (Figure I.2).
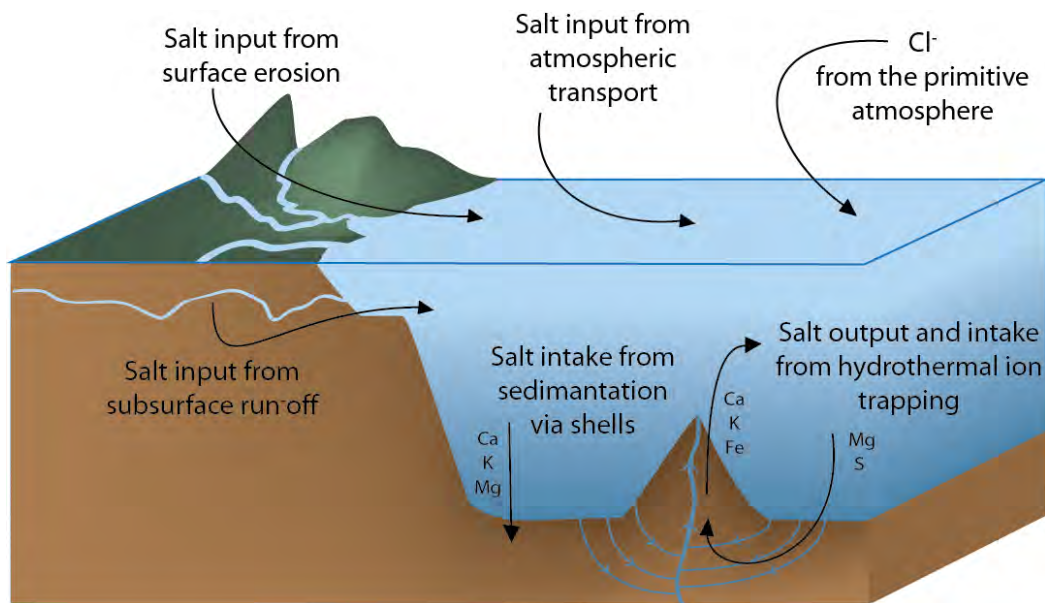


Figure I.2 The simplified geological cycle of salt

Two main sinks have been presented: life and hydrothermal ion trapping. Even if seaweeds, algae and fishes intake potassium (K) and magnesium (Mg) for their metabolism, only a small part is exported to the ocean floor where it can get trapped into the sediments. A greater proportion of calcium (Ca) is trapped inside shells and exported. Near the great ridges, water penetrates the oceanic crust and traps mainly Mg and sulphur (S), releasing Ca, K, iron (Fe) … The chloride ion ($Cl^-$) provenance is unclear as its concentration in the continental bedrock is very low, and therefore cannot be brought in the ocean by the rivers. It is though to come from the primitive atmosphere, and has stayed in the ocean since then. Sodium ($Na^+$) and $Cl^-$ have by far the greatest residence time in the ocean, 58 and 95 million years.

At present, the seawater salinity is on average 35 pss and the total quantity of salt represents 100 m$^3$ per human being.

## II. Importance of Salinity in Oceanography

As noted above, salinity definitions and measurement technics have evolved tremendously for over a hundred years as its scientific relevance has been increasingly recognised by scientists. As a matter of fact, (surface and subsurface) salinity is now recognized as one of the Essential Climate Variables (ECV) within the Global Climate Observing System (GCOS). It is a fantastic tool for tracking the freshwater cycle, water masses displacements and mixing. Salinity also impacts the ocean dynamics through density, as stated above. The following sections emphasise why scientists have expressed more and more interest in salinity.

### II.1.A proxy to track water masses

Historically, scientists have used salinity as a water mass tracer. Water mass as defined by Tomczak (1999) is "a body of water with common formation history, having its origin in a physical region of the ocean". Water masses are usually seen as objective physical entities that move around the ocean at different velocities. Subsurface water masses acquire their homogeneous characteristics at the sea surface or in the mixed-layer where they are formed. Characteristics are given by the atmosphere-ocean interactions (precipitations, evaporation, heating, cooling…). Salinity and temperature are "conservative properties" of theses masses unlike oxygen and nutrients which are consumed by biological processes. Once the water mass leaves the surface to reach deeper layers of the ocean, properties can only change by mixing with nearby water masses. Surface waters have properties varying much faster because of the atmospheric forcing fluctuations.

T-S plots (salinity as a function of temperature) are used to detect and define water masses, deduce their pathways and underline possible mixing with different water masses. For instance, the Tropical Pacific waters are marked by very high salinity whereas the Antarctic Intermediate Waters are characterised by low salinity and lower temperatures (see Figure II.1).
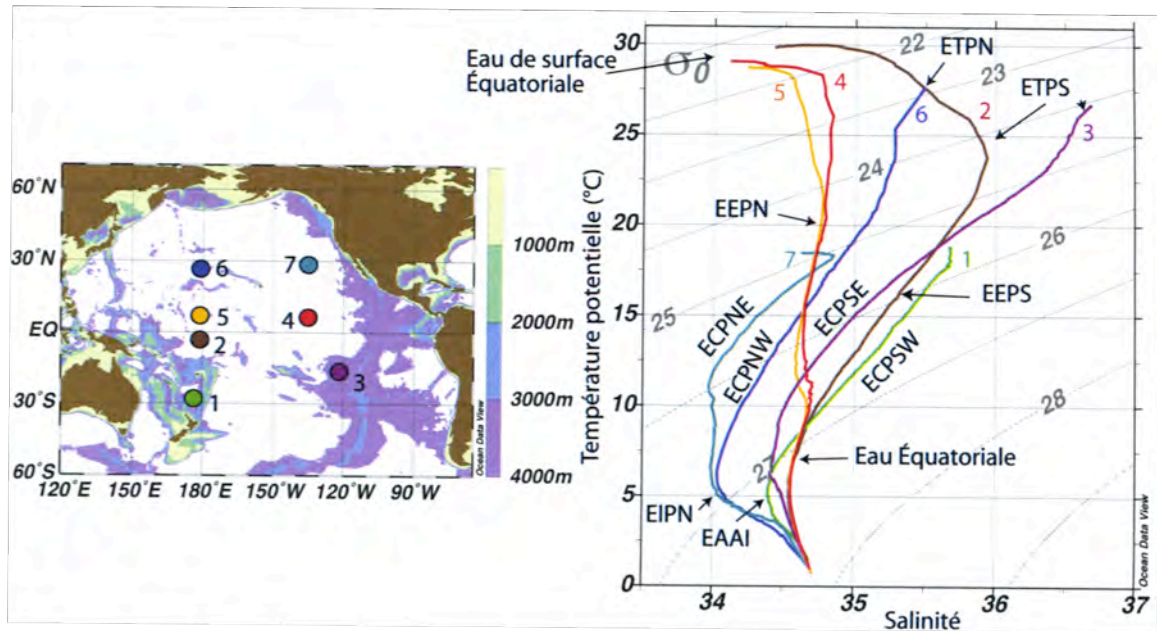
Figure II.1 T–S diagrams of 7 stations in the Pacific Ocean corresponding to thermocline waters of the Pacific Ocean: NE, NW, SE, SW Central Pacific waters (i.e. ECPNE, ECPNW, ECPSE ECPSW), N and S Equatorial Pacific waters (i.e. EEPN, EEPS), N and S Tropical Pacific waters (i.e. ETPN, ETPS), Antarctic Intermediate waters (EAAI) and N Pacific Intermediate waters (EIPN). From Fieux, 2010.

## II.2.A marker for frontal regions

Salinity can also be a good proxy for frontal regions because its interactions with the atmosphere are not as strong as those of temperature. Broad scale surface salinity fronts are indeed usually sharper than temperature fronts, for instance the one observed along the equator by Rodier et al. (2000) in Figure II.2. This particular front will be further described in Section I.12. Strong and fast atmospheric responses to surface temperature fronts reduce their strength. Moreover, because the spatial scale of the atmospheric fronts are much larger than the oceanic ones, the gradient between the sea surface temperature and the air just above can be steep. Static stability is reduced on the warmer side of the front enhancing vertical mixing and winds. The opposite occurs on the cooler side of the front. Therefore, the atmosphere tends to weaken sharp temperature fronts whereas there is no direct atmospheric response to salinity fronts. Examples of salinity front analyses can be found in Picaut et al. (2001) for the western equatorial Pacific Ocean and in Reverdin et al. (1994) for the North Atlantic Ocean.
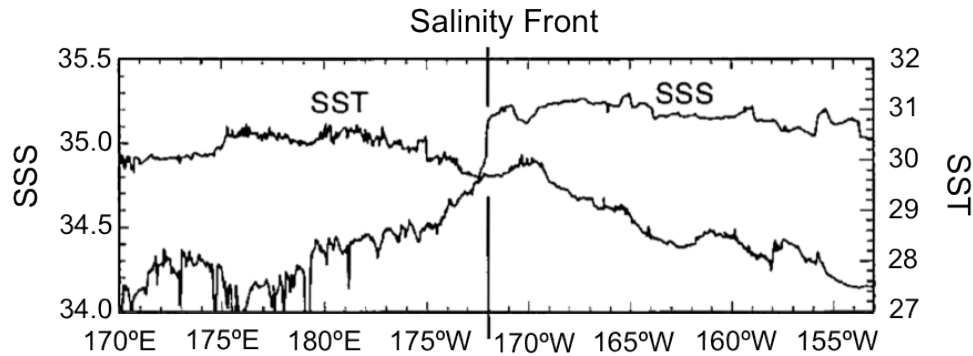
Figure II.2 Zonal distribution of high-resolution SST and SSS data collected from a TSG instrument during the September-October 1994 FLUPAC cruise along the equator (From Rodier et al., 2000). Note the sharp front in SSS and the lack of corresponding front in SST near 172°W.

**II.3. A tool to estimate the freshwater cycle**

Salinity is also thought to be a useful freshwater cycle proxy. Changes in the global hydrological cycle could affect billion of people especially if they imply an intensification of droughts and floods.

The global hydrological cycle corresponds to the freshwater storage and movement between the oceans, the continents, the atmosphere and the cryosphere. Around 80% of this cycle occurs over the oceans (83% of total evaporation and 78% of total precipitations) (e.g. Schanze et al., 2010). However, the ocean is vast and water fluxes are highly under-sampled. Sparse direct measurements are taken at moorings (such as TAO, RAMA, TRITON, PIRATA) and during oceanographic cruises (e.g. dedicated SPURS campaigns). Evaporation and Precipitations are very difficult to measure on the long term and global scale and are often derived from other variables with the help of models (i.e. reanalyses, models). In the early 2000's, the development of satellite based microwave measurement of precipitations and latent heat flux improved our knowledge of large-scale fields. Yet uncertainties in the global hydrological cycle remain large. Using the optimal combination of independent estimates from satellites and in situ over the global ocean, fresh water transport can be assessed. Over the 1987-2006 period Schanze et al. (2010) found 13±1.3 Sv from evaporation, 12.2±0.2 Sv from precipitations and around 1.25±0.1 Sv. from river runoffs (Dai et al., 2009) exhibiting a net imbalance within error estimates. Looking at faint long-term changes in the hydrological cycle using atmospheric data is highly challenging due to large uncertainties (Lagerloef et al., 2010).
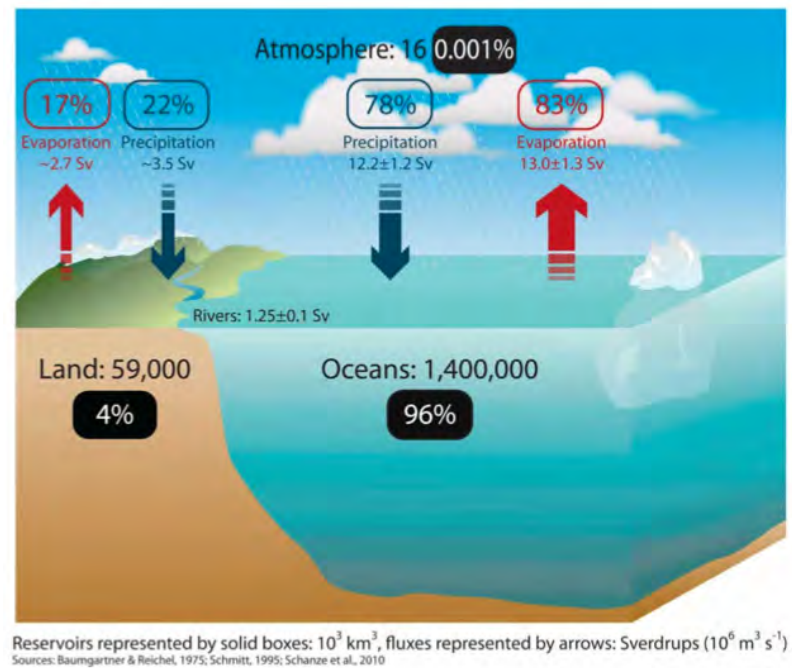
Figure II.3 Schematic of the global water cycle. Reservoir estimates represent storages in $10^3$ km$^3$, flux estimates represent transports in Sverdrup ($10^6$ m$^3$ s$^{-1}$) and values within boxes represent the approximate percentage of total storage for the global surface. Adapted from Schmitt (1995) and Schanze *et al. (*2010) by *Paul Schanze*.

Several studies have underlined the possible use of ocean surface salinity as an inverse rain gauge [e.g. Schmitt et al., 2008; Lagerloef et al., 2010]. To the first order, the freshwater cycle is reflected on the surface salinity fields. For instance a small 0.2 pss salinity decrease in a 35m depth mixed layer is equivalent to a notable 20% increase in precipitations (in common regions where the mean salinity and precipitaion are of the order of 35 pss and 1m/year, respectively). However, it remains challenging to link surface salinity with freshwater fluxes. Salinity is not solely driven by freshwater fluxes but also by complex upper ocean dynamical processes as will be presented in the following sections.

Delcroix et al (1996) found correspondent patterns of standard deviation of in-situ surface salinity and satellite derived precipitations in the heavy rainfall regions of the tropical Pacific. The Empirical Orthogonal Function (EOF) analysis of both parameters showed their link at the seasonal and interannual timescales. The authors also argued that surface salinity could be used to determine the phasing of precipitations changes but not the magnitude at both timescales.

Yu (2011) investigated the relation between the difference of Evaporation and Precipitations (E-P) and surface salinity on the seasonal timescales for the global ocean. From observations, Yu (2011) found E-P controlling salinity in only two regions: where P is strongly dominant (tropical convergence zones) and where E is strongly dominant (western North Pacific and Atlantic). Within these regions, E-P accounts for 40-70% of the surface salinity variance. More recently, Vinogradova and Ponte (2013) studied the interaction between salinity and the freshwater fluxes using a numerical model assimilating observations. They found on average a non-negligible part of salinity variability due to upper ocean processes, which correlates poorly to freshwater fluxes. At the global scale they showed a quasi non-existent relation between salinity and E-P. At the seasonal timescales, results are consistent with what was found earlier by Yu (2011)

At longer timescales, Durack and Wijffels (2010) looked at salinity variations and their link to E-P. They showed a strong connection between basin-wide averaged salinity and E-P in simulations from the Coupled Model Intercomparison Project (Phase 3; CMIP3). They put to light a 50-year trend pattern in salinity resembling what we can expect from an intensification of the global water cycle under global warming. The increasing difference in salinity between the Atlantic and Pacific Oceans is thought to be a remarkable indicator of the intensifying water cycle. (Salinity differences between the Atlantic and Pacific Oceans are discussed below.) Terray et al. (2012) focused on the tropical oceans over the late twentieth century with both observations and model simulations. They also concluded on a strengthened marine tropical hydrological cycle deduced from surface salinity variations, which they linked to anthropogenic forcing via detection / attribution methods.

## II.4. The Seawater Equation of State

We have noted earlier that salinity measurements are primordial to compute another critical physical quantity: density. Seawater absolute density is (almost never) measured directly. Oceanographers use relative density anomaly (σ) computed from measurements of temperature (T), salinity (S) and pressure (P). The relative density is computed relative to standard seawater of known composition as shown below.

$$\sigma = \frac{\rho(s_{sample}, T, P)}{\rho(S_{normal}, T, P)} - 1000$$

The Gibbs equation gives us the empirical relation between ϱ and salinity (S), temperature (T) and pressure (P).

Because of its effect on density, salinity plays a key role in the ocean dynamics influencing dynamic height anomaly (and thus geostrophic currents), vertical mixing, subduction, etc. Subtle changes in salinity can lead to strong density anomalies as shown in

Table II.1. A temperature change of 1ºC corresponds to a change in salinity of 0.11 and 0.44 pss for cold (2-3°C) and warm (28-29°C) waters, respectively. This underlines the deeper effect of salinity changes on density in cold waters.

| | Temperature (T) | Salinity ($S_A$) | Density Anomaly (σ) | Δ T | Δ$S_A$ | Δ σ |
|---|---|---|---|---|---|---|
| **Cold waters** | 2ºC | 35.00 pss | 27.84 kg/m³ | - 1ºC | 0 | + 0.09 kg/m³ |
| | 3ºC | 35.00 pss | 27.75 kg/m³ | | | |
| | 3ºC | 35.11 pss | 27.84 kg/m³ | 0 | + 0.11 pss | + 0.09 kg/m³ |
| **Warm waters** | 28ºC | 35.00 pss | 22.27 kg/m³ | - 1ºC | 0 | + 0.33 kg/m³ |
| | 29ºC | 35.00 pss | 21.94 kg/m³ | | | |
| | 29ºC | 35.44 pss | 22.27 kg/m³ | 0 | + 0.44 pss | + 0.33 kg/m³ |

Table II.1 Changes in density for a 1-degree change in temperature in warm and cold waters, and equivalent salinity change for the same change in density.

Dynamic height anomaly relative to a given reference level is commonly deduced from temperature and salinity fields and can present great differences when using different methodologies. When salinity profiles were sparse, the traditional methodology was to use the available temperature profiles and mean climatological T-S curves (Emery and Wert, 1976). However, these climatological TS curves are not as stable as previously thought, especially near the surface, leading to dynamic height computation errors. These different approaches can result in large errors in dynamical height anomalies and thus in geostrophic currents and transports (e.g., Delcroix et al., 1987; Menkes et al., 1995; Ueki et al., 2002). For example in the equatorial Pacific (at 165°E), the effect of variability in the mean TS curves can result in errors of the order of 6 dyn.cm and 10 cm/s in surface dynamic height and geostrophic current, respectively. The Kessler/ linear TS-scheme approach led to a net improvement when computing dynamic height from surface salinity data, mean TS curves above the thermocline and the mean T-S relationship only below the thermocline (Kessler and Traft, 1987). Ideally,

both salinity and temperature profiles are needed simultaneously to get the dynamic height, which has been made possible in the recent decades (see Section III).

**II.5.Role on deep waters formation (high latitudes)**

The Meridional Overturning Circulation (MOC) is the global circulation responsible for a large part of oceanic heat redistribution (Figure II.4). Warm waters are advected from low to high latitudes through western boundary currents. Cold waters are transported in the opposite direction in depth through the North Atlantic Deep Waters and Antarctic Bottom Waters. The MOC is mainly caused by temperature and salinity horizontal and vertical gradients but also winds. Salinity is of central importance in the deep convection processes by which deep waters are formed. The best illustration is the lack of deep convection in the North Pacific Ocean because of its low salinity. Moreover, studies have suggested that the North Atlantic MOC could be weakened due to an increase in fresh water in the northern North Atlantic, possibly linked to the observed ice melting acceleration from the arctic region (Rahmstorf, 1995; Manabe and Stouffer, 1995).

Deep convection occurs in the open ocean, along the coasts and over the continental shelves. Salinity plays an active role mostly in the open ocean deep convection; this has been observed in the Nordic, Labrador, Mediterranean, Weddell and Ross seas. Some evidence also shows probable open ocean deep convection in the Irminger Sea. However, the coastal deep convection in the Labrador Sea seems to be the most efficient process that produces MOC deep waters (Spall and Pickard, 2001).
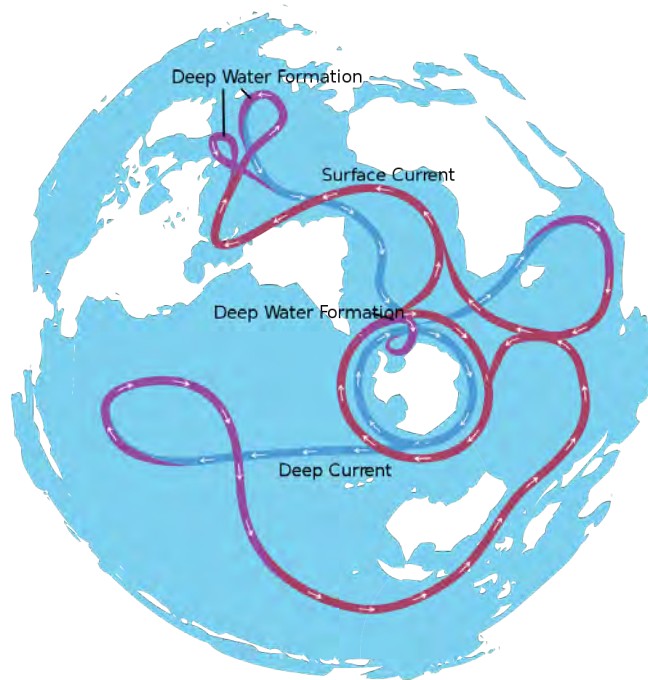
Figure II.4 Schematic representation of the meridional overturning circulation by *Van de Sande (http://wanderingabout.com).*

Open-ocean deep convection occurs seasonally in early winter when the wind curl is maximum. The movement of polar cyclonic gyres are strengthened and more isopycnals reach the surface. Surface waters become heavier under the action of atmospheric cooling and brine rejection from sea ice formation. Under these extreme conditions convective instabilities grow (Marshall and Schott, 1999). Deep convection takes place through a set of "plumes" of typically 1 km diameter and surrounding eddies. The heaviest waters are formed through this process.

Atmospheric conditions imprint their characteristics on the diving waters and again salinity can be used as a tracer as shown by Dickson et al. (2002).

## II.6. Role on mixed layer via barrier layer formation (low latitudes)

Barrier layers exist in all oceans, mostly in the tropics, and the largest ones are found in the western Pacific Ocean (de Boyer Montégut et al., 2007). A large volume of waters above 28ºC can be found there from the surface to around 100m depth. This warm water body is called the "western Pacific warm pool". Other warm pools exist such as the one off the coast of Panama. The warm pool is associated with low surface salinity waters west of 170ºE

called "the fresh pool" (Figure IV.3; Delcroix and Picaut, 1998). In contrast with temperature, steep vertical salinity gradients are most often found in the first 50 meters of the fresh pool. The mixed layer is therefore controlled in this region by haline stratification. The layer between the base of the mixed layer (and halocline) and the thermocline is called "the barrier layer" (Lukas and Lindstrom, 1991; cf. Figure II.5).
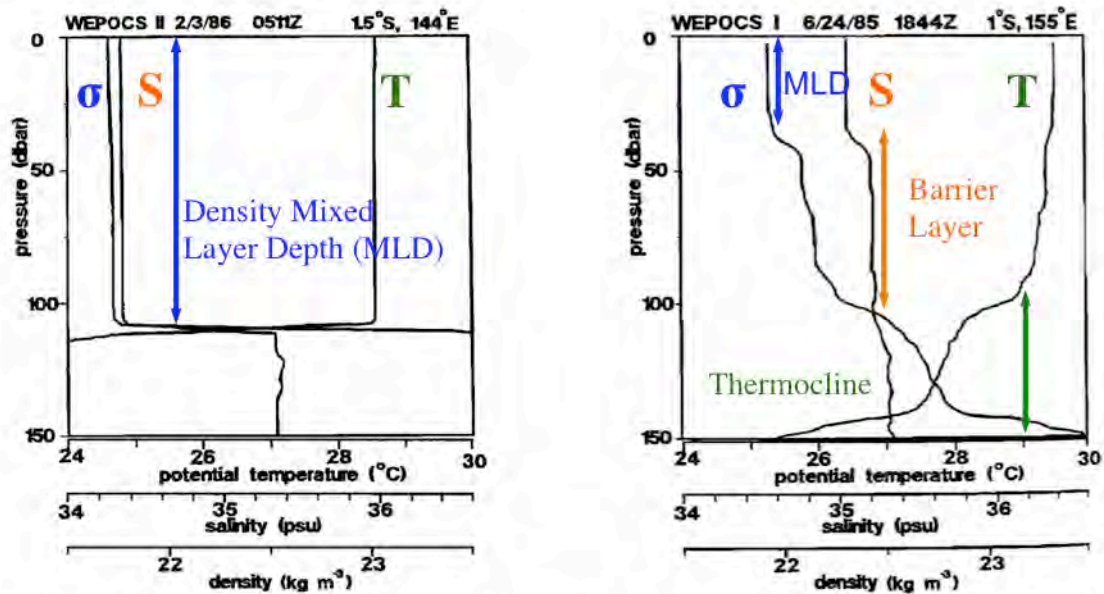


Figure II.5 Potential temperature, salinity and potential density from CTD profiles at 1.5ºS, 144ºE in February 1986 (Left) and at 1ºS, 155ºE in June 1985 (Right). The left panel shows a mixed layer under "normal" conditions and the right panel shows the presence of a barrier layer. (Adapted from Lukas and Lindstrom, 1991)

A subtle balance between surface forcing, vertical mixing and large-scale dynamical processes is associated with the formation and maintenance of the barrier layer (Lukas and Lindstrom, 1991). They argued that the oceanic convergence described above brings higher salinity waters from the equatorial cold tongue. These waters subducting below the fresh pool create a strong halocline and the barrier layer. The convergence and subduction processes were also pointed out in numerical studies (Vialard 1998ab). However, Cronin and McPhaden (2002) referred to this mechanism as a maintaining process rather than a formation one. Temporal phasing was found between the barrier layer thickness and the precipitations anomalies underlying the importance of dynamical processes in the barrier layer variability (Ando and McPhaden, 1997). Cronin and McPhaden (2002) summarized four different mechanisms for the formation of barrier layer as: the local surface processes (heavy rain, low

wind, etc…), dynamic processes (subduction and advection) and the salinity front "tilting/shearing" under the effect of westerly wind bursts. These mechanisms were tested against observations by Bosc et al. (2009) during the 2000-2007 period.

The salinity barrier layer has an impact on atmosphere-ocean interactions. As salinity shoals the mixed layer, wind-forcing momentum and surface heating are distributed over a shallower layer and are thus more efficient (Vialard et al., 1998b). Furthermore, the barrier layer isolates the warm pool from cold waters below, reducing the impact of vertical mixing and entrainment. The warm pool is also isolated from the cold tongue waters by a zonal salinity front (Rodier et al., 2000; Picaut et al., 2001). Studies have also shown the importance of the barrier layer in the onset of the greatest mode of variability in the Pacific Ocean: the El Niño Southern Oscillation (ENSO). The barrier layer's presence leads to an increase in temperature for instance by up to 0.8ºC during the 1997-1998 ENSO event (Lukas and Lindstorm, 1991, Vialard et al. 2002). Vialard et al. (2002) also found an increase by up to 0.2 m.s$^{-1}$ in the surface current during the same ENSO experiment.

## II.7.Salinity assimilation and impact on ENSO prediction

The effect of surface salinity assimilation in the model performance has been investigated by several studies. The assimilation of surface salinity alone has been found not to be sufficient to correct subsurface salinity biases (Reynolds et al., 1998). Using a complex assimilation method based on the Kalman filter theory and twin experiment approaches, Durand et al. (2002) showed the constraint of salinity related variables by assimilating surface salinity. In particular, the zonal velocity and the barrier layer were particularly better simulated during ENSO events. (The crucial influence of both etrms on ENSO will be described in following sections). Moreover, a reduction in precipitations estimation errors emerged when assimilating surface salinity data into an ocean model (Yaremchuk, 2006). With an assimilation scheme similar to the one used by Durand et al. (2002), experiments were carried out to evaluate the assimilation of simulated data from SMOS and Aquarius/SAC-D (Tranchant et al., 2008). The authors showed an improvement of their forecasting system and underlined the importance of specifying the observation error. At the time of writing, no published results can be found on assimilating satellite based salinity data. Assimilating surface salinity in a hybrid-coupled model leads to an increased correlation for 6-12 month forecasts by 0.2-0.5 and a reduction RMS error by 0.3ºC-0.6ºC (Hackert et al., 2011). The forecast of ENSO events is also improved.

Note that surface salinity can also be used as a statistical proxy to help predict ENSO (Ballabrera-Poy et al., 2002). Surface salinity does not impact ENSO now-casting (lag 0) but does increase the predictability of ENSO with lags from 6 to 9 months.

## III.   In situ S data Programs

Before the 1990s, salinity measurements in the open tropical oceans remained rather sparse in space and time. Most pre-1990 salinity measurements were made by Voluntary Observing Ships (VOS, Figure III.1 right) and sporadic oceanographic cruises. On VOS, bucket samples were usually collected by ship officers every 100 to 200 km and stored in bottles. Salinity was then measured in an oceanographic laboratory a few weeks later. A key VOS program was developed by ORSTOM (now called IRD) in Nouméa, New Caledonia, by the end of the 1960's (see Donguy and Hénin, 1976). This program, still ongoing, is now part of the French SSS Observation Service described in Section 2.

Following the strong 1982-1983 ENSO event, the Tropical Ocean Global Atmosphere (TOGA) program (1985-1994) was created as a major component of the World Climate Research Program (WCRP). One of the objectives of the TOGA program was "to provide the scientific background for designing an observing and data transmission system for operational predication". Observing systems have been strongly developed since. Automatic ThermoSalinoGraph (TSG) instruments were installed on the VOS (Figure III.1) in order to increase the spatial resolution of along track data (Hénin and Grelet, 1996). TSG were also installed on moorings (McPhaden et al., 1990) to produce long-term high temporal resolution salinity measurements. Ship tracks and moorings will be described in more details in the Data section.

Figure III.1 Left: Thermosalinograph installed on R.V. Nokwanda. Right: R.V. Rio Blanco (photos: C. Diverrès, IRD). Adapted from the French SSS observation Service web site.

TOGA decade induced improvements in monitoring mainly involve near-surface observations. Apart from the CTD cast data, salinity has only been measured at different depth since the years 2000s, from autonomous Argo floats (Roemmich et Owens, 2000; Figure III.2) and eXpendable Conductivity Temperature Depth (XCTD) transects (Sprintall and Roemmich, 1999). Nowadays, the spatial distribution of salinity measurements at the surface and at different depth enables the production of gridded datasets such those used in the following chapters.
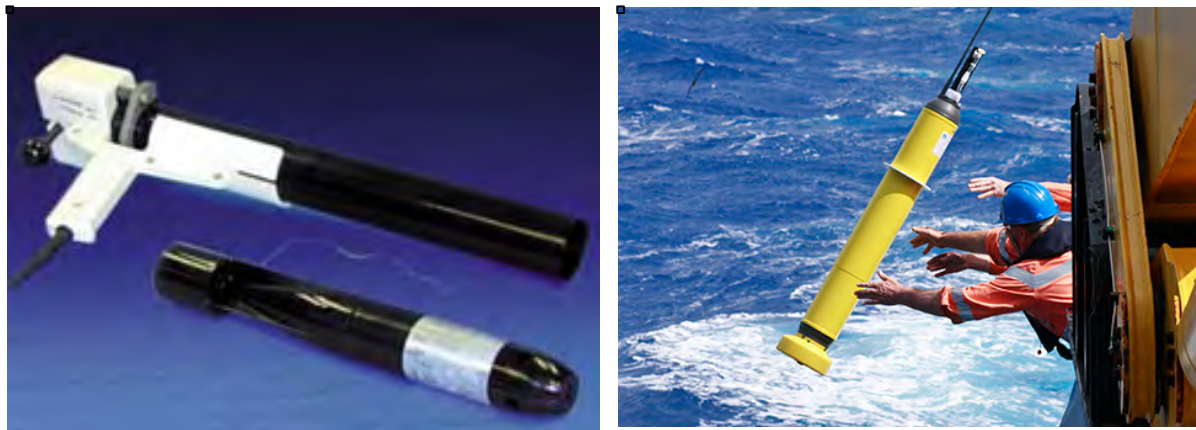


Figure III.2 Left: XCTD . Right: Argo deployment by the CSIRO (Photo A. Navidad)

Because salinity measurements at depth were so scarce before the last decade, most of the earlier studies examined the sea surface salinity. Even if gridded products with different depth levels are improving, their length depends on the Argo floats' deployments and they do not go back before 2002. In this context, numerical modelling has become more and more attractive to study ocean and atmosphere processes. Indeed, model performances have improved greatly in the last decades and they provide a full set of data in the 4 dimensions on regular grid points. Moreover, coupled models are independent of observation and can provide climate projections. However, we must keep in mind that even when using numerical models, salinity observations are still vital to assess model performances.

# IV.    Description of SSS patterns – Mean state

Even though findings on salinity have been constrained to the observations' scattering and model ability to reproduce salinity, the overall distribution of salinity and its large scale variability is rather well know thanks to numerous scientific studies. These studies were made possible by the scientists' and institutions' willpower to gather observations in databases available to everyone such as Levitus (1982) and following atlases. Many studies will not be cited in this manuscript. This poorly expresses my gratitude to the salinity "early explorers" for all their baseline studies.

This section is a literature review of what is known about the salinity mean state salinity in the Global Ocean, continuing with a focus on the tropical Pacific Ocean.

## IV.1.    Mean SSS in the Global Ocean

The mean surface distribution of salinity reveals patterns within basins but also from one basin to another (Figure IV.1). The Atlantic Ocean is significantly saltier than the Pacific Ocean even though they have similar large-scale fields. In both oceans, to the first order, the salinity distribution corresponds to the mean distribution of Evaporation minus Precipitations and River runoff (E-P-R). Low salinity regions roughly correspond to the Intertropical Convergence Zones (ITCZ) and South Pacific Convergence Zone (SPCZ) where precipitations are high and wind low. High Salinities are located in the subtropical basin centre, where evaporation is dominant. The river runoffs affect surface salinity as shown by the well-marked plumes of the Amazon, and to a lesser extent the Congo and Niger rivers in the Atlantic Ocean. No river with comparable runoff marks the tropical Pacific SSS.
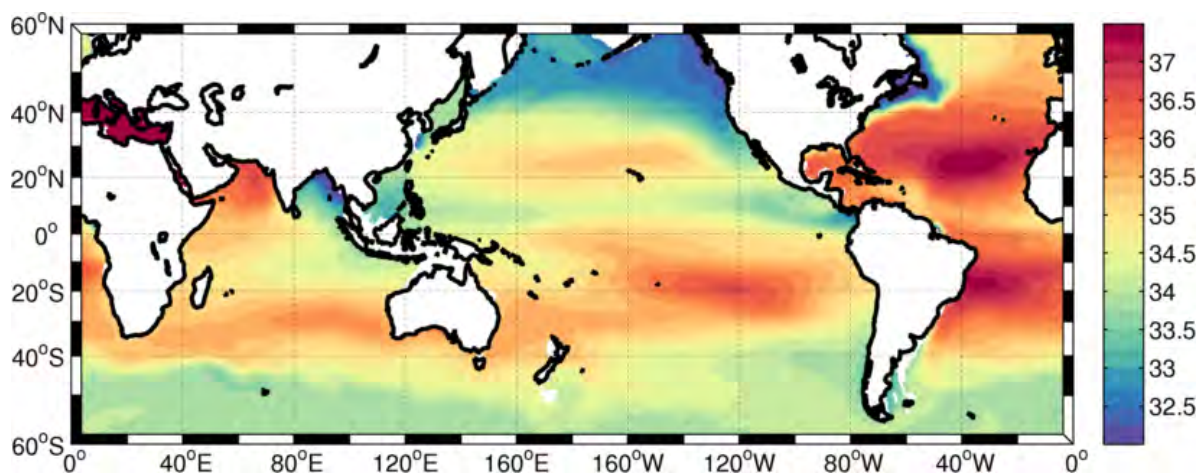


Figure IV.1 Global map of surface salinity from the ISAS dataset (described in Chapter 2) averaged over 2004-2012.

As stated earlier, the Atlantic Ocean is on average a few pss saltier than the Pacific Ocean. Evaporation is directly linked to the relative humidity of the air above the sea surface. The Atlantic is under the influence of dry continental air and evaporation is intense (Schmitt et al., 2008). Moisture from the Atlantic Ocean is then transported across Central America to the Pacific Ocean in air masses advected by the Trade Winds (Weyl, 1968). Evaporation in the Pacific Ocean cannot therefore be as strong as in the Atlantic. As a consequence, evaporation dominates precipitations in the equatorial Atlantic basin whereas the equilibrium is reversed in the equatorial Pacific basin.

The Indian Ocean is very peculiar with a strong zonal gradient across the Indian subcontinent. Very salty waters are found in the Arabian Sea and very fresh waters in the Bay of Bengal. On the one hand, the salty waters can roughly be explained by the advection of very high salinity from the Red Sea through the Gulf of Aden and from the Persian Gulf. On the other hand, the Bay of Bengal's extremely fresh waters result from both extreme rainfall and the Ganges and Brahmaputra rivers runoff.

Many studies have tried to understand the reasons for these mean salinity patterns. Near surface salinity is a balance of surface fresh water fluxes, advection in the three directions and other processes such as turbulence, diffusion etc.

Based on satellite and other in situ estimates, Johnson et al (2002) investigated the equilibrium between freshwater fluxes from the atmosphere and advective processes of the ocean. The mean horizontal salinity advection they found is qualitatively comparable to the surface processes in both large-scale magnitude and spatial variance (correlation of 0.63). They found however substantial differences in the details. Excess of evaporation over the subtropical gyres more than compensates the excess of precipitations in the convergence zones (Johnson et al., 2002). There is also a poleward shift between the precipitations maxima and low salinity waters of the convergence zones, underlying the effect of horizontal advection (Delcroix et al., 1998). A similar shift is found between positive salinity advection and the compensating effect of the heavy precipitations (Johnson et al., 2002). Moreover, salinity advection over-compensates the salinity decrease in the tropical convergence zone (Lagerloef et al., 2010, Figure IV.2). Analogous processes are observed in the subtropical evaporation- dominated regions with shifts between the evaporation and salinity maxima (e.g. Delcroix and Henin, 1991). A shown on Figure IV.2, there is no balance in this region

between observed salinity divergence and surface fluxes suggesting the importance of inaccuracies and the other processes (Lagerloef et al., 2010).
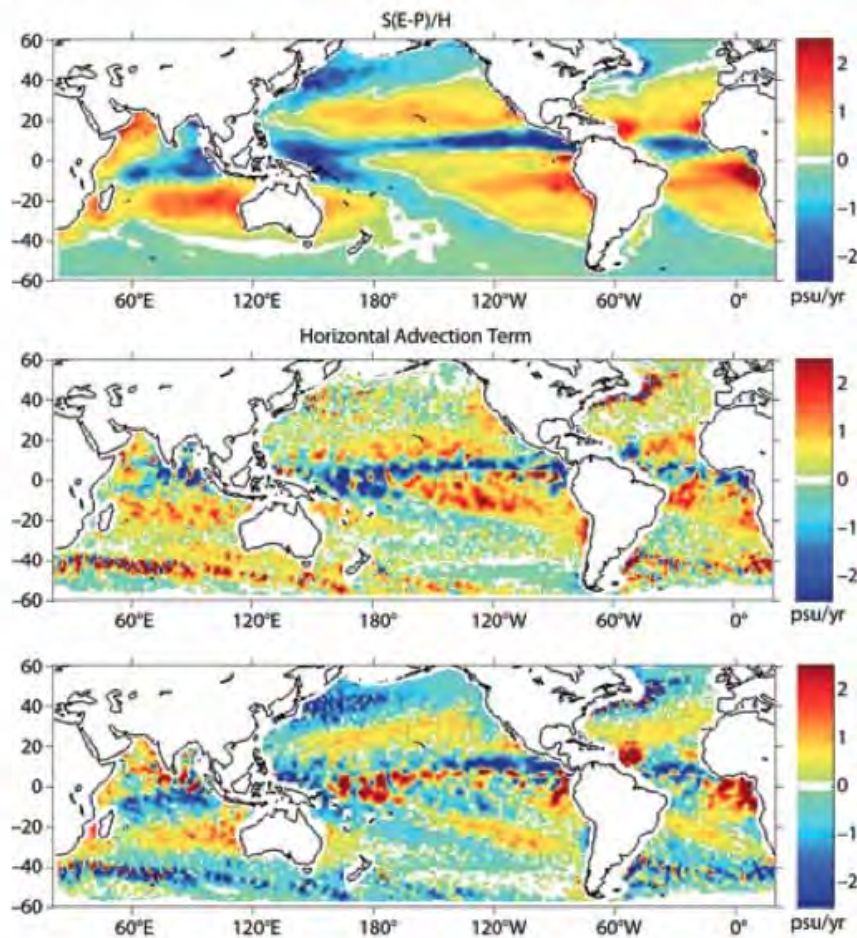


Figure IV.2 Top: Atmospheric forcing term averaged over 2005-2008 using Global Precipitations Climatology Project (GPCP) and "Objectively Analysed" Ocean-Atmosphere flux (OAFlux) products (both will be described in Chapter 2). Middle: Horizontal salinity advection for the same years using Near real-time Global Ocean Surface Currents (OSCAR). Bottom: The difference field. From Lagerloef et al (2010).

Differences between surface forcing and horizontal advection (Figure IV.2) do not only represent the processes at work at the mixed layer base but also unknown bias errors in the surface forcing, horizontal advection and the salinity trend (depending greatly on the timeseries length). The errors to the salinity transport are difficult to specify especially because of the lack of SSS data. The eddy fluxes are not sampled in this study (using climatologic salinity) and are thought to be of prime importance in the salinity transport in the equatorial Pacific (Vialard et al., 2002).

## IV.2. Mean SSS in the tropical Pacific Ocean

The tropical Pacific Ocean presents specific regional features in its surface salinity distribution such as the low salinity in the ITCZ, SPCZ and western Pacific warm pool as well as salinity maxima centred on 15ºN and 20ºS.

Along the equator, the surface salinity increases from the American coast to the central Pacific and decreases from there to the western boundary (Figure II.2, Figure IV.3 and Figure V.1). The unsteady decrease creates a steep surface salinity gradient and a front around 165°E. To the west of this front low salinity waters form the fresh pool mentioned earlier (Delcroix and Picaut, 1998).
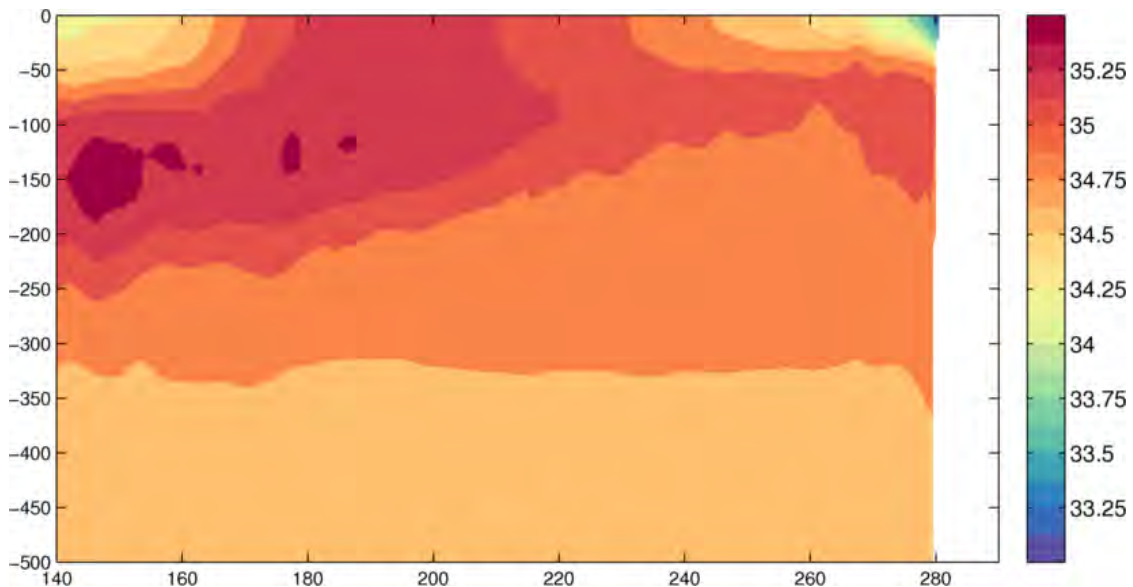


Figure IV.3 Longitude against depth salinity field along the equator averaged over 2004-2012, as obtained from the ISAS dataset (described in Chapter 2).

The low salinity waters of the fresh pool extend to 15ºS in the South Pacific Convergence Zone (Figure IV.1). A secondary surface salinity front is present between the southeast oriented fresh waters associated with heavy precipitations from the SPCZ and the westward oriented salty waters of the south Pacific salinity maximum advected by the southern branch of the South Equatorial Current (SEC) (Gouriou and Delcroix, 2002). The surface temperature field does not show any significant front with quasi-zonally oriented isotherms. Similarly, fresh waters are found roughly in the ITCZ region (5-10ºN, 120-140ºW) under the effect of strong precipitations and low salinity waters advected by the NECC from the west (Delcroix and Hénin, 1991).

The surface salinity absolute minimum (below 33.5 pss) spreads roughly from the American coast to 120ºW and between the equator and 10ºN (Figure IV.1; Figure IV.3). These low salinity waters are trapped between two distinctive systems: the eastern Pacific warm pool and the cold tongue of the equatorial Pacific upwelling system (Alory et al., 2012). This fresh pool corresponds mainly to an excess of precipitations over evaporation under the ITCZ and freshwater from the Andes and Caribbean regions.

Away from these SSS minima, large-scale high-salinity cores are centred within about 15-30° latitude in each hemisphere of the Pacific Ocean (Figure IV.1). Theses cores are also present in each hemisphere of the Atlantic Ocean and most studies have focused either on their global scale signature or on the North Atlantic core. These analyses have pointed out a 5 to 10º latitude shift between the cores and the evaporation-precipitations maxima due to the wind-driven Ekman salt transport (e.g., Delcroix and Hénin, 1991; Foltz and McPhaden, 2008; Qu *et al.*, 2011).

# V. SSS variability in the tropical Pacific Ocean– a brief literature review

As presented above, salinity is affected by atmospheric forcing, advection and mixing. In consequence, salinity shows variability at all time and space scales. In this section, we give examples of salinity variability in the tropical Pacific Ocean from small time/space scales to changes over multiple decades.

## V.1. Small time/space scales

Several studies have tried to quantify SSS variability at scales under a month and a few km. However, few measurements can be of use for this matter. Indeed, times series with very high resolution are needed such as for instance VOS-TSG (for the space-scale) and TAO-TSG (for the temporal-scale). Lagerloef and Delcroix (2001) examined high-resolution data sets and also focused on sampling errors from different resolutions in the western Pacific warm-pool region only. They under-sampled SSS from the original VOS along-tack 0.02º resolution to 2º samples and from the original TAO from under an hour resolution to 10-day sample. The sampling error was found to be less than 0.1 pss in most cases but reaches 0.3 in the vicinity of steep SSS fronts. Delcroix et al. (2005) expanded this study to the three

tropical oceans along 13 well-sampled ship tracks. Standard deviations of the VOS SSS over 0.5º, 1º and 2º degrees of latitude and 1º, 2º and 5º degrees of longitude intervals were computed in order to estimate the SSS variability at these 'small' spatial scales (Figure V.1).
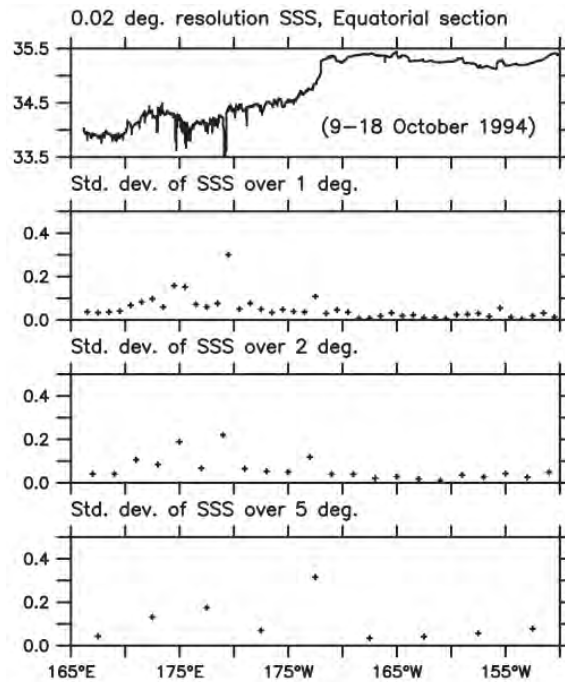


Figure V.1 Examples of high-resolution SSS observations recorded along the equator during 9-18 October 1994, and standard deviations of SSS computed over 0.5º, 1º and 2º longitudes. From Delcroix et al. (2005).

Studies mentioned above all showed small-scale variability of the order of 0.1 pss but as observed by Lagerloef and Delcroix (2001), occasionally reaching 0.2 to 0.4 pss. Furthermore, the 10-and 30-day standard deviations from the TAO SSS are usually less than 0.2 but reached 0.5 during the 1994 ENSO event. These errors are associated with sharp SSS front but also heavy precipitations in the western half of the equatorial Pacific Ocean. Results from Lagerloef and Delcroix (2001) and Delcroix et al. (2005) underline the high salinity variability at small scales, which could affect the interpretation of irregularly collected observations and therefore studies at all scales.

## V.2. Intraseasonal time scales

Intraseasonal variability is considered as corresponding to a temporal scale of variability of about a month and to spatial scale of a thousand kilometres. TIWs (Tropical

Instability Wave) were first characterized by meanders in the meridional SST front as seen from satellites with 1000km wavelength and with a 25-day period in the eastern equatorial Pacific (Legeckis, 1977). The TIW are westward propagating waves and exist in the equatorial regions of both the Atlantic and Pacific Oceans. Following Kessler et al. 's (1996) study, Lyman et al (2007) described the TIW of the Pacific Ocean with observations from the TAO buoy array. They identified two distinct TIWs with periods of 17- and 33-day, with similar characteristics to a Yanai/surface trapped instability and an instable first meridional mode Rossby wave. Reinforced by evidence from modelling, the 17-day TIW was found to imprint its variability within two degrees off the equator on meridional velocity and subsurface temperature. In constrast, the 33-day TIW variability is reflected on subsurface temperature at 5º North of the Equator.
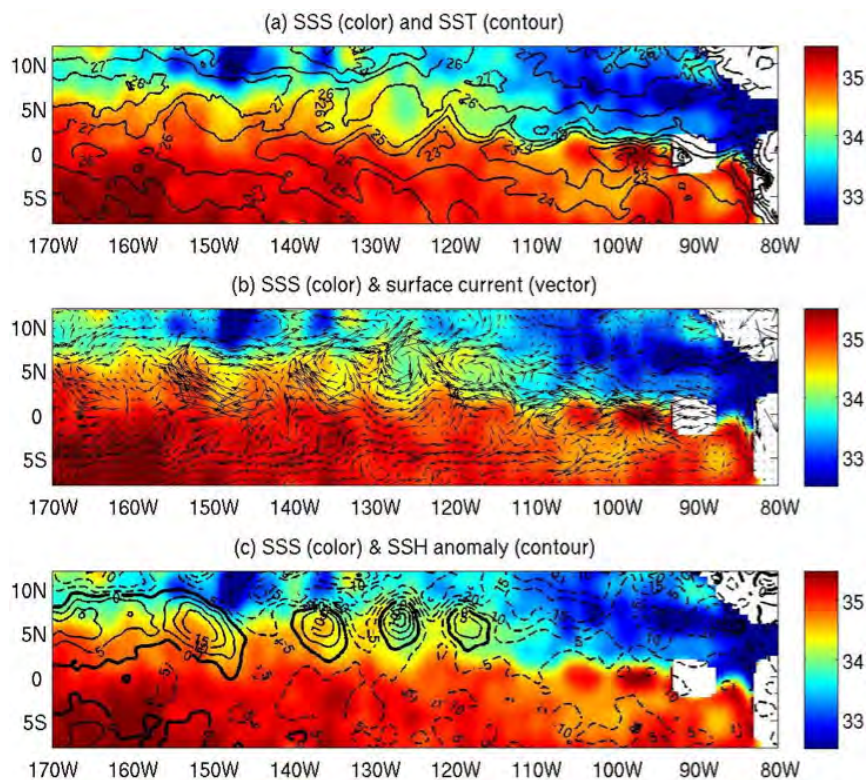


Figure V.2 7-day averages of SSS (pss) derived from Aquarius/SAC-D (colour shading in a-c), SST (ºC, contours in a), surface current (m/s, vectors in b) and sea surface height anomaly (cm, SSHA) (contours in c) centred on December 18, 2011. Surface currents are 10-day average centered on Dec. 18. From Lee et al. (2012).

The first Aquarius/SAC-D measurements reveal SSS variability linked to the TIWs (Lee et al., 2012). (Note that SMOS quasi-repeat period is 18-day, and unfortunately cannot

be of much help to study with accuracy the TIW). The SSS structures captured by Aquarius (Figure V.2) match the TIW ones obtained from SST and sea surface height (SSH). The three parameters have meridional gradients and therefore are affected by the TIWs differently. The maximum meridional gradients of SSS, SSH and SST are centred on the equator, 2ºN and 4ºN respectively. High resolution SSS is therefore ideal to detect and study the 17-day TIW. TIWs show some variability in their intensity which could impact locally SSS. Indeed, the TIWs activity depends on the equatorial current shear. The likely role of TIW on the salt budget is still an open question.

### V.3. Seasonal variability

The seasonal variability of salinity has been shown to account for about 53% of the total suface salinity variability in the tropics (Johnson et al., 2002). The maximum seasonal SSS variability in the tropical Pacific is located in the ITCZ, SPCZ and western Pacific (Delcroix and Hénin, 1991; Delcroix, 1998) where the seasonal cycle characterises more than half of the signal (Delcroix et al., 2005). In some parts of the Pacific Ocean, the seasonal cycle represents only less than 25% of variance, highlighting variability dominated by other scales.

Observed sea surface salinity variability at the seasonal time scale reveals a 6-month lag between cycles along the ITCZ and SPCZ. Salinity is minimum in October in the ITCZ and in April in the SPCZ (Delcroix, 1998). Seasonal salinity variations in the ITCZ are consistent with 2- to 3-month lags with the variations of precipitations (Delcroix and Henin, 1991; Delcroix et al., 2005). Gouriou and Delcroix (2002) focused on the SCPZ and found SSS variations lagging precipitations by around 3 months with maximum intensity over the exact same area. Indeed, the well-known ITCZ and SPCZ atmospheric seasonal cycles show high deep convection activity during boreal and austral winter respectively and low deep convection activity during summer (Meehl, 1987; Vincent, 1994).
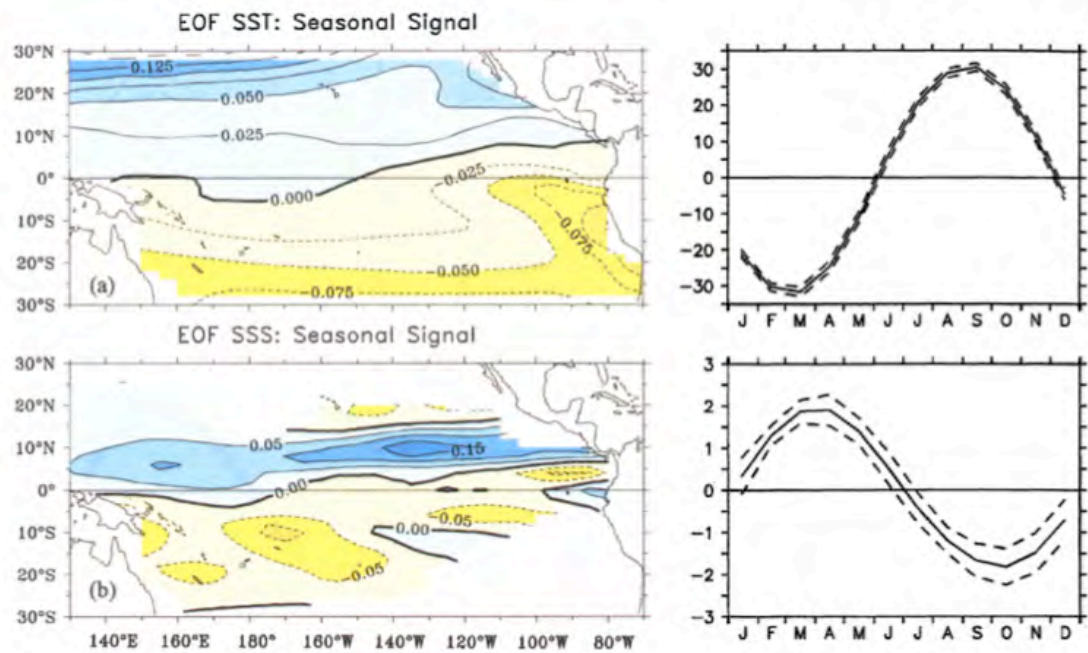
Figure V.3 (left) spatial patterns and (right) associated time function of the 1<sup>st</sup> mode of the Empirical Orthogonal Function (EOF) of the seasonal surface (top) temperature and (bottom) salinity. Computed over 1962-1993 and 1973-1992 respectively. The time functions correspond to the average month by month (solid line) bracketed by ±1 monthly standard deviation (dashed lines). The units are defined by the EOF so the product of the spatial pattern and time series gives ºC for the temperature and pss for the salinity. From Delcroix (1998)

Despite the unmistakeable impact of surface fluxes on seasonal variability, Delcroix (1998) evidenced the probable effect of salt advection seasonal variability from both the North and South Equatorial Counter Currents (NECC and SECC), which have well marked seasonal cycles themselves. In the ITCZ, salinity seasonal variations are coherent with a 2- to 3-month lag with maximum freshwater eastward flow of the NECC (Delcroix and Henin, 1991; Delcroix et al., 2005). Furthermore in the central part of the Basin, the meridional Ekman advection is in phase with the precipitations seasonal variability (Delcroix and Henin, 1991). The freshwaters from the equatorial upwelling advected by the Ekman currents could therefore reinforce the precipitations' impact.

Note that the 2- to 3- month lag between maximum E-P and minimum SSS (with E-P leading) can be explained mostly by the effect of E-P on salinity changes (dS/dt) and not by salinity directly, as discussed by Hires and Montgomery (1972; see also Equation II.1 below).

### V.4. Interannual variability

ENSO is the principal variability mode of the Pacific Ocean at the interannual time scale. ENSO is an atmosphere-ocean coupled phenomena with a periodicity between 2 to 8 years. It includes a warm phase, El Niño, and a cold phase, La Niña (see Philander, 1985; 1990). The strength of El Niño / La Niña is usually estimated using the Southern Oscillation Indice (SOI), which corresponds to the normalized sea level pressure difference between Tahiti (French Polynesia) and Darwin (Australia) shown in Figure V.4.
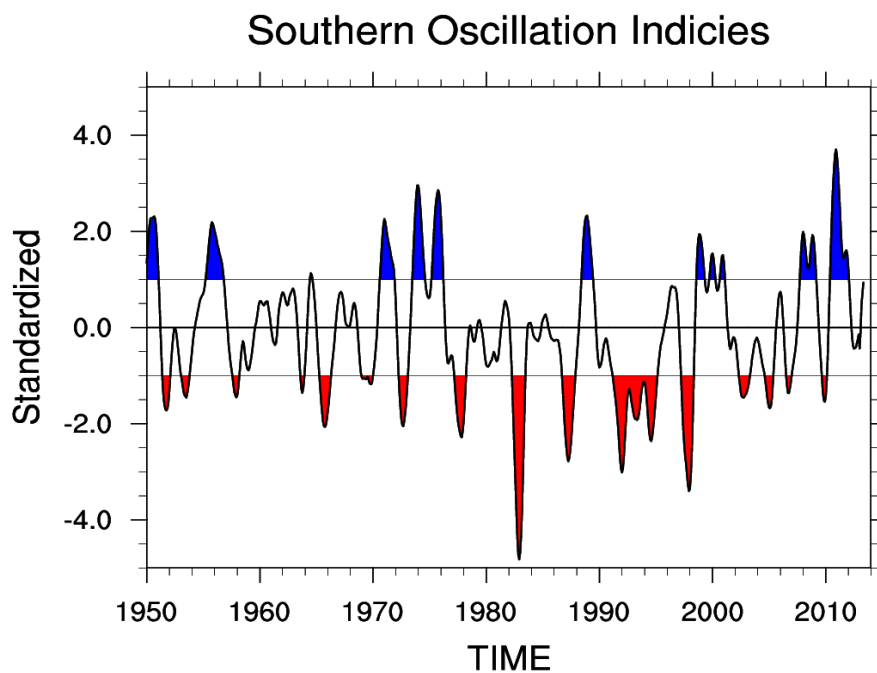


Figure V.4 Time series of the SOI . Variability below 8-month has been filtered out. Data is derived using normalization factors derived from monthly values. Blue correspond to La Niña events and red to El Niño events. Downloaded from the National Center for Atmospheric Research (NCAR) Earth System Laboratory.

ENSO has been thoroughly studied using observed SST, SSH and other parameters. We will remind here conditions associated with the so-called normal, El Niño and La Niña situations (Figure V.5).
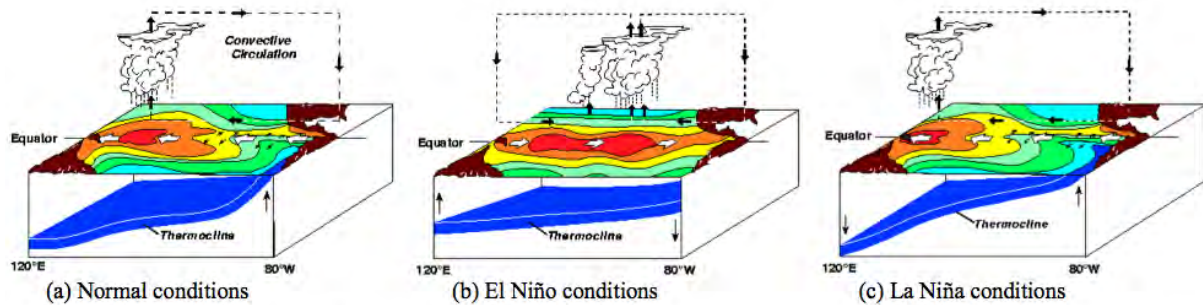
Figure V.5 Schematic plots of: (a) Normal, (b) El Niño and (c) La Niña conditions. Coloured surface contours represent the surface temperature. Back (white) arrows denote the main equatorial atmospheric winds (oceanic currents). Adapted from (http://pmel.noaa.gov/tao/elNiño/Niño-home.html)

When the tropical Pacific Ocean is under 'normal' conditions the warm pool is trapped to the west under the effect of the trade winds. Additionally, the warm pool provides heat for the deep atmospheric convection of the Walker ascending branch. In the east, the equatorial eastern Pacific upwelling system brings cold waters up and shoals the thermocline.

The relaxation of trade winds and/or westerly wind anomalies in the warm pool forces the fresh pool eastern edge convergence to move eastward. As a consequence, the warm and fresh waters from the warm pool spread in the central and in some cases in the eastern equatorial Pacific. Changes in temperature deepen the eastern thermocline and lessen its tilt leading to a weakening or complete shut off of the equatorial upwelling. Furthermore, the deep convection systems follow the warm waters modifying the Waker circulation. Wind stress convergence regions are also modified and the ITCZ and SPCZ both shift equatorward.

The La Niña conditions are analogous to the normal phase but intensified. The warm pool is shifted to its westernmost position and the SEC is intensified. Associated deep convection follows the warm pool back west and the Walker circulation is restored. The ITCZ and SPCZ both swing back poleward to their original positions.

The surface salinity ENSO signal was isolated using EOFs applied to a low-pass filtered SSS gridded field derived from in-situ measurements (Delcroix, 1998, see Figure V.6). The first EOF time function is highly correlated to the SOI with a 4-month lag. The associated spatial field shows a boomerang-shape of high-values (negative in their study). Changes in the warm pool reach 1 pss. More recent studies with longer time series including more numerous ENSO events obtain consistent patterns (e.g. Gouriou and Delcroix, 2002; Singh et al., 2011).
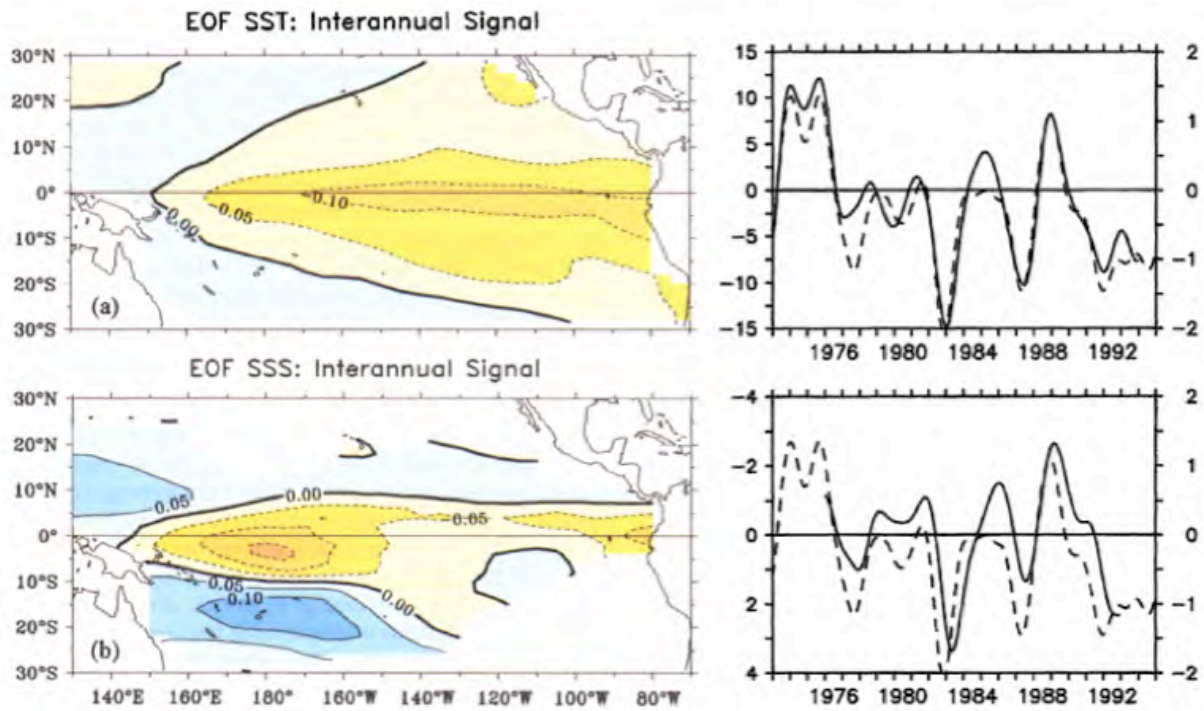
Figure V.6 Analogous to Figure V.3 but for the interannual signal. The dashed lines in the right panels correspond to the SOI.

Different analyses have focused on the processes behind the observed SSS interannual variability. The warm pool eastern edge convergence follows the ENSO cycle (Picaut et al., 2001). The oceanic convergence zone (i.e. zonal salinity front) is displaced east as the warm pool extends eastward during El Niño by zonal advection (Picaut et al., 1996; Cronin et al., 1998). The convective cells follow this displacement and sustain the salinity front (Picaut et al., 2001). The eastward warm pool displacement also increases the fetch of westerly winds over warm waters enhancing their penetration in the central equatorial Pacific Ocean. Furthermore, the weakening of the SEC during El Niño together with the anomalous eastward mass fluxes reduces the quantity of saline water subducting under the warm pool. This reduction erodes the barrier layer (Lukas and Lindstrom, 1991).

Moreover the zonal salinity gradient maximum (salinity front) associated with the barrier layer depth described earlier follows the warm pool displacements at the ENSO time scale (Delcroix and McPhaden, 2002; Bosc et al, 2009). Thick barrier layers in central and eastern Pacific precede El Niño MLT and precipitations anomalies by one or two seasons (Maes, 2006; Ando and McPhaden, 1997). The authors hypothesized that the barrier layer may contribute to an increase of the mixed layer temperature in the cold tongue region, which in turn increases precipitations.

36

During La Niña, waters in the central and eastern Pacific are unusually cold with dry conditions. The warm pool is confined to the westernmost part of the equatorial Pacific, the barrier layer develops only west of 160ºW (Ando and McPhaden, 1997).

Unlike SST, there is also a peak in interannual SSS variability located along the SPCZ main axis (Delcroix and Hénin, 1991; Gouriou and Delcroix, 2002). In the SPCZ region, SSS increases during an El Niño event whereas it decreases during a La Niña event with a magnitude twice as high as the seasonal cycle (Gouriou and Delcroix, 2002). Highest correlation was found between the secondary SSS front and the SOI with a 5-month lag. This variability is however not always as correlated with SOI. Indeed, authors pointed out the 1993-1995 unusual quasi-permanent El Niño conditions at the equator which had no impact on the secondary SPCZ front.

Under the SPCZ, Delcroix and Henin (1989) observed a strengthening of the SEC during the 1982-1983 El Niño. This underlines the importance of horizontal advection in the interannual displacement of the secondary SSS front. Gouriou and Delcroix (2002) found a northeast-southwest displacement of the SPCZ SSS front consistent with the atmospheric deep convection movements.

### V.5. Decadal variability

The Pacific Decadal Oscillation (PDO, Hare, 1996) is believed to be the main decadal signal over the Pacific Ocean. The PDO is an oscillatory pattern of climate variability over the North Pacific (Mantua et al., 1997) with cold and warm phases north. The PDO index is based on an EOF analysis of the Pacific SST north of 20ºN (Figure V.8, bottom) but impacts the whole basin variability. The PDO embodies anomalous patterns in surface and subsurface temperature, sea level pressure and surface wind stress fields (Figure V.7), all rotating clockwise around the North Pacific Gyre (Zhang and Levitus, 1997). The warm phase shown on Figure V.7 (right panel) corresponds to cooler than average SST anomalies in the North-western Pacific and warmer than average on the American coast but also negative sea level pressure in the central part of the basin. The cold phase is roughly the opposite (Figure V.7, left panel).
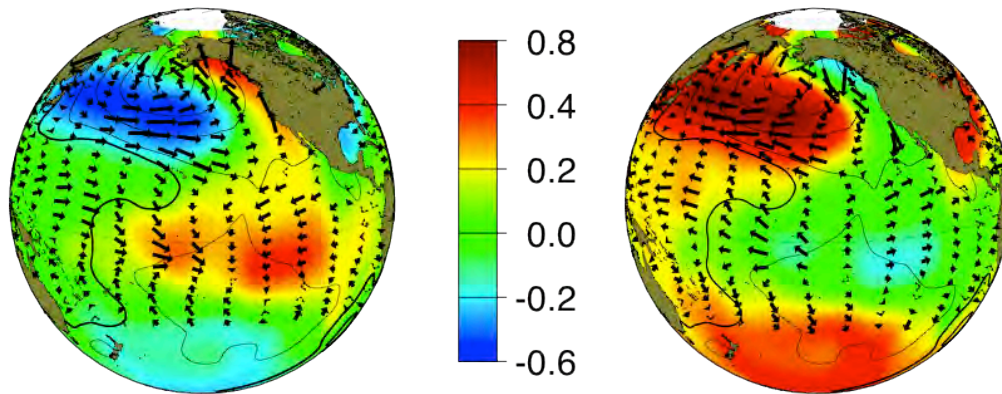
Figure V.7 Sea surface temperature (colours), sea level pressure (contours) and surface wind stress (vectors) anomaly patterns of the PDO cold (left) and warm (right) phases. From Mantua (http://jisao.washington.edu/pdo/).

Several other decadal signals in the Pacific Ocean have also been identified: the interdecadal Pacific Oscillation (IPO, Power et al., 1999), the quasi-decadal oscillation (Mann and Park, 1994) and the bidecadal oscillation (Minobe et al., 2002). Whether these signals are independent or not and what are their underlying mechanisms is still widely debated.

Delcroix et al. (2007) analysed SSS changes at the decadal time scales over the 1970-2003 period along three main shipping tracks. A PDO-like signal was shown in the main areas of variability: the warm-pool, the SPCZ and the equatorial cold tongue. Cravatte et al. (2009) regressed SSS values from a gridded field onto PDO time series. The obtained pattern (Figure V.8 top) is similar to the interannual SSS variability presented earlier, with the strongest signal in the SPCZ and Warm Pool region and is consistent with the north-eastward displacement of the SPCZ during positive PDO phase (Salinger et al., 2001; Folland et al, 2001). Moreover, the pattern in Figure V.8 is also very much consistent with the precipitations regressed on the PDO pattern of Delcroix et al. (2007).
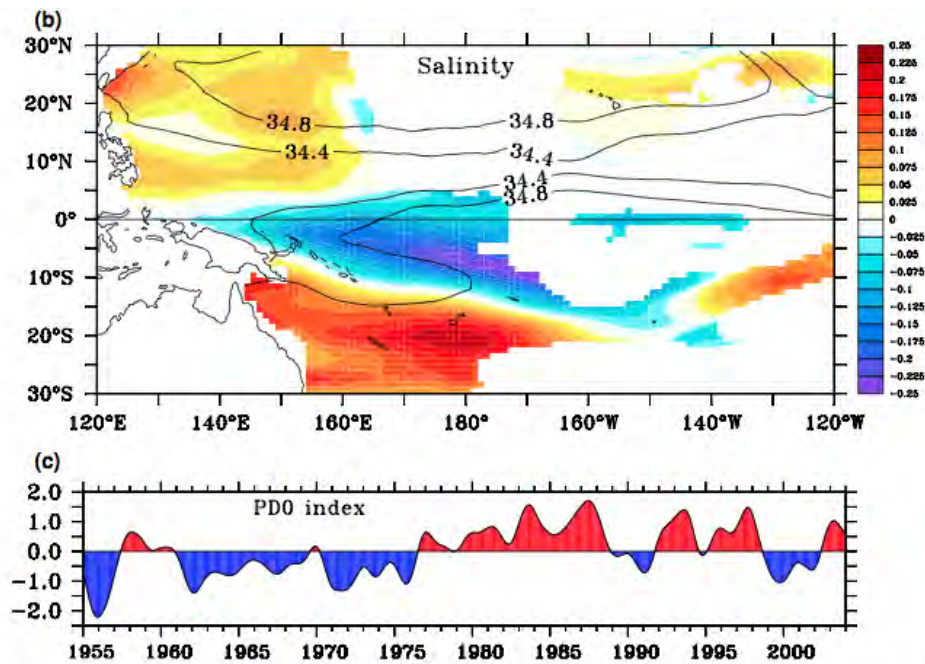
Figure V.8 (Top) Regression between the 1955-2003 detrended SSS and PDO leading the SSS by 6 months. Overlaid are the mean 34.4 and 34.8 isohalines. (Bottom) PDO index, smoothed with a 25-month Hanning filer. From Cravatte et al., 2009.

## V.6. Climate shifts

A significant positive shift occurred in the Pacific surface temperature in the mid-1970s, concomitant with increasing global atmospheric temperature (Meehl et al, 2009). A large body of literature has documented similar shifts in other oceanographic and atmospheric parameters (e.g. Trenberth, 1990; McPhaden and Zhang, 2002; Deser et al., 2004). Several studies showed that these shifts could be part of interdecadal variability, whose dominant time scale is around 50-70 years as computed from tree-rings (Minobe, 1997). Meehl et al. (2009) underlined the contributions from both changes in external forcing and inherent decadal fluctuations of the Pacific climate system. There are almost no studies looking at climate shifts in SSS time series, except the one from Cravatte et al (2009) in which the authors found a brutal shift in SSS in the mid-1990s already mentioned using other variables (Mantua and Hare, 2002).

## V.7. Tendency in recent decades

Despite the uneven distribution of data in time and space, Boyer et al. (2005) observed salinity trends at the global scale and from the surface to the deep ocean over a 44-year period (1955-1998). They reported large-scale coherent trends in each basin. Salinity decreases

everywhere in the Pacific Ocean except for the subtropical Pacific, roughly between 30 to 10ºS. Delcroix et al. (2007) study based on VOS data in the tropical Pacific Ocean confirmed these results. They found a decrease in SSS over a few decades along the New Zealand to Japan and New Caledonia to Tahiti ship routes. An increase was recorded along the Tahiti to Panama, across the South Pacific subtropical gyre. However, only around one decade of timeseries was available along that route at the time. Cravatte et al. (2009) investigated linear trends over the 1955-2003 based on gridded SSS field. They found a significant freshening in the well-sampled western tropical Pacific, particularly in the heavy precipitations zones (SPCZ and Fresh Pool). An increase in SSS is found in the subtropical gyres when data is available and in the Coral Sea. The authors found a strong decrease in the south-eastern Pacific, which is inconsistent with what was found by Delcroix et al. (2007). It can however be explained by a climate shift in the mid 1990s introduced above, leading to an abrupt salinity decrease that the Delcroix et al (2007) timeseries did not cover.

These changes are consistent with Durack and Wijffels (2010) findings from historical and Agro profiles. The 50-yr salinity trend found is heterogeneous with a positive salinity trend in the subtropical gyres and freshening in the tropical and high-latitude heavy rainfall regions. Furthermore, Schmitt et al. (2008) reported a freshening between the pentads 1975-1979 and 2000-2004 in the western tropical Pacific Ocean. Salinity change patterns similar to Cravatte et al. (2009) were found by Terray et al (2012), with an extended dataset (Figure V.9).
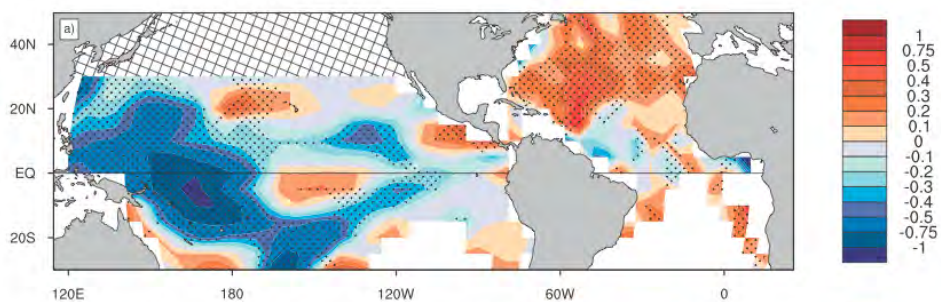


Figure V.9 Linear trend in SSS in pss/33-year (1970-2002). Stippled regions correspond to areas where trends are statistically significant from 0 at the 5% level using a two-sided Student's t test. (Terray et al. 2012)

However, one should bear in mind that only a limited number of in situ timeseries are of help when studying SSS at such a long time scale. Salinity model simulations and/or paleo-salinity data (e.g., Juillet-Leclerc et al., 2006) over long periods, both validated with in situ data, seems to be a complementary and necessary tool to better understand long-term changes.

## V.8. Projected SSS changes under Global Warming

In the context of anthropogenic global warming, several studies have tried to identify corresponding changes in the salinity mean patterns and variability. Terray et al (2012) have tested the ability of models from the CMIP experiment (phase 3) to produce consistent patterns of SSS in the projected 21$^{st}$ century. The authors stated, "The multi-model mean can be used as a robust estimate of the response to anthropogenic forcing, at least in the tropical and subtropical oceans". The multi-model projection is very much consistent with the observed trends discussed above with a freshening of the warm-pool and increasing salt content of the subtropical south Pacific surface salinity maximum.

These changes are consistent with the recently identified "rich-get-richer" mechanism (Chou and Neelin, 2004; Chou et al, 2009). This mechanism is based on the observed and modelled increase of atmospheric moisture predicted by the Clausius Clapeyron relationship in a warming world. Under this paradigm, the convergence zones get higher than usual precipitations and the subsidence zones lower than usual. Brown et al. (2012) illustrate the "rich-get-richer" mechanism in the 21$^{st}$ century projections of the 26 Coupled Model Intercomparison Project Phase 5 (CMIP5) models. They found increased precipitations due to thermodynamic changes in the ITCZ and SPCZ.

## VI. Thesis aims

Even though important aspects of the tropical Pacific salinity variability have been described in numerous studies at nearly all possible time and space scales, there are still insufficiently explored issues:

(1) While mechanisms responsible for SSS are qualitatively well known, quantifying those mechanisms is still under debate. This is extremely difficult based on observations and even on model output archived every 5 days. Indeed, on one hand observations are irregularly distributed over the entire Pacific Ocean and forced models are not able to satisfyingly reproduce salinity without fresh water fluxes corrections. Moreover, there is almost no information based on observations regarding processes happening at the mixed layer base such as mixing and entrainment (from the mixed layer depth variations).

(2) A very large body of literature has given a comprehensive description of ENSO and especially its warm phase: El Niño. Only a small number of studies on La Niña events

can be found. Furthermore, as seen on Figure V.4, strong La Niña events have been becoming more frequent during the last decade. Studies have hypothesized that ENSO could be dominated by La Niña events. It is therefore crucial to understand better the associated mechanisms and in particular the ones behind the salinity signature.

(3) Many studies dealing with SSS changes have focused on the precipitations dominant regions of the tropical Pacific Ocean such as the warm pool, the ITCZ and SPCZ. These zones present fortuitously both the maximum variability and the highest density of surface salinity observations.

As already described, subtropical Pacific maximum surface salinity cores are due to the evaporation dominated freshwater fluxes and wind-driven Ekman salt transport. Salinity changes in these cores could affect, on seasonal to decal timescales, the source branches of Shallow Tropical-subtropical overturning Cells (STCs) and the generation of spiciness anomalies (McCreary and Lu, 1994; Gu and Philander, 1997; O'Conner *et al.*, 2002; Nonaka and Sazaki, 2007; Kolodziejczyk and Gaillard, 2012). Observations and models have evidenced tropical-subtropical exchanges following different subsurface export pathways. After subduction in the subtropics, waters reach the equator either by following the western boundary current or directly through the interior of the basin. Anomalies in salinity can therefore be exported to the equator and can influence low-frequency tropical variability (Schneider *et al.*, 1999; McPhaden, and Zhang, 2004; Laurian *et al.*, 2009). Indeed, under the "rich-get-richer" mechanism, one would expect a decrease of precipitations and thus probably an increase of surface salinity in the high salinity core.

As a contribution to the three major issues cited above, my Ph.D. research work aims at (1) quantifying mechanisms responsible for the tropical Pacific Ocean SSS variability (mainly at seasonal and ENSO time scale), (2) describing and assessing mechanisms behind the 2010-2011 La Niña SSS changes and (3) analysing the formation and variability of the south Pacific subtropical high salinity core (at the same time scales).

Studies based on these three axes are gathered in three papers, one of which is published in the Ocean Dynamics journal, the second one is accepted for publication in the Journal of Geophysical Research (JGR) and the last is submitted to the JGR special section on SMOS and Aquarius/SAC-D. It is important to note that the second and third papers use for the first time an early version of promising surface salinity data derived from SMOS, the first satellite from which scientists can estimate surface salinity.

These three published or submitted papers constitute Chapters 3, 4 and 5 of the present Ph.D. manuscript, respectively. Data and methodology used are presented in chapter 2. The last chapter contains conclusions and overall perspectives related to the work carried out.

# Chapter 2. Data and Methodology

## I. Data description

Analyses led for this Ph.D. are based on complementary salinity data sets from *in-situ* and satellite measurements as well as from a numerical simulation. Each dataset brings different information, which are all necessary for the cross-comparison/validation and better understanding of salinity at various time and space scales.

### I.1. In-situ observations

#### *I.1.1. VOS Bucket samples and TSG*

Surface salinity has been measured in the Pacific Ocean at least since the early 1900's. The data density markedly increased starting from the early 1970's when measurements were made by mean of bucket samples collected on VOS as described in the first chapter. From 1991, the French SSS Observation Service has installed TSG on nearly 40 different VOS. The TSGs, mainly SeaBird SBE21 type, are attached to the VOS engine cooling systems and connected to a computer in the upper deck. Seawater is pumped into the cooling system and part is deviated into the TSG for measurements. The temperature data is usually not used for scientific purposes because it is biased by a few tenths of a degree (of the order of 0.2-0.5°C) as the TSG can be quite far from the original water intake. SSS is usually measured every 15s and median values over 5min are stored. Because of the ships' average draught and speed (20-25 knots), it is estimated that the measurements represent an average of the first 10 meters depth and have on average a 3 km resolution along track.
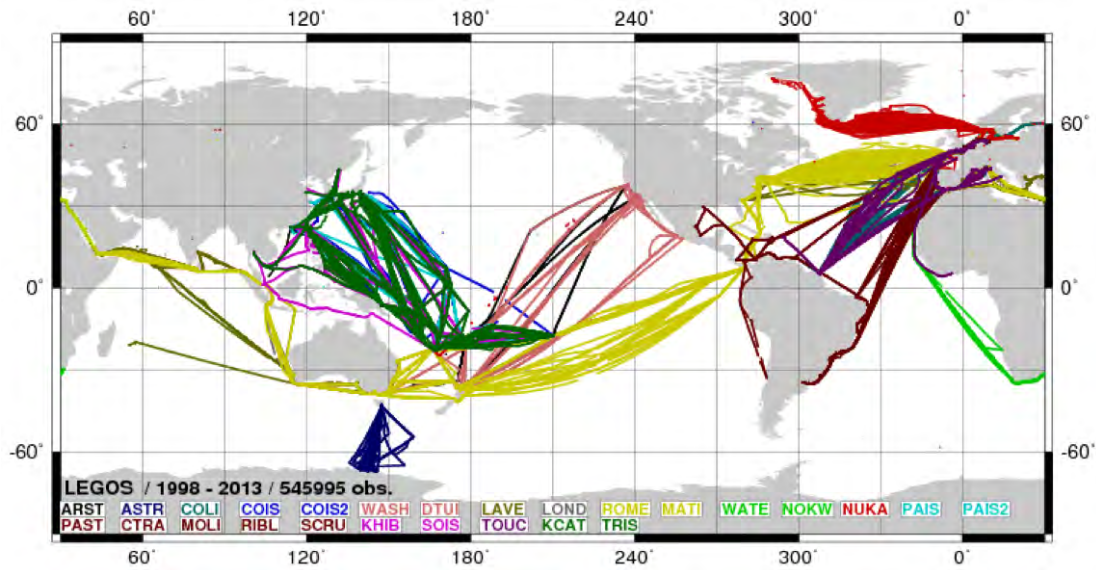
Figure I.1 1998-2013 distribution of real-time (1h resolution) SSS data collected along VOS tracks from the French SSS Observation Service.

Data from TSG, times and the on-board Global Positioning System (GPS) sigal are sent hourly via satellite (Inmarsat or Iridium) to the French SSS Observation Service, which distributes real-time and delayed mode SSS as well as evaluated research products. Only the validated delayed mode data and the last version of a gridded SSS product (Delcroix et al., 2011) were used for the purpose of the studies included in the present PhD thesis. Regarding the delayed mode data, a quality-control algorithm involving comparison with climatology, daily bucket samples collected on board and collocated near-surface Argo data processes surface salinity. The accuracy of SSS values (of the order of 0.02 pss) is a function of the linear-fit adjustment between TSG versus bucket samples and collocated Argo measurements (see Alory et al., 2013, for details). Only "Good" and "Probably Good" flagged data were kept for our study. (See below for the accuracy of the gridded product).

### I.1.2. Other Salinity Observations

Other salinity in-situ observations encompass mainly autonomous measuring systems which have been developed and widely deployed in the recent decades, but also classical data from oceanographic cruises. We give here a quick description of the three main salinity data sources: CTD, Argo and TSG installed on moorings, whose spatial distribution is given below.

46

**Annual salinity observations at 10 m. depth.**
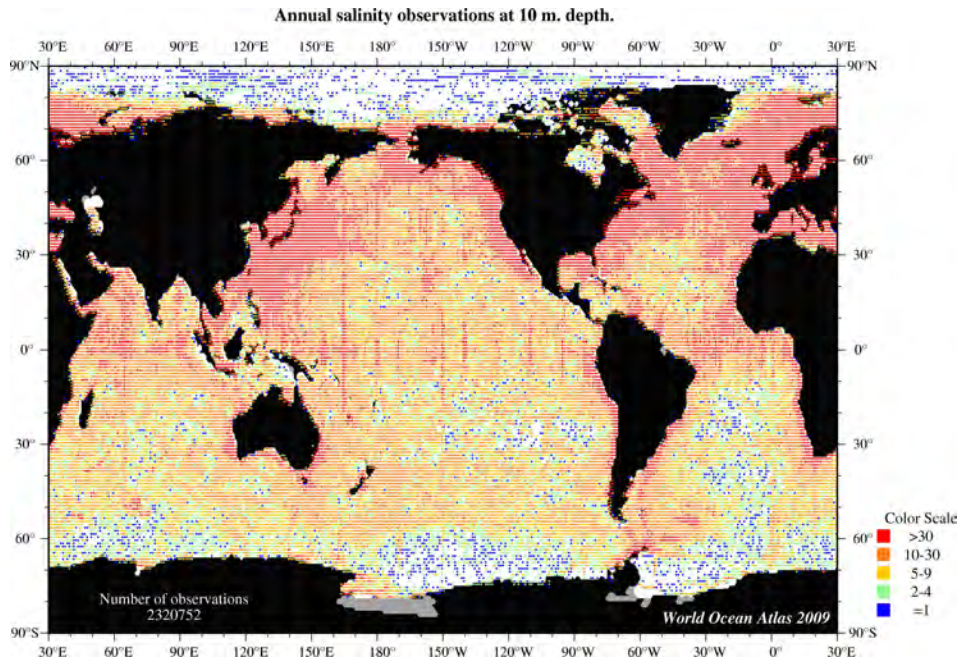


Figure I.2 Data distribution of 10m depth salinity measurements from the World Ocean Atlas 2009

- Conductivity – Temperature – Depth (CTD) casts

CTD measurements are carried out during oceanographic cruises. During stations, the rosette carrying the CTD is put into water to a maximum depth sometimes reaching over 5000 meters. Salinity is derived from conductivity measurements, usually with a one-meter vertical resolution, and is calibrated with in situ data from the rosette bottle samples at a several depths. Historical CTD data covers mainly the northern hemisphere oceans and are subject to seasonality, as the ability to make measurements depends on the state of the sea.
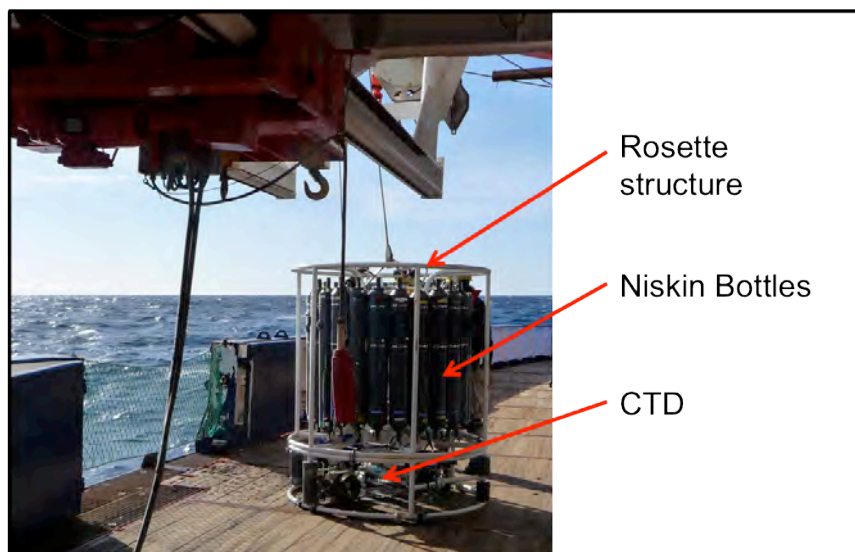


Figure I.3 Rosette from the R.V. Polarstern (March 2009)

• Argo profilers

The Argo project was created in the 1990s and deployments of Argo floats started in the early 2000s on a global scale (Roemmich and Owens, 2000). No less than 53 countries support the Argo program and over 3500 active floats are operating in June 2013 over the Global Ocean (Figure I.2).

The floats monitor the temperature and salinity over the first 2000 meters of the ocean with a vertical resolution of 5 to 10 meters and with a nominal 10-day repeat cycle. After completion of the cycle (Figure I.4), temperature and salinity data is transmitted via the Argos satellite system to Global Data Acquisition Centers (GDAC) such as Coriolis in France. These centres deliver real time data as well as delayed-mode controlled and/or adjusted data.
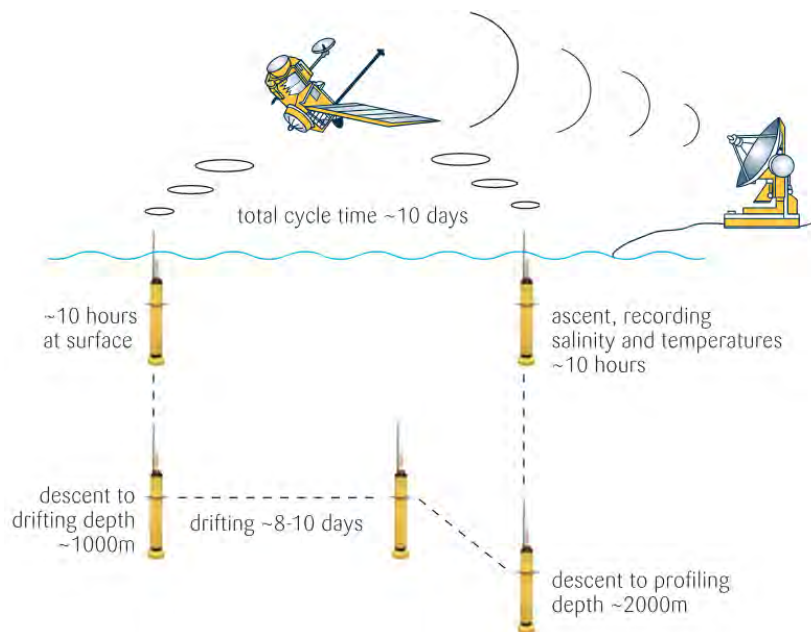


Figure I.4 Argo profiler cycle

• Moorings TSG

TSG were deployed on the New Generation ATLAS (Autonomous Temperature Line Acquisition System) buoys of the TAO (Tropical Atmosphere Ocean project) developed during the TOGA decade and of the TRITON (TRIangle Trans-Ocean Buoys Network) arrays. TAO/TRITON moorings are located in the equatorial Pacific Ocean (8ºS-8ºN, 137ºE-95ºW). Ocean temperature, salinity and ocean currents are monitored over the first 500 meters (Figure I.5) with high temporal resolution. Atmospheric parameters are also recorded, such as air temperature, relative humidity and rain-rate. Data is transmitted via satellite to dedicated

centres and made available in real-time by the NOAA Pacific Marine Environmental Laboratory (PMEL) at http://www.pmel.noaa.gov/tao/data_deliv/deliv.html.
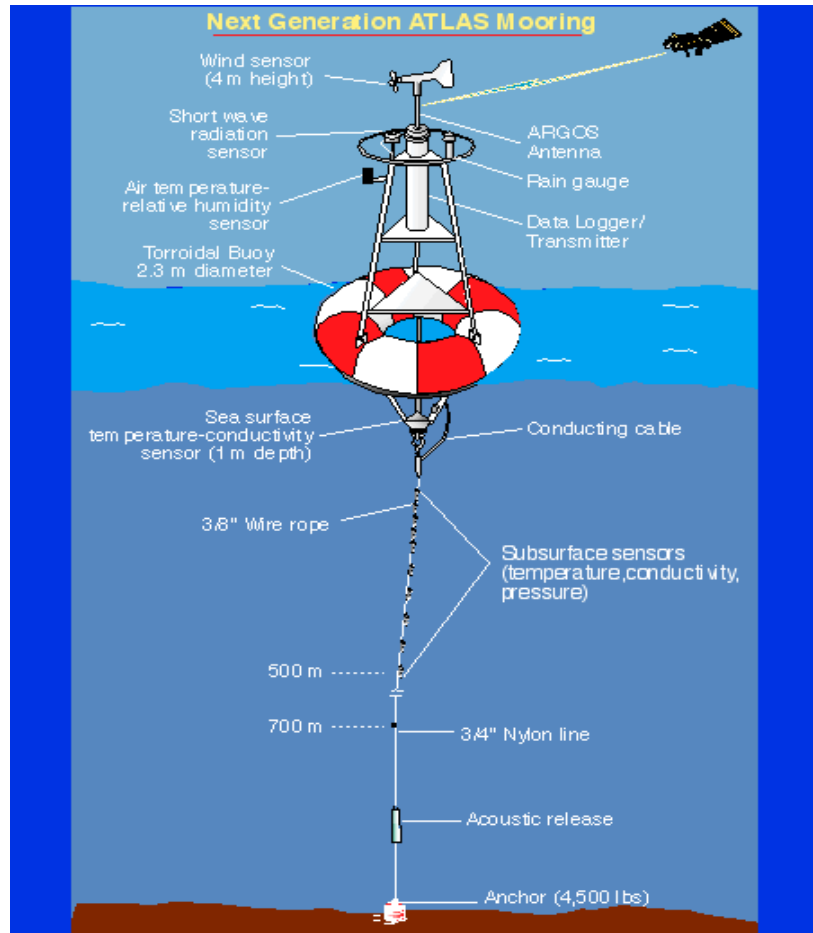


Figure I.5 Next Generation ATLAS Mooring

## I.2. Gridded Products

The two different gridded products introduced in this section are based on the in situ data we just presented and are used in the studies included in this manuscript.

### I.2.1.The tropical Pacific SSS Product

The surface salinity gridded product described in Delcroix *et al*. (2011) covers the tropical Pacific Ocean within 30°S-30°N, 120°E-70°W. Values of salinity representative of the 10 first metres average were derived from over one million records of in situ data described above and represented in Figure I.6. For all data but the VOS-TSG, the value closest to 5-metre depth is kept. The dataset spans monthly from 1958 to 2009 (extended

since Delcroix et al., 2011) over a 1° longitude by 1° latitude spatial grid. Values of associated errors are also available within the domain.
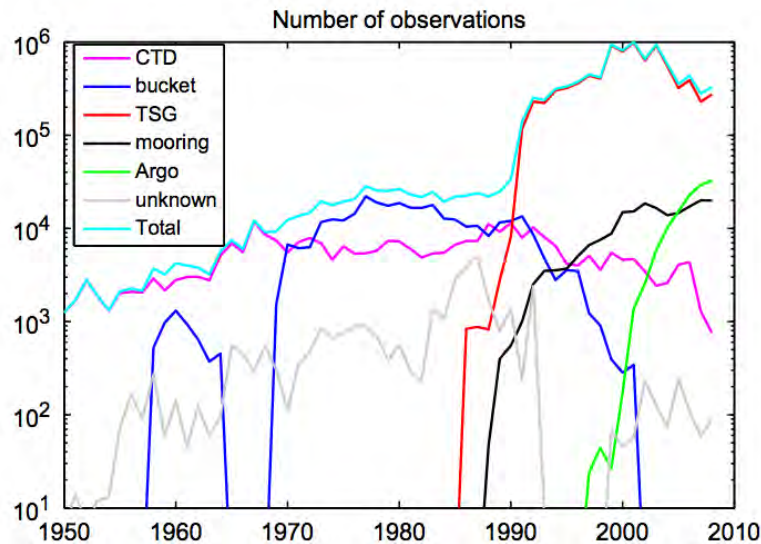


Figure I.6 Yearly distribution of SSS observations collected from different instrument types denoted by color codes. Note that the vertical axis is expressed in decimal logarithm. (From Delcroix et al., 2011)

Information about the data and the blending techniques are described in Delcroix et al. (2005, 2007, 2011) and Cravatte et al. (2009). Some data are readily discarded such as duplicates and data failing basic statistical tests. Surface salinity medians are then computed over 5 days and 1° longitude by 1° latitude grid elements. Following Cravatte et al. (2009) the obtained median data is then analysed with an optimal interpolation method (De Mey and Ménard, 1989) to produce the final interannual monthly field. Data within an ellipsoid with axes of 2000 km in longitude, 500 km in latitude and 2 months in time are included in the central data point calculation. The data is then mapped with a two-step methodology which takes in account the time and space scales of the involved physics (Delcroix et al., 2011).

This product is generated and distributed by the French SSS Observation Service. It is made freely available at http://www.legos.obs-mip.fr/observations/sss/datadelivery/products.

### I.2.2. ISAS

The ISAS (In-Situ Analysis System) data set is a uni-variate objective analysis (OA) giving optimal values of temperature and salinity for each horizontal and temporal grid point from 2002 to 2011.

It is based on the Argo network of profiling floats, TAO-TRITON moorings and CTD casts presented in Section I.1.2 but also on complementary datasets such as the one obtained from marine mammals in southern oceans. Note that the last version we will consider does not yet include VOS data. The temperature and salinity profiles are first interpolated to 152 standard depths from 0 to 2000 metres. The ISAS OA algorithm (v.6) is then applied to the profile, which results in fields on the global ½ °x ½ ° horizontal mesh (77ºS-66.5ºN). The reference field needed for the OA is based on the overall 2004-2012 average and 2002-2012 variance. Around each grid point, only data included in the ellipsoid defined in dimensions by $L_x$=600 km of longitude, $L_y$=300 km of latitude and $L_t$=3 weeks are included in the analysis, using covariance scales of 300 km in longitude, proportional to the Rossby radius of deformation in latitude, and 3 weeks in time. The accuracy of the objectively analysed T and S gridded values thus depends on the number of nearby data. If there is no data within the ellipsoid then the data corresponds to a first guess reference field. This OA is produced at the Laboratoire de Physique des Océans (LPO)/ IFREMER (France); details can be found in Gaillard et al. (2009). The previous version technical report can be found at http://wwz.ifremer.fr/lpo/SO-Argo/Products/Global-Ocean-T-S/ISAS/Documentation/ISAS-V6-Method-and-config.

### I.3. SMOS

The SMOS satellite and its main instrument have been briefly presented in the introductory chapter. The SMOS mission is a joint ESA/CNES/CDTI Earth Observation Program and was selected as the 2nd Earth Explorer Opportunity Mission. SMOS MIRAS is designed for the measure of soil moisture and SSS, a first from a single spaceborne instrument. MIRAS calibration is very challenging and requires sophisticated corrections as well as pre- and post-processing algorithms.

The satellite control centre is installed within the CNES premises in Toulouse. L1 and L2 products are developed by an ESA dedicated mission centre.

Two centres were created for the level 3 and 4 data development in France and Spain.

- The SMOS Barcelona Expert Centre (SMOS-BEC) is a joint initiative of the Spanish Research Council and the Universitat Politècnica de Catalunya.
- CP34-BEC centre, which moved from ESAC to the BEC in July 2013

- The Centre Aval de Traitement des Données SMOS (CATDS) is divided in two centres focusing on salinity:
- The Data Production Centre (CPDC) at IFREMER (Brest)
- The Ocean Salinity Expertise Centre (CEC-OS) at both IFREMER (Brest and Toulon) and LOCEAN (Paris)

Ground segments for SMOS level 3 and 4 data are in charge of:

- SMOS L3/L4 products (from L1B products from the ESA Data Processing Ground Segment) production and distribution
- SMOS L3/L4 products reprocessing when necessary
- Proposing improvements for the L0 to L2 processing chains (possibly helping to fine tune the calibration aspects).
- Providing services & hot-line support to L3/L4 users
- Development, test and validation of L3 and L4 processing chains algorithms in close cooperation with the scientific community

All centres deliver one or more L3 SSS products. At the time of writing, their main characteristics are summarized in the Table below.

| | CP34-BEC | CPDP | | | CEC-OS IFREMER | | | CEC-OS LOCEAN | |
|---|---|---|---|---|---|---|---|---|---|
| Product version | V1.1 | V2.6 | | | Ifremer V02 | | | LOCEAN v2013 | |
| SSS Retrieval | L2OSOP v5.50 | L2 OS v5 | | | SSS ($T_{bx}+T_{by}$) | | | L2 OS v5 | |
| Reprocessed L3 data | Jan 2010 to Dec 2012 | Jan 2010 to Apr 2012 | | | May 2010 to Dec 2012 | | | Jan 2010 to Dec 2012 | |
| Real time | Up to now | Up to now | | | None | | | None | |
| Temporal windows | 3-day 9-day Monthly Seasonal Annual | Monthly | 10-day | Daily | Monthly | 10-day | Daily | 10-day | Monthly |
| Spatial Resolution | ¼° | 200km | 100km | 50km | 1° | ½° | ¼° | 100km then sampled over ¼° | |
| Calibration | Variable OTT (~every 2 weeks) | Variable OTT (~every 2 weeks) | | | Single OTT + Daily 5° adjustment with respect to SSS climatology | | | Variable OTT (~every 2 weeks) | |

Table I.1 Main characteristics of the different L3 SSS products delivered by the L3/L4 ground segments.

Data from January to June 2010 must be interpreted with care, as, during the satellite commission phase period, the calibration control parameters of the instrument were quite variable.

The L3 SSS produced by the CEC-OS LOCEAN was chosen for the analyses presented in this manuscript. The first reason for this choice was our close contacts and scientific collaboration (and publications) with the CEC-OS teams. Moreover, the LOCEAN product is not adjusted to climatology making it more appropriate for our variability analyses. However, its RFI filter is not performing as well as the CEC-OS IFREMER, but our study region is rarely affected.
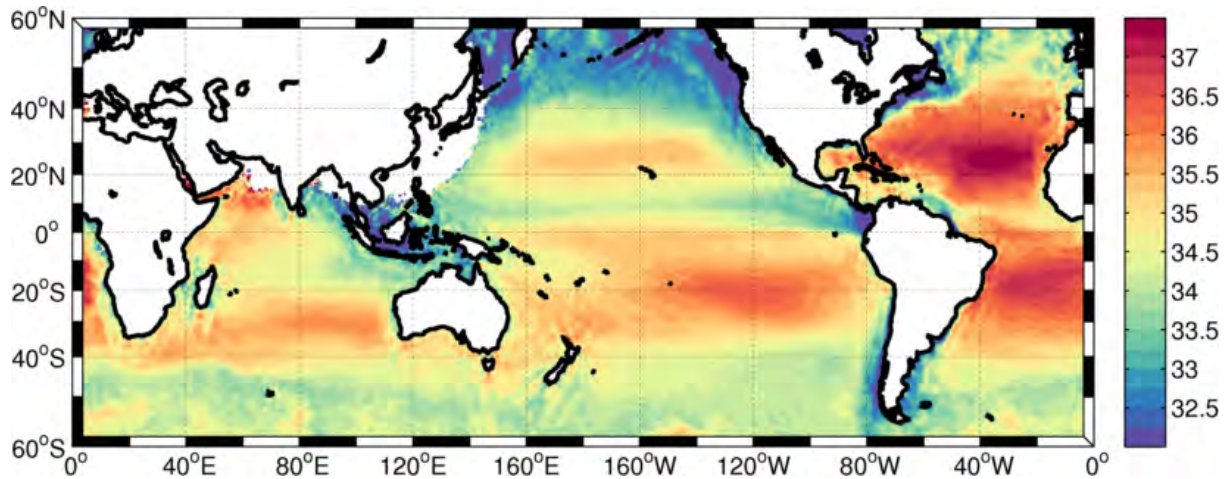
Figure I.7 CEC-OS LOCEAN V2013 SSS

The LOCEAN SSS dataset uses the L2OS 'retrieval flags' and L2OS Radio Frequency Interference (RFI) flag. The 2 weeks averaged variable Ocean Target Transformation (OTT) corrects most of the seasonal biases.

The monthly product used in the following studies are obtained using the weight averaging method described in Yin et al. (2012) and the flag sorting described in Boutin et al. (2013). Furthermore, the galactic noise flag was not tested (data affected by large galactic noise are nevertheless sorted out), and land mask is only 40km.

### I.4. Model Simulation MRD911

The Ocean General Circulation Model (OGCM) simulation used in the following studies has been run by the DRAKKAR group based in the Laboratoire des Écoulements Géophysiques et Industriels (LEGI, France). The OGCM corresponds to the version 3.2.1 NEMO (Nucleus for European Modelling of the Ocean) z-coordinate model (Madec *et al.* 2008). The simulation configuration (so called ORCA025.L75-MRD911, hereafter MRD911) has 75 vertical levels, with as much as 21 levels in the upper 70 m to resolve well the mixed layer. The ORCA025 model configuration covers the Global Ocean with a tripolar grid of a ¼° nominal horizontal resolution leading to a 28km resolution near the equator and 10 km near the Arctic Ocean and Antarctic continent (Figure I.8).
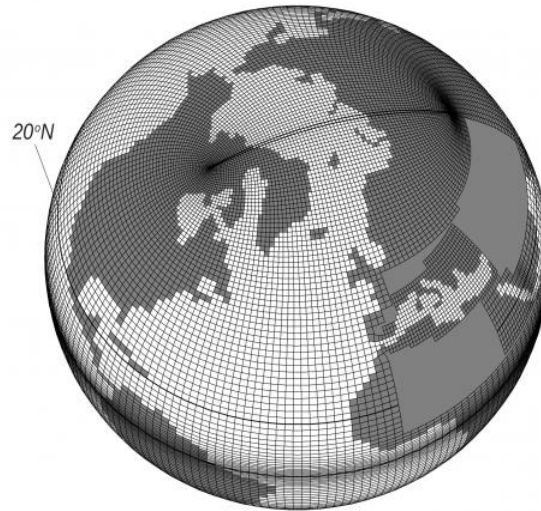
Figure I.8 Tripolar grid of DRAKKAR ORCA025 configuration (Barnier et al. 2011)

Partial steps represent the bottom topography, and a Laplacian operator on neutral surfaces enables isopycnal diffusion with a coefficient of 300 m$^2$ s$^{-1}$ for tracers. The vertical turbulent scheme is the TKE (Blanke and Delecluse, 1993) and vertical background diffusivity was set to 10$^{-5}$ m$^2$ s$^{-1}$. Additional details about the model configuration can be found in Barnier *et al*. (2006) and Penduff *et al*. (2010).

The atmospheric forcing of the model was derived from a 3 hourly ERA-interim reanalysis for the 1990-2009 period, with corrected radiative fluxes towards Gewex satellite data as in the GLORYS2V2 reanalysis (Ferry *et al*., 2011). Surface fluxes are computed based on global aerodynamical formulae proposed by Large and Yeager (2004).

The key MRD911 peculiarity that sets this simulation apart from others is the correction applied to the E-P budget, which prevents from using a direct SSS relaxation. Everywhere but in the presence of sea-ice a climatological monthly corrective term for E-P is computed and averaged on the 1990-2009 period, based on the surface salinity restoring term of a parent simulation ORCA025.L75-MJM95 (Barnier *et al*., 2011). The only difference between the two simulations is the SSS restoring which is rather strong (60 days for 10m), limited to the open ocean (at least 150 km away from the coast) and caped at 4 mm/day. This corrective term is quite small compared to the other terms in the E-P balance but reduces greatly model surface and subsurface salinity biases, which are 3 times larger when no restoring or correction on E-P are applied.

The simulation was originally run from 1990 to 2009 with a 960 seconds time step and was later extended to 2011. The output is averaged and archived every 5 days on the original global Mercator 1/4° grid mesh.

The DRAKKAR team routinely evaluates their simulations outputs. A thorough assessment of the model via comparison with observed datasets (not only SSS) are presented in dedicated sections of the three following chapters.

## I.5. Additional datasets

### *I.5.1. Near-surface currents*

Ocean Surface Current Analyses – Real time (OSCAR) provides zonal and meridional near-surface currents (Bonjean and Lagerloef, 2002). OSCAR is based on satellite scatterometer vector winds and altimeter sea level, which enables the computation of the Ekman and geostrophic current components, respectively. The OSCAR currents are available on a monthly filtered 1° longitude by 1° latitude grid, from October 1992 till present. The NOAA Satellite and Information System (NESDIS) make data available at http://www.oscar.noaa.gov.

### *I.5.2. Precipitations*

The Global Precipitations Climatology Project (GPCP; Adler *et al.*, 2003) provides monthly estimates of mean precipitations (P) on a 2.5° spatial grid from 1979 to present. The GPCP merges together infrared, passive microwave data from geostationary and low-orbit satellites. The global analysis calibrates and validates the merged product with over 6,000 rain gauge stations as well as sounding observations. Data can be downloaded freely on the NOAA National Climatic Data Centre website (http://www.ncdc.noaa.gov/oa/wmo/wdcamet-ncdc.html).

### *I.5.3. Evaporation*

The evaporation (E) data is obtained from the OAFlux project dataset (Objectively Analysed air-sea Fluxes; Yu *et al.*, 2008), and is available monthly on a 1° spatial grid from 1958 to 2012. The OAFlux project gives optimal estimates of flux-related surface meteorology through an objective analysis and computes the global fluxes by using state-of-the-art bulk flux parameterizations. Data is developed and made available by the Woods Hole Oceanographic Institution (http://oaflux.whoi.edu/data.html).

### *I.5.4. Mixed Layer Depth*

The 2° latitude by 2° longitude seasonal climatology of mixed layer depth (H) is derived from approximately 780,000 CTD and Argo profiles taken from 1961 to 2008 (de

Boyer Montégut *et al.*, 2004). The mixed layer depth is first estimated from the independent vertical profiles with a $0.03 \text{kg.m}^3$ difference to the surface criterion. After basic quality controls, this preliminary dataset is delivered under the "L2 Point wise data" label. Data is then binned in the final grid and the median is computed. Statistical interpolation is used wherever data is lacking. The final "L3 Gridded data" can be downloaded from: http://www.ifremer.fr/cerweb/deboyer/mld/Data.php.

## II. Methodology

### II.1. Mixed Layer Salinity (MLS) budget

The tropical ocean surface layer is usually turbulent and well mixed within a seasonally varying depth of 50 to 100 metres. This surface layer, called "the mixed layer", is under the direct effect of the horizontal ocean circulation, surface wind, surface waves breaking, evaporation and precipitations (i.e., fresh water exchanges), and heat exchanges with the atmosphere. Subsurface processes such as vertical advection and mixing, diffusion and entrainment also affect the mixed layer through its base. These subsurface processes cannot be discarded when looking at variations of surface salinity.

The time evolution of salinity in the mixed layer may be written as:

$$\underbrace{\partial_t \langle S \rangle}_{I} = \underbrace{\frac{(E-P)}{H} \cdot \langle S \rangle}_{II} - \underbrace{\langle \vec{u}_h \cdot \vec{\nabla}_h S \rangle}_{III} + \underbrace{\frac{(w_e + d_t H) \cdot \delta S}{H}}_{IV} + \underbrace{\langle \vec{\nabla}_h (K_h \cdot \vec{\nabla}_h S) \rangle}_{V} + \underbrace{\frac{\partial_z (K_z \cdot \delta S)}{H}}_{VI} \quad (1)$$

where $\langle X \rangle = \frac{1}{H} \int_{-H}^{0} X(z) dz$, S denotes salinity within the mixed layer of depth H, (E-P) the Evaporation and Precipitations difference (defined as positive out of the ocean), $u_h$ the horizontal velocity vector averaged within the mixed layer (having (u) and (v) components defined as positive eastward (x) and northward (y), respectively), $w_e$ the entrainment velocity at the base of the mixed layer, δS the salinity jump at the base of the mixed layer, and K the diffusion coefficient. (Note that river runoffs were considered negligible for our studied region). In the following study, term (I) in Equation II.1 is referred to as the salinity tendency, term (II) as the surface forcing, terms (III) and (V) as the horizontal advection, and terms (IV) and (VI) together as the subsurface forcing.

All terms presented above but the entrainment are computed at each model time-step and then averaged and archived online every 5 days.

## II.2. Signal Processing

In all following studies, mean seasonal and interannual signals are systematically extracted from the original signal to be studied apart. We present here in more details the data treatment we apply for this purpose.

The Figure below shows a theoretical time series constructed by adding variability at 25-day (intraseasonal), 1-year (seasonal), 1.5-year (interannual, CP- El Niño), 6-year (interannual, EP- El Niño), and 20 years (decadal) time-scales. A linear trend was also simulated (Figure 9a, solid black line). As seasonal and higher time scales are investigated in the following studies, the first step was to create monthly means of the time series (Figure 9a, solid grey line). In the first two chapters, the trend was removed from all variables as illustrated by Figure 9a (dashed grey line).
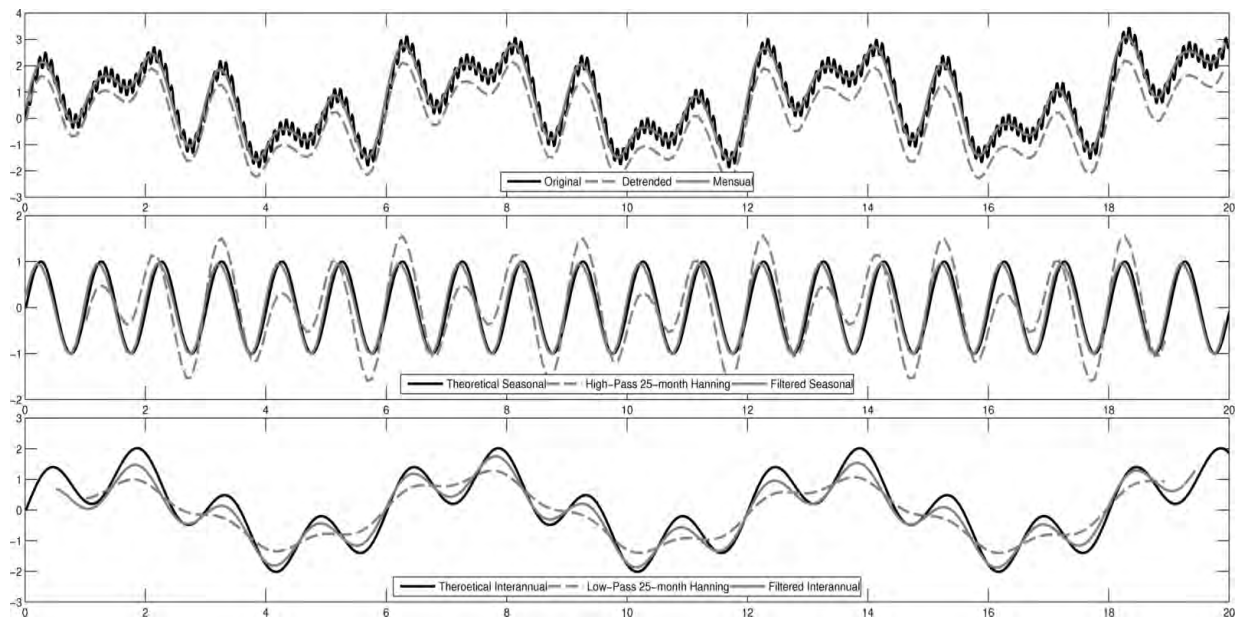


Figure I.9 Theoretical Filter Assessment of a simulated timeseries whose equation is

$$f(x) = \sin(x) + 1.2 \cdot \sin(x/6) + 0.9 \cdot \sin(x/1.5) + 0.3 \cdot \sin(x/0.1) + 0.3 \cdot \sin(x/20) + 0.01 \cdot x$$

### II.2.1. Mean seasonal signal

In order to obtain the mean seasonal signal, a three-step methodology was applied.

As stated above, the linear trend is removed from the time series to filter out very long-term variations.

A high-pass 25-month Hanning filter is applied to filter out any variability above a year, hence including the ENSO signal (Figure 9b, dashed grey line).

The data is then averaged month-by-month to create the monthly climatology. Figure 9b shows the theoretical seasonal signal in black and the obtained filtered signal in solid grey.

The theoretical and filtered seasonal signals are very much alike and show the ability of our methodology to filter out signal below a year, specifically the 1.5-year interannual signal.

## *II.2.2. Interannual signal*

Filtering the interannual signal is tricky, as the signal from both the Central and Eastern Pacific El Niño must be kept. They do not have the same periodicity and duration. It is particularly challenging to isolate the CP El Niño signal as its periodicity is close to a year. In our theoretical test, we assumed its periodicity to be 1.5 year.

A two-step methodology is used:

The mean seasonal climatology is removed from the original signal

A low-pass 13-month Hanning filter is applied to further smooth the residual interannual variability.

The simple low-pass 25-month Hanning filter (Figure 9c, dashed grey line) is not as efficient when separating the interannual signal (solid black line) compared to the approach described above (solid grey line).

## **II.3. Computing procedures**

All of the data cited above and used in the present PhD were usually available in the Network Common Data Format (netCDF). The largest files such as the model ones were handled with the netCDF Operator (NCO) programs. The model simulation represents over 1.5 To of data in the tropical Pacific Ocean alone. NCO was therefore needed to manipulate such large dataset and produce files that would be more adequate for further calculations.

Data was then treated with the Matrix Laboratory (MatLab) high-level technical computing language (version 2009b) for numerical calculations and plotting. MatLab was chosen because of the many existing toolboxes already available in the software and from the dedicated file exchange forum. Moreover, MatLab was able to read all the needed data and store values in standard matrices. This was particularly useful when filtering data as described above corresponding to many variables from many datasets. While the present PhD will focus on and mostly present scientific results, one must bear in mind that data treatment represented at least 50% of the devoted time.

# Chapter 3. The Mixed Layer Salinity Budget in the Tropical Pacific Ocean

## Foreword

This chapter focuses on quantifying the mechanisms behind the salinity patterns in the tropical Pacific Ocean looking at a 2-decade long mean as well as the seasonal and interannual time-scales. As presented in the introduction, salinity plays a central role in the ocean dynamics at these time-scales and better understanding its variability is essential. SMOS salinity datasets were not yet available at the time of writing this paper, so we decided to take advantage of all possible datasets to first evaluate why salinity changes with time. Most previous studies documenting SSS changes in the tropics have focused on the responsible mechanisms in a qualitative way only. This puts to light either the lack of observations to properly evaluate all forcing terms and/or the moderate performance of past model outputs in reproducing salinity variability.

## Article

This paper has been published in the Ocean Dynamics magazine in January 2013.

Hasson, A. E. A., T. Delcroix, and R. Dussin (2013), An assessment of the mixed layer salinity budget in the tropical Pacific Ocean. Observations and modelling (1990-2009), *Ocean Dynamics*, *63*(2-3), 179-194, doi:10.1007/s10236-013-0596-2.

# An assessment of the mixed layer salinity budget in the tropical Pacific Ocean. Observations and modelling (1990–2009)

Audrey E. A. Hasson · Thierry Delcroix · Raphaël Dussin

**Abstract** This paper investigates mechanisms controlling the mixed-layer salinity (MLS) in the tropical Pacific during 1990–2009. We use monthly $1° \times 1°$ gridded observations of salinity, horizontal current and fresh water flux, and a validated ocean general circulation model with no direct MLS relaxation in both its full resolution (0.25° and 5 days) and re-sampled as the observation time/space grid resolution. The present study shows that the mean spatial distribution of MLS results from a subtle balance between surface forcing ($E-P$, evaporation minus precipitation), horizontal advection (at low and high frequencies) and subsurface forcing (entrainment and mixing), all terms being of analogous importance. Large-scale seasonal MLS variability is found mainly in the Intertropical and South Pacific Convergence Zones due to changes in their meridional location (and related heavy P), in the North Equatorial Counter Currents, and partly in the subsurface forcing. Maximum interannual variability is found in the western Pacific warm pool and in both convergence zones, in relation to El Niño Southern Oscillation (ENSO) events. In the equatorial band, this later variability is due chiefly to the horizontal advection of low salinity waters from the western to the central-eastern basin during El Niño (and vice versa during La Niña), with contrasted evolution for the Eastern and Central Pacific ENSO types. Our findings reveal that all terms of the MLS equation, including high-frequency (<1 month) salinity advection, have to be considered to close the salinity budget, ruling out the use of MLS (or sea surface salinity) only to directly infer the mean, seasonal and/or interannual fresh water fluxes.

## 1 Introduction

Several studies have shown the importance of analysing salinity changes for monitoring, understanding, and/or improving prediction of the ocean and climate variability at different time scales. Salinity (together with temperature and pressure) is required to compute the ocean density and provides key information about water mass formation, mixed layer depth, barrier layer depth and geostrophic circulation. It is also used to trace the circulation of ocean water masses, to estimate fresh water exchanges between the ocean and the atmosphere and to improve the El Niño Southern Oscillation (ENSO) prediction lead time (e.g. Sverdrup 1943; Donguy and Henin 1980; Gill 1982; Lukas and Lindstrom 1991; Ballabrera-Poy et al. 2002). The scientific relevance to measuring and analysing salinity changes is increasingly recognized (see Lagerloef et al. 1999, 2010). It has for a large part motivated the development of the Argo program (Roemmich et al. 1999) and of the dedicated SMOS and Aquarius satellite missions (Kerr et al. 2001; Lagerloef et al. 2008) to enhance global salinity observations.

Due to the weak number of in situ salinity data (as compared to temperature for instance), documentation and analyses of 3D salinity changes are rather limited, especially before the Argo era. In the tropical oceans, most published results make use of sea surface salinity (SSS), focusing on changes at seasonal, interannual and decadal time scales, as

⌗ Springer

well as on long-term trend (e.g. Delcroix and Henin 1991; Dessier and Donguy 1994; Donguy and Meyers 1996; Gouriou and Delcroix 2002; Grodsky et al. 2006; Delcroix et al. 2007; Cravatte et al. 2009; Durack and Wijffels 2010). Moreover, most studies documenting SSS changes in the tropics have focused on the responsible mechanisms in a qualitative way only. This puts to light either the lack of observations to properly evaluate all forcing terms and/or the moderate performance of past model outputs in reproducing salinity variability. The goal of this paper is to assess in a quantitative manner all mechanisms affecting the mixed-layer salinity (MLS). The emphasis will be put on the mean MLS budget as well as on changes occurring at the seasonal to interannual time scales in the tropical Pacific Ocean. This will be conducted using in situ and remotely sensed observations as well as a state-of-the-art ocean model forced over the 1990–2009 time period. A brief overview of past observational and model studies is first presented in the following paragraphs.

The mean distribution of observed SSS in the tropical Pacific Ocean is reminded in Fig. 1a (see Section 2 for the data origin). It is characterised by two relative maxima centred on the subtropical gyre centres: one northwest of the Hawaii archipelago and the other southeast of the Polynesian Islands. The lowest SSS values are found in three regions: along the basin wide Intertropical Convergence Zone (ITCZ) between 5 and 10°N; in the South Pacific Convergence Zone (SPCZ), roughly between Papua New Guinea and Fiji/Samoa; and in the western equatorial Pacific. This last region, with sea surface temperature (SST) warmer than 28–29 °C and SSS below 34.5 pss, has been called the western Pacific Fresh Pool (FP; Delcroix and Picaut 1998) and/or Warm Pool (WP).

The distribution of the standard deviation of observed SSS is shown in Fig. 1c. It reveals high SSS variability over the three minimum salinity sectors described above, and mainly reflects the combined effects of the seasonal and interannual variability. Changes at the seasonal time scale have been shown to be the highest in the ITCZ and SPCZ regions, with SSS maxima in May–June and August–September, respectively. This seasonal variability results mostly from the seasonal precipitation regime (the SSS maxima lagging the P minima by 2–3 months) together with the seasonal salinity advection by the North and South Counter Currents (NECC, SECC) (Delcroix and Henin 1991; Bingham et al. 2010; Yu 2011). Changes at the interannual time scale have been shown to be chiefly due to ENSO and located in the warm pool and SPCZ regions as well as near the equatorial American coast (Delcroix 1998).

Mechanisms responsible for the ENSO-related interannual variability of SSS in the WP have been particularly well discussed. The El Niño signal is predominantly characterised by a SSS freshening in the western-central equatorial Pacific due to an eastward migration of the eastern edge of the WP and of the associated thick barrier layer (Picaut et al. 1996, 2001; Vialard and Delecluse 1998a, b; Maes et al. 2006; Bosc and Delcroix 2008). El Niño is also characterised by increased SSS along the mean position of the SPCZ due to its equatorward migration and the related heavy rainfall (Delcroix and Henin 1991; Gouriou and Delcroix 2002). Changes at the decadal time scale in relation to the Pacific Decadal Oscillation, as well as long-term changes in relation to climate changes, were documented from in situ
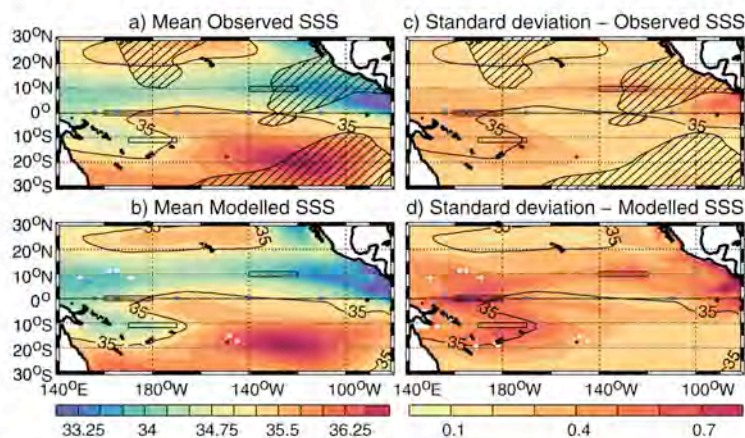


**Fig. 1** (*Left panels*) means and (*right panels*) standard deviations of the (*upper panels*) observed and (*lower panels*) modelled sea surface salinity (practical salinity scale) in the tropical Pacific, calculated from monthly averaged values covering the 1992–2008 period. The *hatched zones* in the *upper panels* denote regions where the mean normalized errors are greater than 0.7. *Blue stars* correspond to the equatorial TAO moorings location discussed in Section 2 and Table 1. The three 20° longitude by 2° latitude *rectangles* highlight the so-called ITCZ (9–11° N, 140–160°W), SPCZ (10–12°S, 170°E–170°W) and warm pool (1° N–1°S, 160°E–180°) regions discussed in Figs. 2, 5 and 7

observations in recent years (Delcroix et al. 2007; Cravatte et al. 2009; Durack and Wijffels 2010; Terray et al. 2012), but is beyond the scope of this study.

Furthermore, model results provide relevant information regarding the mechanisms responsible for the MLS balance in the tropical Pacific Ocean, and on the role of salinity in ENSO events. Following a few pioneer studies (e.g. Miller 1976; Cooper 1988) highlighting the importance of an accurate representation of vertical salinity gradients in modelling, Vialard and Delecluse (1998a) conducted a set of numerical simulations to test the sensitivity of their mean modelled MLS to different atmospheric forcing. Their simulated SSS is found to be very sensitive to freshwater flux ($E-P$), especially in the Costa Rica minimum and subtropical gyres maximum SSS regions. In the heavy P regions (ITCZ and SPCZ), improvement in the $E-P$ forcing does not however lead to improvement in their modelled SSS indicating the potential importance of balancing mechanisms. Furthermore, Vialard and Delecluse (1998a) modelled SSS is very sensitive to the horizontal advection of salinity gradients by the mean oceanic circulation, especially the variable zonal extensions of the SEC to the WP. Strong entrainment of saltier subsurface waters was thought to be a cause of unrealistic SSS as well as resolution and parameterisation of the ocean model itself. In a more recent study, Vialard et al. (2002) discussed the respective influence of surface forcing, horizontal advection (high and low frequencies), entrainment and vertical mixing in shaping the mean and variability of their modelled MLS. They emphasised the important role of strong precipitations in the ITCZ, fresh water advection by the SEC and high frequency currents near the equator. At the interannual time scale, and in agreement with observation-based studies, changes in modelled SSS are found to be maximum in the western tropical Pacific and in the equatorial band (Vialard and Delecluse 1998b; Yim et al. 2008). Mechanisms associated with these changes differ from one region to another. Vialard and Delecluse (1998b) concluded that SSS changes mostly stem from horizontal advection in the FP frontal region whereas they mainly result from subsurface waters entrainment and freshwater fluxes to the west.

Model studies of mechanisms affecting MLS were also conducted in the other tropical oceans. For example, in the Atlantic Ocean, the freshwater fluxes only explain half of the SSS variability, being of equal importance with advection, vertical entrainment, eddies and small-scale processes (Qu et al. 2011). In the Indian Ocean, SSS is shown to be strongly affected through precipitations and river runoffs modulated by the monsoon on the seasonal time scale and by the

Indian Ocean Dipole and ENSO on the interannual time scale (Vinayachandran and Nanjundiah 2009).

Aside from quantifying the main factors responsible for MLS changes, sensitivity experiments were also conducted to assess the possible impact of salinity on the tropical Pacific climate variability, especially on ENSO dynamics and thermodynamics. Results from Vialard and Delecluse (1998a) indicated that salinity weakly modifies the 1993–1996 Pacific circulation (period thought to be representative of the mean state). Contrastingly, they showed the strong effect of salinity during the 1997–1998 El Niño through its impact on vertical mixing and horizontal pressure gradient (Vialard et al. 2002). Numerous modelling studies were also conducted on the zonal displacement of the eastern edge of the WP/FP, the related barrier layer formation and their relation to ENSO (see Picaut et al. 2001, and references therein). Of note, the importance of the salinity barrier layer (BL) as a key parameter to set up the ocean state prior to ENSO was clearly identified in a coupled model (Maes et al. 2006). The BL forces the density mixed layer to shoal increasing the warm pool temperature by limiting both the entrainment and the volume into which the solar heat is distributed. The BL also strengthens surface currents through the enhanced response to wind forcing due to the shallow density mixed layer (e.g. Vialard and Delecluse 1998a, b; Vialard et al. 2002).

Given the large body of literature stemming from different time periods, observational data sources and model simulations, as partly reminded above, we now believe appropriate to present a concise investigation of the MLS budget using a newly derived observed gridded SSS field and a validated state-of-the-art model output. In this goal, the remaining part of this paper is organized as follows. Section 2 presents the methodology to study the MLS budget, the used observations, the Ocean General Circulation Model (OGCM) and the OGCM ability to reproduce the MLS mean and variability. The mean MLS budget is analysed in Section 3.1 from observations and OGCM output, the latter being considered both in its full resolution and resampled as the observation time/space grid resolution in order to assess the approximation done by analysing MLS budget with observations only. The modelled MLS budget is then examined in Sections 3.2 and 3.3 at the seasonal and ENSO time scales, respectively. The ENSO signal is further detailed in Section 4, contrasting the mechanisms responsible for the MLS changes during the 1997–1998 Eastern Pacific and 2002–2003 Central Pacific (hereafter EP and CP) El Niño events. Discussion and conclusion are presented in the last section.

## 2 Methodology, data and model description

### 2.1 Methodology

The time evolution of salinity in the mixed layer may be written as:

$$\underbrace{\partial_t \langle S \rangle}_{I} = \underbrace{\frac{(E-P)}{H} \cdot \langle S \rangle}_{II} - \underbrace{\langle \vec{u}_h \cdot \vec{\nabla}_h S \rangle}_{III} + \underbrace{\frac{(w_e + d_t H) \cdot \delta S}{H}}_{IV}$$

$$+ \underbrace{\langle \vec{\nabla}_h (K_h \cdot \vec{\nabla}_h S) \rangle}_{V} + \underbrace{\frac{\partial_z (K_z \cdot \delta S)}{H}}_{VI} \qquad (1)$$

where $\langle X \rangle = \frac{1}{H} \int_{-H}^{0} X(z)dz$, $S$ denotes salinity within the mixed layer of depth $H$, $(E-P)$ the evaporation and precipitation difference (defined positive out of the ocean), $u_h$ the horizontal velocity vector averaged within the mixed layer [having $(u)$ and $(v)$ components defined positive eastward $(x)$ and northward $(y)$, respectively], $w_e$ the entrainment velocity at the base of the mixed layer, $\delta S$ the salinity jump at the base of the mixed layer and $K$ the diffusion coefficient. (Note that river runoffs were considered negligible for our studied region). In the following study, the term $(I)$ in Eq. (1) is referred to as the salinity tendency (or MLS trend), term $(II)$ as the surface forcing, terms $(III)$ as the horizontal advection, and terms $(IV)$ and $(VI)$ together as the subsurface forcing. Note that horizontal mixing (term $V$) is added to the horizontal advection in the study based on the model output (see Sections 3 and 4) in order to group all horizontal processes.

### 2.2 Observational data

The 1950–2008 SSS gridded product described in Delcroix et al. (2011) is used both to evaluate the modelled salinity and to analyse the MLS mean balance from observations. The SSS data were obtained from near surface (0–10 m) in situ observations collected mainly from Voluntary Observing Ships, TAO/TRITON moorings, Argo buoys and CTD casts. Values of SSS and their errors are available monthly on a 1° longitude by 1° latitude spatial grid, within the 30°S–30°S, 120°E–70°W domain. Following Singh et al. (2011), only values with normalized errors less than 0.7 will be hereafter considered. Values with errors above this threshold are hatched on Figures.

The zonal $(u)$ and meridional $(v)$ near-surface currents were obtained from the OSCAR (Ocean Surface Current Analyses—Real time; Bonjean and Lagerloef 2002) product. These products are based on satellite vector winds and altimeter sea level to compute the Ekman and geostrophic current components, respectively. The OSCAR currents are available on a monthly 1° longitude by 1° latitude grid, from

1992 to 2010. Note that, strictly speaking, both observed SSS and current data represent values in the upper 0–10 m and not averages of the mixed layer as in Eq. (1).

The Global Precipitation Climatology Project (Adler et al. 2003) provides monthly mean precipitation $(P)$ fields on a 2.5° spatial grid from 1979 to 2010. The evaporation $(E)$ data are obtained from the OAFlux dataset (Yu et al. 2008), and are available monthly on a 1° spatial grid from 1958 to 2010. Finally, the 2° latitude by 2° longitude seasonal climatology of mixed layer depth $(H)$ is derived from around 780,000 CTD and Argo profiles taken from 1961 to 2008 (de Boyer Montégut et al. 2004). The above data set was regridded onto a common 1° longitude by 1° latitude by 1 month grid using bilinear interpolation, whenever needed. The 1992–2008 period, common to all observational data sets, is considered when they are combined such as for the computation of any term of Eq. (1).

### 2.3 Model data

The OGCM has been run by the DRAKKAR group using the NEMO $z$-coordinate model (Madec 2008) in version 3.2.1. The simulation configuration used in the present study (so-called ORCA025.L75-MRD911, hereafter MRD911) has 75 vertical levels, with as much as 21 levels in the upper 70 m to resolve well the mixed layer. Partial steps represent the bottom topography, and a Laplacian operator on neutral surfaces enables isopycnal diffusion with a coefficient of 300 $m^2 s^{-1}$ for tracers. The vertical turbulent scheme is the TKE (Blanke and Delecluse 1993), and vertical background diffusivity was set to $10^{-5} m^2 s^{-1}$. More details about the model configuration can be found in Barnier et al. (2006) and Penduff et al. (2010).

The atmospheric forcing of the model was derived from three hourly ERA-interim reanalysis for the 1990–2009 period, with corrected radiative fluxes towards Gewex satellite data as in the GLORYS2V2 reanalysis (Ferry et al. 2011). The MRD911 simulation peculiarity is the correction directly applied to the $E-P$ budget, preventing from using a direct SSS relaxation. A climatological monthly corrective term is computed in terms of equivalent $E-P$ from the restoring term of a parent simulation (so-called ORCA025.L75-MJM95), averaged on the 1990–2009 period (Barnier et al. 2011). The only difference between the two simulations being the SSS restoring, which is rather strong (60 days for 10 m), limited to the open ocean (at least 150 km away from the coast) and capped at 4 mm/day. This corrective term is quite small compared to the other terms in the $E-P$ balance but reduces greatly model surface and subsurface salinity biases, which are three times larger when no restoring or correction on $E-P$ is applied. The simulation is run from 1990 to 2009 with a 960 s time step. All terms of Eq. (1) but entrainment, which is a residual, are computed at each time step, averaged

and archived every 5 days on 0.25° latitude by 0.25° longitude grid mesh.

### 2.4 Model assessment

The ability of the model to reproduce observed features is now considered. Values within the eight first model layers (from the surface down to 9.82-m depth, hereafter called modelled SSS) were averaged to enable better comparison with surface observations. The spatial distribution of the observed and modelled SSS, averaged over 1990–2009 (and over 1° by 1° spatial grid for the model) compares quite well with a correlation coefficient of $R=0.93$ (Fig. 1a, b). When comparing Fig. 1a and b, the model however appears to produce too fresh waters in the ITCZ, SPCZ and in the western equatorial Pacific.

The standard deviations of the observed and modelled monthly SSS are shown in Fig. 1c, d. The model properly replicates the main observed patterns of maximum variability (of the order of 0.2–0.4) in the western equatorial Pacific, in the ITCZ, SPCZ and off Panama, though with a tendency to be more energetic. The SSS seasonal and interannual changes were computed for observations and model output as described below in Section 3. In both datasets, maximum seasonal variability is found in the convergence zones and off Panama, and maximum interannual variability is found in the western Pacific WP and in the SPCZ, as expected from previous observational studies (e.g. Delcroix et al. 2011; their Fig. 4b, c).

To further assess the model performance in reproducing SSS variability, Fig. 2 compares the longitude-time plots of the 2°N–2°S averaged observed and modelled SSS time series. It confirms the overall good performance of the model, which shows correct variability at both the seasonal and interannual time scales in the eastern and western-central Pacific regions, respectively. This later variability is highlighted by the ENSO-related zonal displacements of 35 isohaline in the western-central equatorial Pacific, used here as a proxy of the FP eastern edge. As discussed in Bosc et al. (2009; their Fig. 6), the location of this FP eastern edge coincides with the location of the SSS zonal gradient maximum (not shown in Fig. 2). Note that this gradient (or front) is slightly more pronounced in the model than in observations, with fresher (saltier) SSS west (east) of the 35 isohaline. An extreme freshening across the basin occurs around 1997–1998. It corresponds to the well-studied EP El Niño, which will be discussed later (Section 4). A few CP El Niños also stand out roughly around 1992, 1995, 2003 and 2007. The 2002–2003 CP El Niño will be considered as representative and detailed in Section 4.

Figure 3 further compares the observed and modelled SSS time series averaged in two 2° latitude by 20° longitude boxes of maximum SSS variability: one box located in the western Pacific warm pool (1°N–1°S, 160°E–180°) and the other in the SPCZ (12°S–10°S, 170°E–170°W). Figure 3 verifies: (a) the overall agreement between the observed and modelled SSS, the coefficient of correlation $(R)$ is greater than 0.74 for both regions, (b) the model general tendency to produce too fresh waters when salinity is roughly below 34.5 pss and too salty when above 34.5 pss, (c) the strong interannual (ENSO) variability appearing in the equatorial box, with well-marked freshening during the El Niño events and (d) the combined effects of the seasonal and ENSO variability in the SPCZ region.

Finally, the model was tested against time series of 5 days averaged observed surface (10 m) currents obtained from the equatorial TAO moorings situated at 110°W, 140°W, 170°W, 165°E and 156°E. The comparison statistics between the 5-day averages of observed and modelled zonal currents are given in Table 1. The statistics indicates that the model output is highly correlated with the data measured at the moorings, with a mean correlation coefficient of $R=0.8$. The model also has a slight tendency to underestimate the zonal current variability at all locations as the mean ratio of modelled versus observed standard deviation is about 75 %. Finally, the model assessment gives us confidence regarding the model ability to reproduce the near-surface salinity variability for the good reasons.

### 3 Mixed layer salinity budget

The following three sub-sections focus on the mean, seasonal and interannual salinity balances in the mixed layer. The mean balance is analysed from both observations and model data, which are described above, whereas the seasonal and interannual balances are derived from the model output only. We consider the longest available time period common to all the observed and model data (i.e. 1992–2008) in order to estimate the mean of each term in Eq. (1). To study the seasonal and interannual variability, the full-length original model data were looked at (i.e. 1990–2009). The modelled seasonal variability was computed by creating a 12-month average year, from the differences between the original 5-day resolution and the 25-month Hanning filtered (Hf) time series so as to filter out the ENSO influence. The interannual variability was computed by filtering the original data with a 13-month Hf, from which the seasonal signal has been substracted. Several studies have shown that filtering with a 25-month Hf is an adequate methodology to extract the interannual variability, as it passes almost no signal at periods shorter or equal to 1 year (e.g. Emery and Thomson 1998; Delcroix 1998). However, for our study a 13-month Hf is considered as more appropriate to analyse ENSO whose CP flavour duration is less than 1 year (see Ashok et al. 2007). Note that
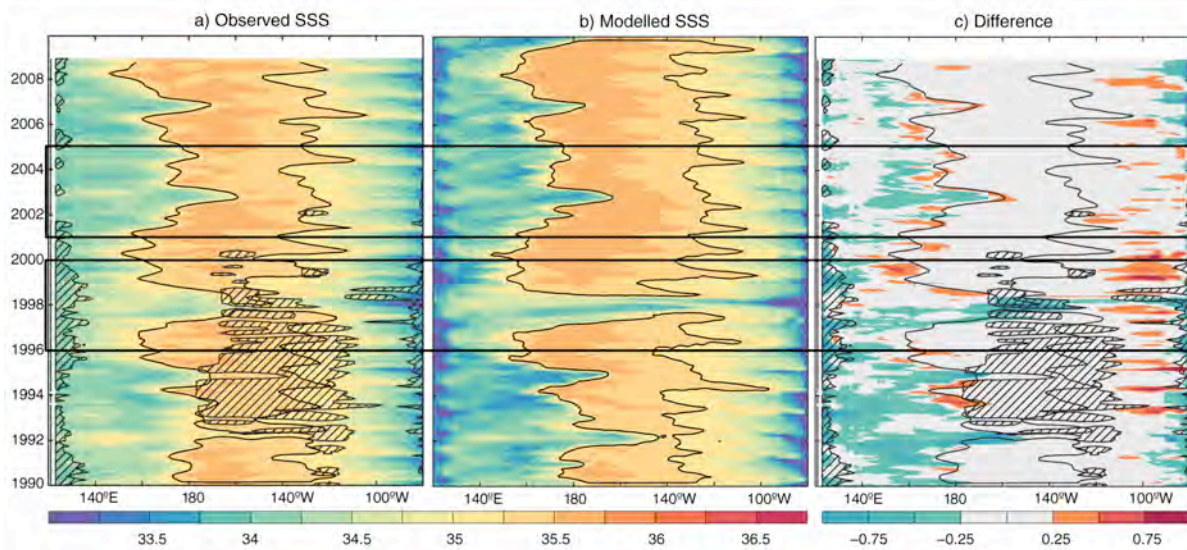
**Fig. 2** Longitude-time distribution of the 2°N–2°S averaged **a** observed and **b** modelled monthly averaged sea surface salinity (practical salinity scale), together with **c** their differences (observed minus modelled). The two *boxes* denote the 1996–1999 and 2001–2004 ENSO periods detailed in Section 4, and the *heavy lines* in (**a**) and (**b**) denote the 35 isohaline. The *hatched zones* denote regions where the mean normalized errors are greater than 0.7. The y-axis ticks denote the beginning of each year

using an $N$-month Hf, the first and last $N/2$ months of each time series cannot be filtered reducing the analysed period by $N$ months.



**Fig. 3** Observed (*red*) and modelled (*blue*) monthly averaged SSS time series (practical salinity scale) averaged in the so-called (*top panel*) warm pool and (*bottom panel*) SPCZ regions shown in Fig. 1

### 3.1 Mean state

Based on the observations averaged monthly on a 1° longitude–latitude grid of $E-P$, $H$, $u$, $v$ and SSS described in Section 2.2, the surface forcing and the horizontal advection processes (terms *II* and *III* in Eq. (1)) are shown in Fig. 4a, b for the mean state. (Note that term *I* in Eq. (1) is zero for the mean state).

The mean surface forcing (Fig. 4a) shows negative values in three regions: the western equatorial Pacific, along the ITCZ extending roughly between 5°N and 10°N from the American coast to the western boundary, and along the SPCZ between Papua New Guinea (PNG) and 15°S–160° W, underlining regions of strong precipitations. It also shows regions of high positive values in both subtropical gyres where evaporation is dominant. Interestingly, the spatial patterns of the horizontal advection (Fig. 4b) are similar to the ones of the surface forcing, stressing the important role of the surface circulation to balance $E-P$ in the MLS budget. Horizontal advection depends on both horizontal currents and salinity gradient. Mean meridional current ($v$ component in term *III* of Eq. (1); not shown here) is northward (positive) in the northern hemisphere and southward (negative) in the southern one because of the equatorial divergence. The salinity meridional gradient is strongly negative (stronger than zonal gradient) around the equator especially in the east (see Fig. 1d). It is furthermore positive north of the ITCZ and SPCZ regions and south of the SSS maximum. Consequently, meridional advection is negative from the equator to the ITCZ and SPCZ and positive east of
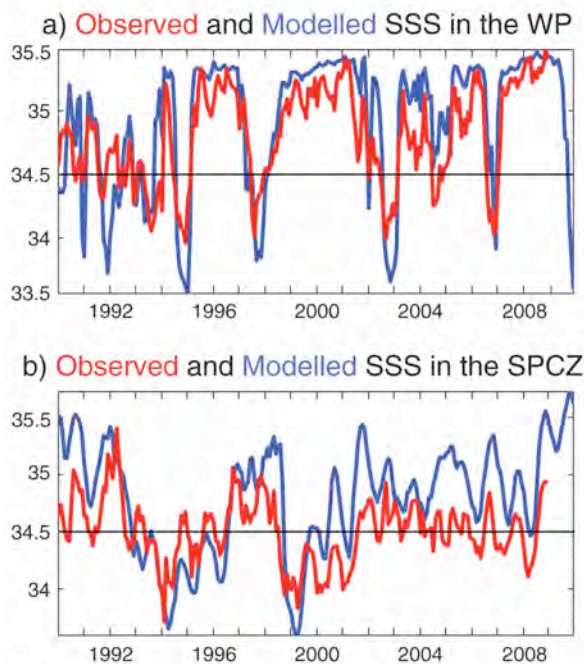
**Table 1** Comparison between the 5-day averaged current meters time series on TAO moorings situated on the equator and the corresponding modelled time series

| Longitude of equatorial mooring | Correlation coefficient | Length of the common time series (5-day periods) | $\sigma_{model}/\sigma_{obs}$ |
|---|---|---|---|
| 156°E | 0.81 | 88 | 0.84 |
| 165°E | 0.87 | 126 | 0.86 |
| 170°W | 0.87 | 67 | 0.76 |
| 140°W | 0.68 | 174 | 0.69 |
| 110°W | 0.77 | 174 | 0.67 |

Blue stars on Fig. 1 represent the mooring locations. Current meters are at 10 m depth and compared to the nearest vertical model level that is at 9.82 m depth

160°W from the equator to the southern SSS maximum latitude. Zonal currents are particularly strong in the central basin within 10° off the equator where are located the westward-flowing South Equatorial Current (SEC) and the eastward-flowing North Equatorial Counter Current (NECC). They are however associated with weak zonal salinity gradient. Zonal advection is therefore significant only where the gradient is non-null, which is west of the dateline between 0 and 10°S, and east of about 140°W under the SEC and NECC latitudes. Note that the SEC results in positive zonal advection, which is counteracted by negative meridional advection from the equatorial divergence. Even though the surface forcing tends to be compensated by the horizontal advection, the difference between these two terms (Fig. 4c) is however not negligible. This difference corresponds to the combined effects of subsurface forcing [terms *IV* and *VI* in Eq. (1)], observational coarse sampling and measurement errors. These effects cannot be discriminated with observational data. However, it is likely (and confirmed below) that the contribution of the subsurface forcing is dominant in Fig. 4c. Similar analyses conducted for different time periods and using different salinity data sets and surface forcing have reached consistent conclusions (Johnson et al. 2002; Lagerloef et al. 2010).

Not only terms *II* and *III* but also *IV*, *V* and *VI* from Eq. (1) were examined from the model output. As an initial step, the model data were processed to somewhat mirror the calculations we performed with observations. In other words, from the native model grid, we first computed on a 1° longitude by 1° latitude grid monthly averages of *u*, *v*, *S* and *E−P*. We used the surface (average 0–10 m) *u*, *v* and *S* to represent values in the mixed layer, and a mean monthly climatology for the MLD (*H*). Note that the modelled horizontal diffusion was left out as there exists no equivalent
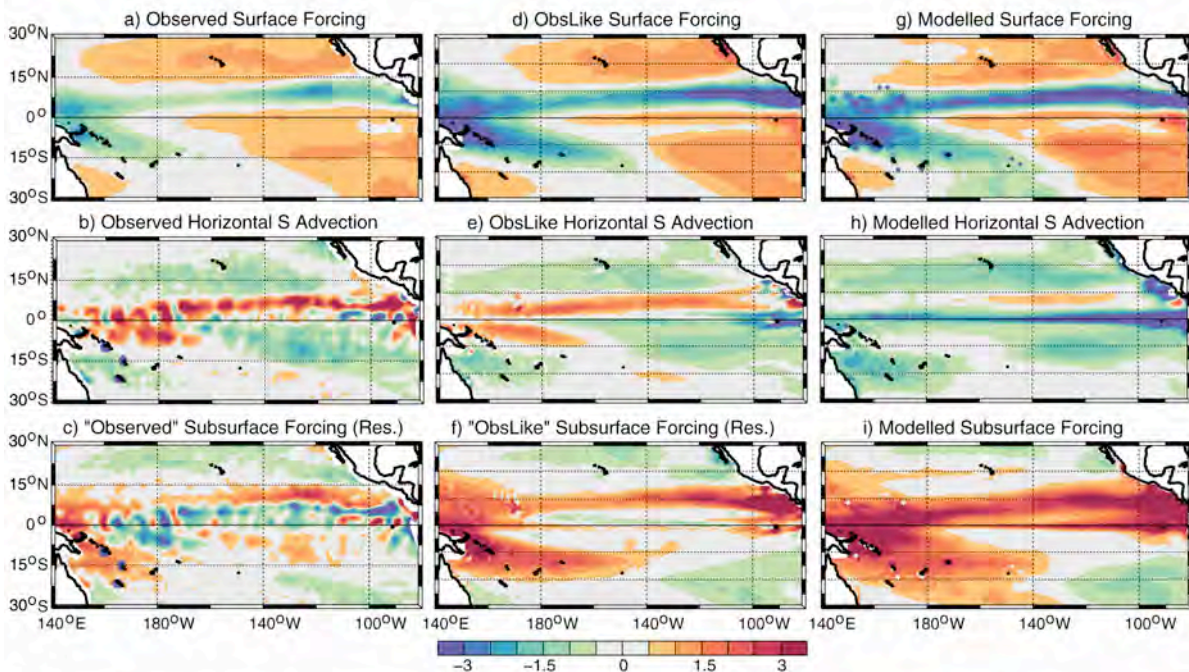


**Fig. 4** Contribution of the (*top panels*) surface forcing terms, (*middle panels*) horizontal advection terms and (*bottom panels*) subsurface forcing terms to the mean mixed-layer salinity budget as described in Eq. (1). The *left columns* are obtained from observed values, the *middle columns* from the so-called ObsLike modeled values, and the *right columns* from the online-computed modelled native-grid values. See Section 2 for details. Units are practical salinity scale per year

🦋 Springer

observational dataset. The "observation-like" (hereafter, ObsLike) modelled surface forcing and horizontal advection are shown in Fig. 4d,e as well as their difference in Fig. 4f. Both forcing terms clearly bear some pattern resemblances with the observed ones (Fig. 4a, b), reinforcing our confidence in the way the main processes are simulated.

The modelled ObsLike surface forcing (Fig. 4d) is slightly too intense, as compared to the observed one (Fig. 4a), with too strong precipitations in the fresh pool, ITCZ and SPCZ areas, and too strong evaporation in the subtropical regions. This is consistent with differences between the mean ObsLike modelled and observed SSS discussed above for Fig. 1. Yet, it must be kept in mind that the mixed layer depth (MLD) definitions for the observed and modelled data sets are slightly different. The density criteria used are respectively 0.003 and 0.001 kgm$^{-3}$. On average within 30°N–30°S, the modelled ObsLike MLD is 21 % (11 m) shallower than the observed MLD. However, patterns of MLD differences are heterogeneous in space, and the MLD difference can reach as much as 60 % (equivalent to 40 m) on the equator. This is partly responsible for the stronger modelled impact of the surface forcing on the MLS. [Recall that the MLD appears in the denominator of the surface forcing term in Eq. (1)].

The modelled ObsLike horizontal advection term (Fig. 4e) tends to balance the modelled surface forcing term, as was obtained above with observations. Note that the related spatial patterns appear less patchy than the observed ones. The simulated ObsLike difference (Fig. 4f) shows (as the observed one) its importance in closing the salinity budget. This difference term does not only encompass the subsurface forcing (terms *IV* and *VI* in Eq. 1) but also the high frequency and/or small-scale signal that is *not* caught by our monthly 1° longitude by 1° latitude gridded dataset, as discussed below.

The mean MLS budget was further examined using the native-grid high-resolution online computed values of the modelled terms *I* to *VI* in Eq. (1). The trend in MLS (term I) is again found negligible. The surface forcing (term *II*), horizontal advection (terms *III* and *V*) and subsurface forcing (terms *IV* and VI) are displayed in Fig. 4g, h, i, respectively. The surface forcing pattern (Fig. 4g) is quasi identical to the observations and ObsLike modelled ones, with a slightly higher amplitude. The horizontal advection pattern (Fig. 4h) displays similarities with the two other ones (Fig. 4b, e), such as the two zonal relative maxima, the subtropical gyres and Coral Sea relative minima. It does present however some striking dissimilarities, such as high values of negative *S* advection trapped near the equator. The subsurface forcing, obtained from the model output values, is not the difference between the surface forcing and horizontal MLS advection, as computed earlier, but is however equal to it since term *I* in Eq. (1) is null. The subsurface

forcing (Fig. 4i) is of equal importance than the two other forcings to close the salinity budget in the mixed layer.

Differences between the online and ObsLike values of terms in Eq. (1) reflect the use of different time (1 month versus 960 s archived online every 5 days) and space (1° versus 0.25°) resolutions, MLD calculation (mean monthly year versus 5 days time series and vertical density gradient thresholds) and definition of ML salinity and horizontal currents (0–10 m averages versus integrated over the varying MLD). These differences are worth detailing as they quantify the reliability of the approximation performed when analysing terms of the MLS balance with monthly averaged low-resolution observations. To illustrate, the difference between the online and ObsLike values are shown in Fig. 5 for horizontal advection. The maximum differences (above 1.5 pss/year) appear mainly from the east to the west within about 5° off the equator, with values in the eastern half of the basin being consistent with the so-called eddies described by Vialard et al. (2002). Using the original resolution archived data, this is the region where we found the strongest variability in the high-frequency (<1 month) variability of horizontal advection, and where a FFT analysis showed a relative maximum just below 20 days period (not shown here). Consequently, this suggests that most differences result from high-frequency variability, which cannot be accounted for with low-resolution observations. Likewise, Qiu et al. (2008) showed that east of 150°W, the high MLS variability could be due to mesoscale eddy advection.

This section proves the model's good skills in reproducing the mean contribution of terms involved in the MLS budget. It has been shown that MLS cannot only be derived from *E*, *P* and horizontal advection but also from subsurface processes happening at the base of the ML. This section also puts to light the difficulty to properly evaluate the respective contribution of all terms involved in the MLS balance with
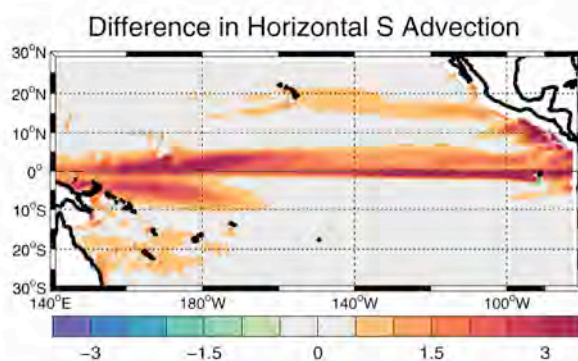


**Fig. 5** Differences between the contributions of the horizontal advection terms to the mixed-layer salinity budget as derived from the so-called ObsLike (see Fig. 4e) and online-computed modelled (see Fig. 4h) values

low-resolution gridded observational data only, as further discussed in the last section.

### 3.2 Seasonal time scale

As described above, a mean year was constructed for each term of Eq. (1) computed from the model native grid. The standard deviation of the 12 mean months ($\sigma_s$) of the MLS trend is used here as a measure of the seasonal variability and is shown in Fig. 6a. The strongest MLS trend seasonal variability is present mostly along mean position of the ITCZ (basin-wide, 5°N to 15°N), and SPCZ (from PNG to Fiji and French Polynesia), in the western equatorial Pacific, in the northern part of the Coral Sea and off Central America. This is consistent with the study of Delcroix (1998) based on observations. The relative contribution of each forcing term to the MLS trend variability is quantified (Fig. 6b–d) following the methodology of Vialard et al. (2011) for the Indian Ocean SST. It is computed as the product of $\sigma_s$ and each forcing term correlation to the MLS trend. With such a normalisation, Fig. 6b–d adds up to Fig. 6a.

In the ITCZ, changes in MLS trend result mostly from a balance of surface and subsurface forcings, with a notable contribution of horizontal advection within 120°W–140°W. The surface forcing seasonal variability is particularly strong due to the seasonal meridional migration of the heavy precipitation band associated with the ITCZ. From observations, precipitations were found to represent about 60 % of the MLS variability in the ITCZ (Yu 2011), and Bingham et al. (2010) described the SSS variability as due to seasonal cycles of currents. A detailed analysis of the contribution and timing of each term of Eq. (1) to the seasonal MLS trend variability is shown in Fig. 7 for the eastern-central part of the ITCZ (Box in Fig. 1). In this region, the MLS decreases (so the trend is negative) from May to September, and increases during the rest of the year. During the first half of the year, the salinity trend follows closely the horizontal advection (timing and amplitude) as the two other terms compensate one another. After July, the trend slightly departs from the horizontal advection curve, as the surface forcing gets more intense in boreal summer. The seasonal changes in MLS trends can therefore not be attributed to horizontal advection only, as they result from a delicate balance between three terms of similar amplitude.

The SPCZ region also holds strong MLS trend seasonal variability (Fig. 6a). The surface forcing drives the seasonal variations of salinity, in relation to the seasonal meridional migration of the SPCZ, whereas the other two terms only modulate it. Subsurface forcing damps the MLS trend variability in the eastern part of the SPCZ, whereas horizontal advection enhances it closer to the equator. This mostly agrees with numerous studies such



**Fig. 6** (From *top to bottom*) Standard deviation of the 12 mean months of modelled seasonal salinity tendency, used as a measure of the seasonal variability, and relative contributions of the surface forcing, horizontal advection and subsurface forcing terms, as described in Section 3.2

as Delcroix (1998), Vialard et al. (2002) and Gouriou and Delcroix (2002).

MLS seasonal variability is also particularly strong east of 110°W to the American coast, north of 10°S. There, all terms are of importance in the MLS balance. Off the American coast, the three forcing terms are alternatively strongly negative and strongly positive. This partly reflects
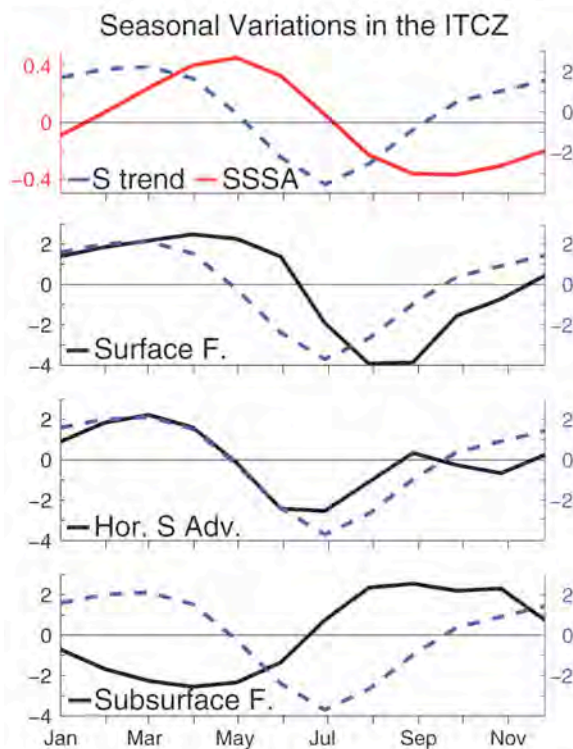
**Fig. 7** Mean seasonal variations of model-derived **a** MLS (*red curve*) and MLS tendency (*dashed blue curve*), and contributions of **b** the surface forcing, **c** horizontal advection and **d** subsurface forcing terms (*black curves*) in the ITCZ region (9–11°N, 140–160°W). The MLS tendency curve is repeated in (**b**–**d**) for clarity. Units are practical salinity scale per year

the effect on ocean dynamics of the annual cycle in the trade winds blowing through gaps in the Central American Cordillera (Kessler 2006). The region where surface forcing restrains MLS variability the most is located in the Costa Rica Dome (CRD). As for the two other forcing contributions, subsurface forcing alternately reinforces and restrains MLS variability on the American coast. Bingham et al. (2010) quantified vertical velocities combining upwelling and vertical motion of the ML base. They only found it to be of any significance around the CRD. Alory et al. (2012), using in situ and SMOS-derived SSS, concluded that both surface forcing, horizontal and vertical advections impact the observed seasonal SSS changes in the Panama bay.

Along the equatorial band, it is worth pointing out that MLS seasonal variability is strong west of the date line where horizontal advection plays a dominant role. In the rest of the equatorial sector, all term contributions counteract one another. Note that the subsurface contribution is very weakly positive which is consistent with Bingham et al. (2010). Yu (2011)) also found that vertical entrainment

was not essential in the tropical Pacific Ocean at the seasonal time scale.

### 3.3 Interannual time scale

Following the methodology described in the first paragraph of Section 3, the modelled interannual signal was extracted for each term of Eq. (1). The MLS trend standard deviation of the interannual time series ($\sigma_i$) is used as a measure of the interannual variability (Fig. 8a). The relative contribution of each term to the MLS trend variability is computed similarly to the previous section (Fig. 8b–d).

The maximum interannual variability of the MLS trend ($\sigma_i$) appears within about 15°N–17°S, with relative maxima: within a few degrees of the equator near the dateline, in the SPCZ region and off the Central American coast (Fig. 8a). Variability on the interannual time scale in the western equatorial Pacific (150°E–170°W) is primarily driven by horizontal advection (Fig. 8c). It should be underlined that the regional steeper-than-observed zonal SSS gradient in the model (see Section 2.2) may result in an overestimation of horizontal advection as compared to the real world. This is consistent with the previously observed and modelled zonal displacements of the eastern edge of the western Pacific warm pool during ENSO events (Picaut et al. 1996, 2001; Vialard et al. 2002). Moreover, Maes et al. (2006) showed the absence of correlation between the observed zonal displacements of that eastern edge and the precipitations in this region. The horizontal advection contribution also has to be considered in the SPCZ region, as suggested earlier from altimetry-derived geostrophic currents (Gouriou and Delcroix 2002). The surface contribution is strong on the equatorial sides of both tropical convergence zones, matching the equatorward migration of the heavy precipitation bands during El Niño events (Ando and McPhaden 1997; Vialard et al. 2002). The subsurface processes modulate both the other contributors, especially damping variability in the southwestern tropical Pacific. It is also worth pointing out that the MLS trend presents a relative minimum in the equatorial region west of the Galapagos' archipelago because a strong positive contribution of the horizontal advection balances the negative contribution of subsurface terms north of the equator (and vice versa to south of the equator).

Figure 9 represents the time series of the interannual variations of SSS, which are compared to the SOI (dashed red), and each term of Eq. (1) for a selected box in the SPCZ (Box in Fig. 1). The two upper time series in Fig. 9 show the signature of ENSO in SSS, with a clear tendency for positive SSS anomalies during most El Niño events (SOI <0), such as the 1991–1992, 1997–1998, 2002, 2004 and 2006 events and negative anomalies during the 1996 and 1998–1999 La Niña events (Gouriou and Delcroix 2002). The MLS trend follows closely the horizontal advection term

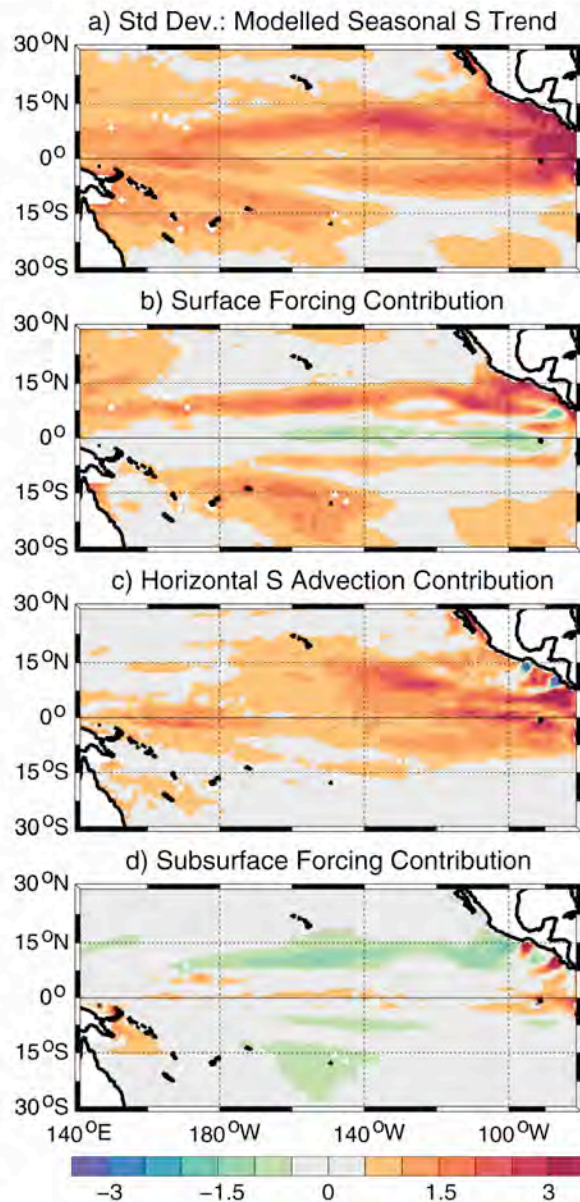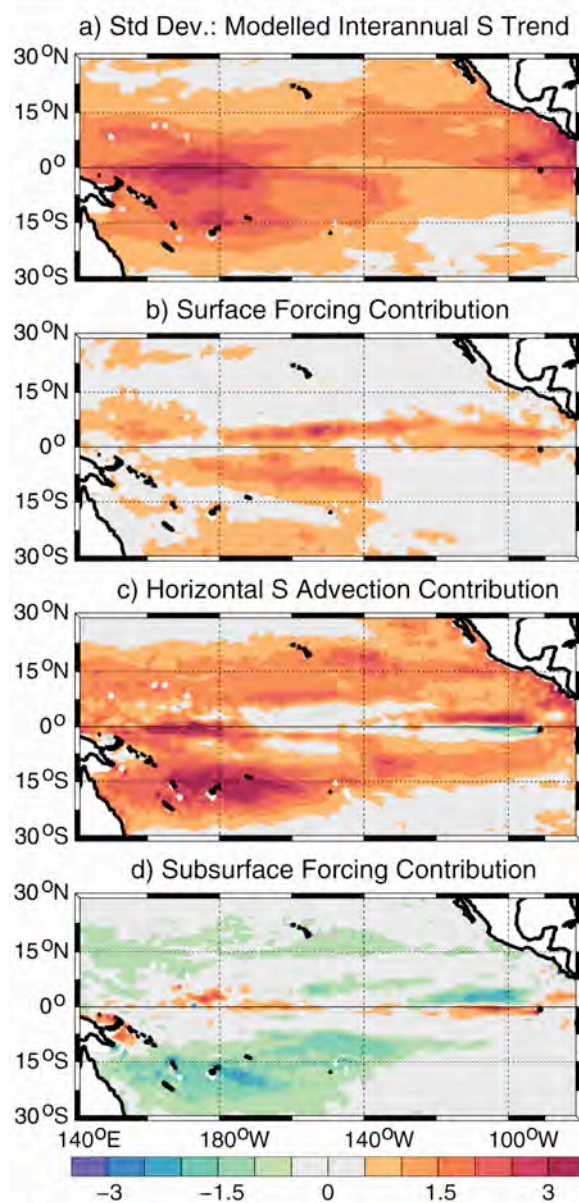**Fig. 8** (From *top to bottom*) Standard deviation of the modelled interannual salinity tendency, used as a measure of the interannual variability, and relative contributions of the surface forcing, horizontal advection and subsurface forcing terms, as described in Section 3.2



**Fig. 9** Mean interannual variations of **a** model-derived MLS (*black curve*) and Southern Oscillation Index (*dashed red curve*), **b** MLS tendency (*dashed blue curve*) and Southern Oscillation Index (*dashed red curve*), and contributions of **c** the surface forcing, **d** horizontal advection and **e** subsurface forcing terms (*black curves*) in the SPCZ region (10–12° S, 170°E–170°W). The MLS tendency curve is repeated in (**c**–**e**) for clarity. Units are practical salinity scale per year

($R$=0.83), with maximum amplitude during the 1998–1999 La Niña event. It is however modulated by both the surface ($R$=−0.11) and the subsurface ($R$=−0.66) forcings, at least during La Niña. Strong MLS interannual variability is also found off the American coast (Fig. 8) where horizontal advection is roughly the only contributor.

This section gives us a broad picture of the mechanisms involved in the mean balance and seasonal and interannual

variability of the MLS. However, interannual variability encompasses a wide range of different ENSO events, in time and space. In particular, Singh et al. (2011) have shown with observations that EP and CP ENSO events have different signatures in observed SSS, and they suggested some possible responsible mechanisms. These mechanisms are quantified from the model data in the next section.

## 4 Contrasting the MLS budget during Eastern and Central Pacific ENSO

In this section, we focus on the modelled MLS budget in the equatorial band for the 1997–1998 EP and the 2002–2003 CP El Niño events. The longitude-time plots of the 2°N–2°S averaged interannual changes of all terms in Eq. (1) are used to describe the chronology of the mechanisms' contributions. They are shown from January 1996 to December 1999 and from January 2001 to December 2004 in Figs. 10 and 11, respectively.
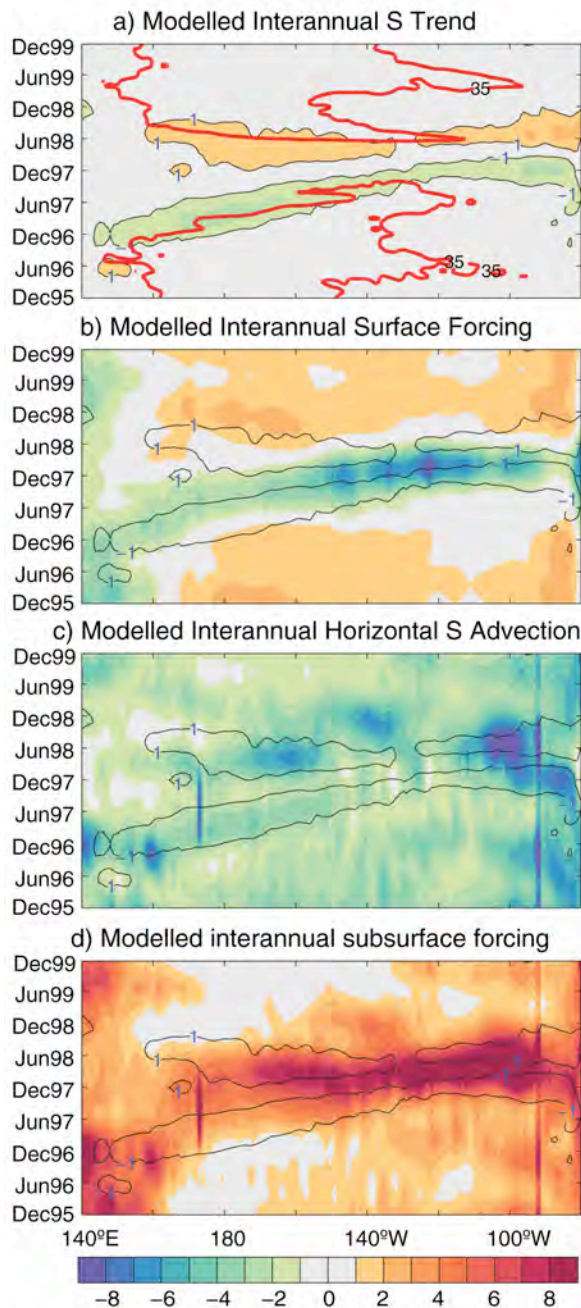
**Fig. 10** Longitude-time plots of the 2°N–2°S averaged interannual changes in model-derived **a** MLS tendency, and contributions of the **b** surface forcing, **c** horizontal advection and **c** subsurface forcing during the 1996–1998 ENSO period. Units are practical salinity scale per year. The *heavy red curves* in (**a**) denote the 2°N–2°S averaged positions of the 35 isohaline denoting the eastern edge of the fresh pool. *Thin black lines* on panel (**a**) are the +1 and −1 pss/year contour of the MLS trend. They are repeated on panels (**b**) to (**d**) to ease interpretation of the figure in the main text. *Narrow vertical bands* of strong values correspond to islands' effect such as the Galápagos' archipelago (91°W) in the model output
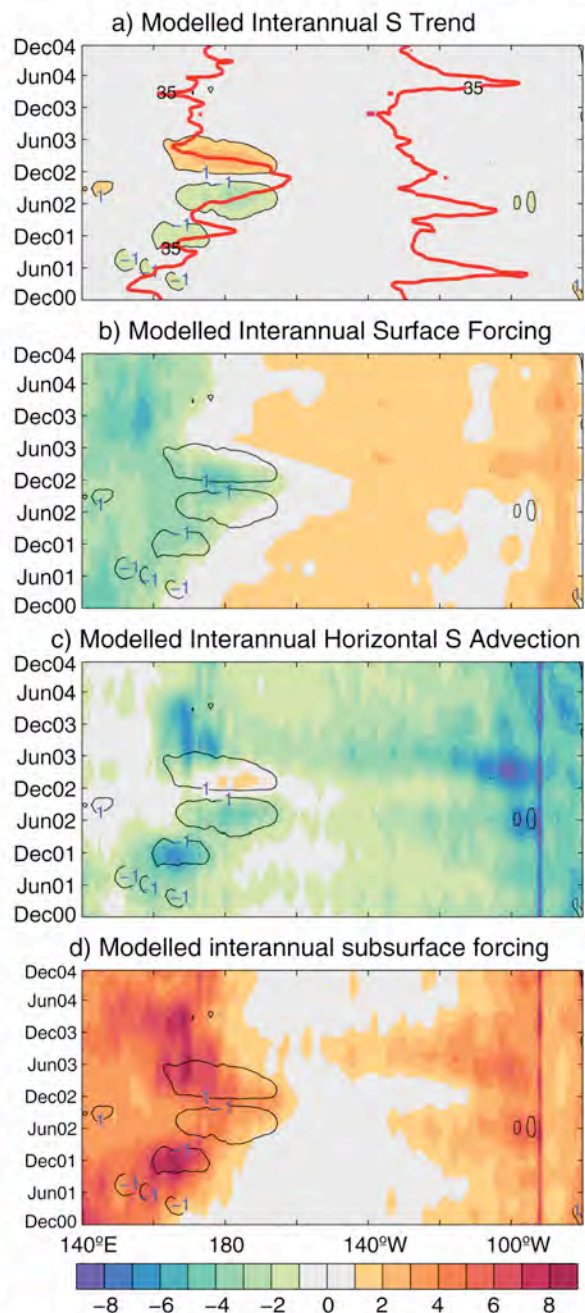
**Fig. 11** As in Fig. 10 for the 2001–2003 period

### 4.1 The 1997–1998 Eastern Pacific El Niño

A small increase of SSS west of 160°E is observed during the first half of year 1996 (Fig. 10a). This period corresponds to an anomalous westward shift of the salinity front, which was described by Vialard et al. (2002). The area is

freshened by both surface forcing (Fig. 10b) and weaker than usual horizontal advection (Fig. 10c). Subsurface processes (Fig. 10d) overcome these two freshening effects. Subsequently, between August 1996 and February 1997, east of 145°E strong processes take place even though no robust changes in the S trend appear. The negative horizontal advection anomaly is attributed to stronger than usual SEC pushing the FP further west. Very strong subsurface processes (Fig. 10d) overcome this freshening effect. Similar results showed strong subsurface forcing at the same period in a mixed-layer temperature variability study (Vialard et al. 2001).

A strong negative anomaly of MLS trend stretches east of the strong subsurface processes region described just above, across the entire basin, from the end of 1996 to the beginning of 1998 (Fig. 10a). This negative MLS tendency, resulting mostly from horizontal advection in the western half of the basin (Fig. 10c), coincides with the eastward displacements of the eastern edge of the fresh pool denoted by the 35 isohaline in Fig. 10a (solid red). As demonstrated by previous authors from observations and model outputs, such advection of low-salinity waters is due to the occurrence of eastward current anomalies characterizing wind-forced downwelling Kelvin waves (e.g. McPhaden and Yu 1999; Boulanger and Menkes 1999; Delcroix et al. 2000), which are well reproduced in the model simulation (not shown). Together with the basin-wide fresh anomaly, high SSTs are spread over the Pacific during this period (not shown), driving the ITCZ to shift closer to the equator (e.g. Ando and McPhaden 1997; Vialard et al. 2002). Its signature can be seen on the surface-forcing map (Fig. 10b) as an intense freshening due to increased precipitations after July 1997 and east of 160°W. Whilst the FP shifts to the east, the gradient between the MLS and S below the ML increases, strengthening the subsurface forcing through the enhancement of entrainment and mixing at the ML base.

In early 1998, a strong reversal in the MLS signal takes place across the basin due to the shift from an eastward to a westward movement of the eastern edge of the FP related to the El Niño to La Niña phase change (Fig. 10a). This phase shift signal in MLS results from the combination of the three forcing terms. In the eastern basin, the MLS increase is mostly due to the subsurface forcing moderated by the horizontal advection east of 110° W. The subsurface forcing remains quite important in the central basin from January to September 1998. Its effects are however counteracted by horizontal advection in the Central basin. Westward current anomalies associated with downwelling Rossby and upwelling Kelvin waves (Delcroix et al. 2000) shift the eastern edge of the FP back to the west bringing low-salinity waters generated by enhanced surface forcing. The conditions go back to 'normal' by the end of 1998.

### 4.2 The 2002–2003 Central Pacific El Niño

Starting at the end of 2001 and lasting for about one year, this El Niño event is quite representative of most CP events (see Fig. 2). Two episodes of freshening between 160°E and 160°W occur from October 2001 to November 2002 (see the green patterns in Fig. 11a). These periods correspond to eastward displacements of the eastern edge of the FP, which reaches its easternmost position by the end of 2002.

The 2002–2003 modelled eastern edge of the FP extends to the centre of the basin only, around 160–170°W, as observed from in situ data (e.g. Singh et al. 2011). The eastward displacements of anomalous precipitations (characterized by the negative surface forcing in Fig. 11b) follow closely the extension of the FP, as expected in the real world as it is also characterized by warm SST inducing enhanced atmospheric activity.

The aforementioned freshening episodes following one another are also both characterised by strong eastward horizontal advection. Fresh waters from the FP are advected zonally towards the dateline. The meridional advection (not shown here) is one order of magnitude weaker. These episodes correspond to two distinct eastward propagating modelled thermocline depth anomalies characterizing downwelling Kelvin waves (not shown here). The first Kelvin wave packet departing the west by the end of 2001 and the second departing in mid-2002 are both drastically damped when reaching the eastern-central basin. This is consistent with a recent study comparing composites of equatorial Kelvin wave evolutions for EP and CP El Niño events (see Dewitte et al. 2012). It is noteworthy that the two freshening events also slightly differ from one another regarding the magnitude of subsurface processes (Fig. 11d). Saltening subsurface processes largely damp the first freshening event, whereas they have a lesser effect on the second event. These differences are due to dissimilarities in ML depth (not shown) which is much shallower during the first event.

The shift towards La Niña phase occurs by the end of 2002. This shift is associated with the appearance of positive MLS trend anomaly whose pattern is confined in the western-central Pacific, much alike the El Niño freshening. The maximum surface freshening occurs during the El Niño/La Niña transition, and decreases as La Niña grows. Contrastingly, the horizontal advection forcing becomes positive in the western-central Pacific bringing high-salinity waters from the central basin. It is worth pointing out that during the second half of 2003 and beginning of 2004, even though no notable changes in MLS trend can be observed in the equatorial band (Fig. 11a), saltening zonal advection and subsurface processes offset strong freshening due to precipitations and meridional advection.

## 5 Conclusion

A two-decade long mixed layer salinity (MLS) budget in the Tropical Pacific Ocean was assessed using observations and model outputs. For the observations, we used 1° latitude by 1° longitude by 1-month gridded fields of sea surface (0–10 m) salinity, horizontal currents, $E-P$ and climatological ML depths to compute the MLS tendency, horizontal advection and surface forcing terms involved in the MLS balance equation. The subsurface forcing term, not quantifiable directly from observations, was inferred as a residual. For the model, we used online values computed at every time step and archived every 5 days on a 0.25° latitude by 0.25° longitude grid of all terms involved in the MLS equation. The model reliability in reproducing observed features was shown from different sets of in situ products.

The mean MLS budget was first investigated with three datasets: the observations, the full resolution model and the modelled dataset modified to mirror the observation temporal and spatial grid resolutions. This latter dataset (called 'ObsLike') was built to underline the observational data ability to catch the full MLS variability. Only the original model dataset actually includes diffusion/mixing, vertical advection and entrainment at the ML base, non-linear terms, as well as high-frequency (<1 month) and small-scale (<100 km) variability. Therefore, it does not consider the subsurface forcing as a residual in the MLS budget.

All three datasets show almost identical spatial distributions for the surface forcing and horizontal advection patterns. The surface forcing reveals regions of dominant precipitations in the ITCZ, SPCZ and WP region and dominant evaporation in both subtropical gyres, resulting in negative and positive MLS tendency, respectively. Horizontal MLS advection shows transports of low-salinity waters by the NECC and SECC and by the mean eastward current in the western equatorial Pacific (i.e. negative MLS tendency) but also of high-salinity waters by the NEC and SEC off the equatorial band (i.e. positive MLS tendency). High values of positive MLS advection and subsurface forcing are shown to be trapped near the equator with the full model resolution only. Our results suggest that this mainly reflects the occurrence of high-frequency (<1 month) variability that cannot be accounted for with low-resolution observations. Patterns of the surface forcing (for the three datasets) show similar magnitude and opposite signs to the ones of the horizontal MLS advection. They however do not balance each other, pointing out the importance of all terms (including the subsurface forcing term) to close the mean MLS budget.

Both seasonal and interannual MLS variability were examined from the model output only. The strongest MLS seasonal variability is present mostly along the ITCZ, SPCZ, in the western equatorial Pacific, in the northern part of the Coral Sea and off Central America. In the ITCZ, the

seasonal changes in MLS result from a delicate balance between the horizontal advection and the surface and subsurface forcing of similar amplitude. The surface forcing drives the seasonal variations of MLS in the SPCZ, whereas the other two terms only modulate them.

The maximum interannual variability of the MLS is linked to ENSO and trapped around the equator, in the SPCZ region and, to a lesser extent, off the Central American coast. It is primarily driven by horizontal advection in the western equatorial Pacific, as demonstrated in numerous previous studies. The surface contribution is strong on the equatorial sides of both convergence zones, matching the equatorward migration of the related heavy precipitation bands during El Niño events. The subsurface processes modulate both the other contributors, damping variability. Variations of the MLS in the SPCZ are mainly due to horizontal MLS advection but are modulated by both the surface and the subsurface forcings. Horizontal advection is roughly the only contributor to the interannual variability off the American coast.

The ENSO-related MLS changes were further analysed in the equatorial band, contrasting the 1997–1998 EP and the 2002–2003 CP El Niño events. For both the EP and CP El Niño events, we showed that the appearance of low salinity waters (i.e. negative MLS tendency) in the western-central basin first results from horizontal advection of MLS (i.e. negative MLS horizontal advection) together with the eastward displacements of the eastern edge of the western Pacific FP. These low salinity waters reach the eastern basin during the 1997–1998 EP El Niño only, due to the persistence of negative MLS horizontal advection and enhanced P (i.e. negative surface forcing) in the eastern-central basin due to the equatorward shift of the ITCZ. In contrast, these low salinity waters only reach the central basin during the 2002–2003 CP El Niño, mostly due to the absence of equatorial enhanced P east of 160°W and to the reversal of horizontal advection (i.e. positive MLS horizontal advection). For both the EP and CP events, the MLS subsurface forcing has a clear tendency to increase the MLS.

We have synthetized a picture of the processes responsible for the mean distribution and for the seasonal and interannual changes of MLS in the tropical Pacific. Our findings reveal that all terms of the MLS equation have to be considered to close the salinity budget, ruling out the use of MLS (or SSS) alone to directly infer the mean, seasonal and/or interannual fresh water fluxes. We also stressed that more work still has to be done to better understand the MLS budget, in particular within the equatorial band. As suggested above from the model data, it is likely that high-frequency (<1 month) MLS changes play an important role in closing the MLS budget in the real world. This would be consistent with the observations of energetic high-frequency changes in horizontal velocity (Halpern et al. 1988) and

SSS (Delcroix et al. 2005) at several equatorial mooring sites, but also with observations of 15 to 23-day tropical instability waves in surface and subsurface temperature (e.g. Legeckis 1977; Lyman et al. 2007), and with the recent discovery of such wave signatures in remotely sensed SSS (Lee et al. 2012).

# References

Adler RF et al (2003) The version-2 global precipitation climatology project (GPCP) monthly precipitation analysis (1979–present). J Hydrometeorol 4(6):1147–1167. doi:10.1175/1525-7541(2003)004<1147:tvgpcp>2.0.co;2

Alory G, Maes C, Delcroix T, Reul N, Illig S (2012) Seasonal dynamics of sea surface salinity off Panama: the far Eastern Pacific Fresh Pool. J Geophys Res Oceans 117. doi:10.1029/2011jc007802

Ando K, McPhaden MJ (1997) Variability of surface layer hydrography in the tropical Pacific Ocean. J Geophys Res Oceans 102(C10):23063–23078

Ashok K, Behera SK, Rao SA, Weng H, Yamagata T (2007) El Niño Modoki and its possible teleconnection. J Geophys Res Oceans 112(C11). doi:10.1029/2006jc003798

Ballabrera-Poy J, Murtugudde R, Busalacchi AJ (2002) On the potential impact of sea surface salinity observations on ENSO predictions. J Geophys Res Oceans 107(C12). doi:10.1029/2001jc000834

Barnier B et al (2006) Impact of partial steps and momentum advection schemes in a global ocean circulation model at eddy-permitting resolution. Ocean Dyn 56(5–6):543–567. doi:10.1007/s10236-006-0082-1

Barnier B, Dussin R, Molines JM (2011) Scientific Validation Report (ScVR) for V1 Reprocessed Analysis and Reanalysis: GLORYS2V1. MyOcean FP7-SPACE-2007-1 project, report MYO-WP04-ScCV-rea-CNRSRep

Bingham FM, Foltz GR, McPhaden MJ (2010) Seasonal cycles of surface layer salinity in the Pacific Ocean. Ocean Science 6(3):775–787. doi:10.5194/os-6-775-2010

Blanke B, Delecluse P (1993) Variability of the tropical Atlantic Ocean simulated by a General Circulation Model with 2 different mixed-layer physics. J Phys Oceanogr 23(7):1363–1388

Bonjean F, Lagerloef GSE (2002) Diagnostic model and analysis of the surface currents in the tropical Pacific Ocean. J Phys Oceanogr 32(10):2938–2954

Bosc C, Delcroix T (2008) Observed equatorial Rossby waves and ENSO-related warm water volume changes in the equatorial Pacific Ocean. J Geophys Res Oceans 113(C6). doi:10.1029/2007jc004613

Bosc C, Delcroix T, Maes C (2009) Barrier layer variability in the western Pacific warm pool from 2000 to 2007. J Geophys Res-Oceans 114(C6). doi:10.1029/2008JC005187

Boulanger JP, Menkes C (1999) Long equatorial wave reflection in the Pacific Ocean from TOPEX/POSEIDON data during the 1992–1998 period. Clim Dyn 15(3):205–225. doi:10.1007/s003820050277

Cooper NS (1988) The effect of salinity on tropical ocean models. J Phys Oceanogr 18(5):697–707. doi:10.1175/1520-0485(1988)018<0697:teosot>2.0.co;2

Cravatte S, Delcroix T, Zhang D, McPhaden M, Leloup J (2009) Observed freshening and warming of the western Pacific Warm Pool. Clim Dyn 33(4):565–589. doi:10.1007/s00382-009-0526-7

de Boyer Montégut C, Madec G, Fischer A, Lazar A, Iudicone D (2004) Mixed layer depth over the global ocean: an examination of profile data and a profile-based climatology. J Geophys Res 109:C12003

Delcroix T (1998) Observed surface oceanic and atmospheric variability in the Tropical Pacific at seasonal and ENSO time scales: a tentative overview. J Geophys Res 103:18611–18633

Delcroix T, Henin C (1991) Seasonal and interannual variations of sea surface salinity in the tropical Pacific Ocean. J Geophys Res Oceans 96(C12):22135–22150

Delcroix T, Picaut J (1998) Zonal displacement of the western equatorial Pacific "fresh pool". J Geophys Res Oceans 103(C1):1087–1098. doi:10.1029/97jc01912

Delcroix T, Dewitte B, duPenhoat Y, Masia F, Picaut J (2000) Equatorial waves and warm pool displacements during the 1992–1998 El Niño Southern Oscillation events: observation and modeling. J Geophys Res Oceans 105(C11):26045–26062. doi:10.1029/2000jc900113

Delcroix T, McPhaden MJ, Dessier A, Gouriou Y (2005) Time and space scales for sea surface salinity in the tropical oceans. Deep-Sea Res I Oceanogr Res Pap 52(5):787–813. doi:10.1016/j.dsr.2004.11.012

Delcroix T, Cravatte S, McPhaden MJ (2007) Decadal variations and trends in tropical Pacific sea surface salinity since 1970. J Geophys Res Oceans 112(C3):C03012. doi:10.1029/2006jc003801

Delcroix T, Alory G, Cravatte S, Correge T, McPhaden MJ (2011) A gridded sea surface salinity data set for the tropical Pacific with sample applications (1950–2008). Deep-Sea Res I Oceanogr Res Pap 58(1):38–48. doi:10.1016/j.dsr.2010.11.002

Dessier A, Donguy JR (1994) The sea surface salinity in the tropical Atlantic between 10 degS and 30 degN seasonal and interannual variations (1997–1989). Deep-Sea Res I Oceanogr Res Pap 41(1):81–100. doi:10.1016/0967-0637(94)90027-2

Dewitte B, Choi J, An SI, Thual S (2012) Vertical structure variability and equatorial waves during central Pacific and eastern Pacific El Nios in a coupled general circulation model. Clim Dyn 38(11–12):2275–2289. doi:10.1007/s00382-011-1215-x

Donguy JR, Henin C (1980) Surface conditions in the Eastern Equatorial pacific related to the intertropical convergence zone of winds. Deep Sea Res Oceanogr Res Paper 27(9):693–714. doi:10.1016/0198-0149(80)90023-0

Donguy JR, Meyers G (1996) Seasonal variations of sea-surface salinity and temperature in the tropical Indian Ocean. Deep-Sea Res I Oceanogr Res Pap 43(2):117–138. doi:10.1016/0967-0637(96)00009-x

Durack PJ, Wijffels SE (2010) Fifty-year trends in global ocean salinities and their relationship to broad-scale warming. J Clim 23(16):4342–4362. doi:10.1175/2010jcli3377.1

Emery W, Thomson R (1998) Data analysis methods in physical oceanography. Pergamon, Elsevier Science Ltd, New York, p 634

Ferry N, Parent L, Garric G, Drevillon M, Desportes C, Bricaut C, Hernandez F (2011) Scientific validation report (ScVR) for V1 reprocessed analysis and reanalysis: GLORYS2V1. MyOcean FP7-SPACE-2007-1 project, report MYO-WP04-ScCV-rea-MERCATOR_V1*Rep*

Gill AE (1982) Atmosphere-ocean dynamics, pp. 1–662. Academic Press, doi:10.1016/S0074-6142(08)60026-1

Gouriou Y, Delcroix T (2002) Seasonal and ENSO variations of sea surface salinity and temperature in the South Pacific Convergence Zone during 1976–2000. J Geophys Res Oceans 107(C12):8011. doi:10.1029/2001jc000830

Grodsky SA, Carton JA, Bingham FM (2006) Low frequency variation of sea surface salinity in the tropical Atlantic. Geophys Res Lett 33(14). doi:10.1029/2006gl026426

Halpern D, Knox RA, Luther DS (1988) Observations of 20-day period meridional current oscillations in the upper ocean along the pacific equator. J Phys Oceanogr 18(11):1514–1534. doi:10.1175/1520-0485(1988)018<1514:OODPMC>2.0.CO;2

Johnson ES, Lagerloef GSE, Gunn JT, Bonjean F (2002) Surface salinity advection in the tropical oceans compared with atmospheric freshwater forcing: a trial balance. J Geophys Res Oceans 107(C12). doi:10.1029/2001jc001122

Kerr YH, Waldteufel P, Wigneron JP, Martinuzzi JM, Font J, Berger M (2001) Soil moisture retrieval from space: the soil moisture and ocean salinity (SMOS) mission. IEEE Trans Geosci Remote Sens 39(8):1729–1735. doi:10.1109/36.942551

Kessler WS (2006) The circulation of the eastern tropical Pacific: a review. Prog Oceanogr 69(2–4):181–217. doi:10.1016/j.pocean.2006.03.009

Lagerloef GSE, Mitchum GT, Lukas RB, Niiler PP (1999) Tropical Pacific near-surface currents estimated from altimeter, wind, and drifter data. J Geophys Res Oceans 104(C10):23313–23326. doi:10.1029/1999jc900197

Lagerloef G et al (2008) The AQUARIUS/SAC-D mission: designed to meet the salinity remote-sensing challenge. Oceanography 21(1):68–81

Lagerloef G, Schmitt R, Schanze J, Kao H-Y (2010) The ocean and the global water cycle. Oceanography 23(4):82–93

Lee T, Lagerloef G, Gierach MM, Kao H-Y, Yueh S, Dohan K (2012) Aquarius reveals salinity structure of tropical instability waves. Geophys Res Lett 39(12). doi:10.1029/2012GL052232

Legeckis R (1977) Long waves in eastern equatorial Pacific Ocean—view from a geostationary satellite. Science 197(4309):1179–1181. doi:10.1126/science.197.4309.1179

Lukas R, Lindstrom E (1991) The mixed layer of the western equatorial Pacific Ocean. J Geophys Res Oceans 96:3343–3357

Lyman JM, Johnson GC, Kessler WS (2007) Distinct 17-and 33-day tropical instability waves in subsurface observations. J Phys Oceanogr 37(4):855–872. doi:10.1175/jpo3023.1

Madec G (2008) NEMO ocean engine, edited, p. 300, France, Institut Pierre-Simon Laplace (IPSL)

Maes C, Ando K, Delcroix T, Kessler WS, McPhaden MJ, Roemmich D (2006) Observed correlation of surface salinity, temperature and barrier layer at the eastern edge of the western Pacific warm pool. Geophys Res Lett 33(6):L06601. doi:10.1029/2005gl024772

McPhaden MJ, Yu X (1999) Equatorial waves and the 1997–98 El Niño. Geophys Res Lett 26(19):2961–2964. doi:10.1029/1999gl004901

Miller JR (1976) Salinity effect in a mixed layer ocean model. J Phys Oceanogr 6(1):29–35. doi:10.1175/1520-0485(1976)006<0029:tseiam>2.0.co;2

Penduff T, Juza M, Brodeau L, Smith GC, Barnier B, Molines JM, Treguier AM, Madec G (2010) Impact of global ocean model resolution on sea-level variability with emphasis on interannual time scales. Ocean Sci 6(1):269–284

Picaut J, Ioualalen M, Menkes C, Delcroix T, McPhaden MJ (1996) Mechanism of the zonal displacements of the Pacific warm pool: implications for ENSO. Science 274(5292):1486–1489. doi:10.1126/science.274.5292.1486

Picaut J, Ioualalen M, Delcroix T, Masia F, Murtugudde R, Vialard J (2001) The oceanic zone of convergence on the eastern edge of the Pacific warm pool: a synthesis of results and implications for El Niño-Southern Oscillation and biogeochemical phenomena. J Geophys Res Oceans 106(C2):2363–2386

Qiu B, Scott RB, Chen S (2008) Length scales of eddy generation and nonlinear evolution of the seasonally modulated South Pacific Subtropical Countercurrent. J Phys Oceanogr 38(7):1515–1528. doi:10.1175/2007jpo3856.1

Qu T, Gao S, Fukumori I (2011) What governs the North Atlantic salinity maximum in a global GCM? Geophys Res Lett 38. doi:10.1029/2011gl046757

Roemmich D, Boebel O, Desaubies Y, Freeland H, King B, LeTraon P.-Y, Molinari R, Owens B, Riser S, Send U, Takeuchi K, Wijffels S (1999) ARGO: the global array of profiling floats. CLIVAR Exchanges 13

Singh A, Delcroix T, Cravatte S (2011) Contrasting the flavors of El Niño-Southern Oscillation using sea surface salinity observations. J Geophys Res Oceans 116. doi:10.1029/2010jc006862

Sverdrup HU (1943) On the ratio between heat conduction from the sea surface and heat used for evaporation. Ann N Y Acad Sci 44(1):81–88

Terray L, Corre L, Cravatte S, Delcroix T, Reverdin G, Ribes A (2012) Near-surface salinity as nature's rain gauge to detect human influence on the tropical water cycle. J Clim 25(3):958–977. doi:10.1175/jcli-d-10-05025.1

Vialard J, Delecluse P (1998a) An OGCM study for the TOGA decade. Part I: role of salinity in the physics of the western Pacific fresh pool. J Phys Oceanogr 28(6):1071–1088. doi:10.1175/1520-0485(1998)028<1071:aosftt>2.0.co;2

Vialard J, Delecluse P (1998b) An OGCM study for the TOGA decade. Part II: barrier-layer formation and variability. J Phys Oceanogr 28(6):1089–1106. doi:10.1175/1520-0485(1998)028<1089:aosftt>2.0.co;2

Vialard J, Menkes C, Boulanger JP, Delecluse P, Guilyardi E, McPhaden MJ, Madec G (2001) A model study of oceanic mechanisms affecting equatorial Pacific sea surface temperature during the 1997–98 El Niño. J Phys Oceanogr 31(7):1649–1675. doi:10.1175/1520-0485(2001)031<1649:amsoom>2.0.co;2

Vialard JM, Delecluse P, Menkes C (2002) A modeling study of salinity variability and its effects in the tropical Pacific Ocean during the 1993–1999 period. J Geophys Res Oceans 107(C12). doi:10.1029/2000jc000758

Vialard J, Jayakumar A, Gnanaseelan C, Lengaigne M, Sengupta D, Goswami BN (2011) Processes of 30–90 days sea surface temperature variability in the Northern Indian Ocean during boreal summer. Clim Dyn. doi:10.1007/s00382-011-1015-3

Vinayachandran PN, Nanjundiah RS (2009) Indian Ocean sea surface salinity variations in a coupled model. Clim Dyn 33(2–3):245–263. doi:10.1007/s00382-008-0511-6

Yim BY, Yeh SW, Noh Y, Moon BK, Park YG (2008) Sea surface salinity variability and its relation to El Niño in a CGCM. Asia-Pac J Atmos Sci 44(2):173–189

Yu L (2011) A global relationship between the ocean water cycle and near-surface salinity. J Geophys Res Oceans 116. doi:10.1029/2010jc006937

Yu L, Jin X, Weller RA (2008) Multidecade global flux datasets from the objectively analyzed air-sea fluxes (OAFlux) project: latent and sensible heat fluxes, ocean evaporation, and related surface meteorological variables. *Rep.*, 64pp., Woods Hole Oceanographic Institution, Woods Hole Massachusetts

77

# Chapter 4. Analysing the 2010-2011 La Niña signature in the tropical Pacific sea surface salinity using *in situ*, SMOS observations and a numerical simulation

## Foreword

The greatest mode of climate variability on Earth at the interannual time scale is the ENSO which occurs in the tropical Pacific. Many studies have described this oscillation in details and especially its warm phase: El Niño. However, only a small number of then have focused on its cold phase: La Niña even though it was quite strong in recent years and also negatively affected our environment. It is therefore crucial to understand better the associated mechanisms and in particular the ones behind the salinity signature. A strong La Nina event has spanned from 2010 to 2011. By change, this period has been observed by the SMOS satellite and offers the innovative possibility to observe the associated variations in salinity at the basin-wide scale. In this chapter and in the related submitted article (see below), the 2010-2011 La Nina is described with SMOS *in situ* SSS data sets, and a forced (and, whenever possible validated) model, and the associated mechanisms are analysed with the model solely.

## Article

This article has been submitted to the Journal of Geophysical Research– Oceans in August 2013 special section titled "Early scientific results from the salinity measuring satellites Aquarius/SAC-D and SMOS".

Hasson A., T. Delcroix, J. Boutin, R. Dussin, J. Ballabrera-Poy, "Analysing the 2010-2011 La Niña signature in the tropical Pacific sea surface salinity using *in situ*, SMOS observations and a numerical simulation", *submitted to Journal of Geophysical Research on August 29th, 2013.*

## Abstract

The tropical Pacific Ocean has remained in a La Niña phase from early 2010 to mid-2012. In this study, the well-marked signature of this cold El Niño-Southern Oscillation

(ENSO) phase is described and analysed using a combination of numerical model output, *in situ* data and Soil Moisture Ocean Salinity (SMOS) salinity products. The model outputs are from a validated Drakkar eddy-permitting forced simulation in which all mixed-layer salinity budget terms are computed at each time-step. The *in situ* data include high-resolution voluntary observing ship thermo-salinograph (TSG) measurements and Argo-based gridded Sea Surface Salinity (SSS) products. We use a newly derived SMOS product based on the ESA L2 v5.5. Comparisons of all near-surface salinity products show a good overall agreement between them;, with a mean bias and RMS difference of 0.2-0.3 between TSG-SMOS and TSG-model. The 6 first months of 2010 (La Niña) are characterized by an unusually strong tri-polar anomaly captured by the three salinity products in the western tropical Pacific. A positive SSS anomaly sits north of 10ºS (>0.5), a negative northwest-southeast anomaly lies between 10ºS and 20ºS and a positive one south of 20ºS. In 2011, anomalies shift south and amplify up to 0.8, except for the one south of 20ºS. The associated processes were studied from the simulation output. The SSS meridonal gradient changes because of the meridional advection were found to be mainly responsible for the SSS variations. They result from ENSO-related displacements of the warm pool and South Pacific convergence zone (SPCZ) fresh waters. The modelled SSS is also affected by the surface forcing, mainly due to the effect of ENSO on the Walker circulation. The subsurface forcing has a damping effect on changes in SSS induced mainly by surface forcing, but also on horizontal advection. The observed basin-scale La Niña SSS signal captured by all datasets are finally compared with the historical 1998-1999 La Niña event as represented by the validated model simulation.

## I. Introduction

The El Niño Southern Oscillation (ENSO) event is the strongest climatic signal on Earth at the interannual time scale. Even though it originates in the tropical Pacific Ocean, ENSO has global environmental impacts through the modification of the atmospheric circulation. These changes affect for instance precipitations in the tropical Pacific (Ropelewski and Halpert, 1996), in Northern America (Cole *et al.*, 2002), in Africa (Nicholson *et al.*, 2000) and in Southeast Asia (Kripalani and Kulkarni, 1997). ENSO includes the most-studied warm El Niño phase as well as the less-documented cold La Niña phase (Philander, 1985). These two phases respectively correspond to warmer- and colder-

than-usual Sea Surface Temperature (SST) in the eastern-central equatorial Pacific. Recent studies have described different flavors of El Niño events (e.g., Ashok *et al.*, 2007). Details about ENSO main features and mechanisms can be found in several textbooks, including those of Philander (1989), Clarke (2008) and Sarachik and Cane (2010) to name a few.

A recent overview of the known ENSO signature in Sea Surface Salinity (SSS) was presented in the Introduction section of Hasson *et al.* (2013). Based on sparse *in situ* observations, the ENSO signature in SSS is mainly located in the western half of the tropical Pacific Ocean, with below-than-normal salinity waters in the equatorial band and higher-than-normal values along the mean position of the South Pacific Convergence Zone (SPCZ) during El Niño events. The reverse mechanism occurs during La Niña events (Delcroix and Hénin, 1991; Gouriou and Delcroix, 2002). In contrast, most of the SST ENSO signal was found to be located in the eastern half of the basin, trapped in the equatorial band (Rasmusson and Carpenter, 1982). The ENSO signal amplitude in SSS is of the order of 1 pss, which is two-fold the seasonal SSS signal (see Delcroix, 1998).

The main mechanisms responsible for La Niña-related SSS changes are qualitatively well known (Delcroix and Picaut, 1998; Picaut *et al.*, 2001; Gouriou and Delcroix, 2002; Singh *et al.*, 2011). During La Niña the intensification of the Trade Winds over the Pacific Ocean reinforces the equatorial upwelling penetrating farther to the west. SSS then increases in the western-central equatorial Pacific mostly as a consequence of vertical advection bringing high-salinity waters from below. These easterly wind anomalies also push the equatorial warm and fresh pool farther to the west of the basin. They also generate upwelling Kelvin waves whose associated westward current anomalies enhance the warm/fresh pool displacements to the far west. As a consequence of the enhanced zonal advection and increased precipitation, the western Pacific SSS decreases. In the south-western tropical Pacific, the SSS increases, mainly as a consequence of the southward displacements of the South Pacific convergence Zone (SPCZ) and of its related heavy precipitation regime, with a minor contribution of zonal advection. To sum up, opposite anomalies occur in the western-central equatorial region and along the mean SPCZ position: during La Niña events the equatorial fresh pool shifts westward and the equatorial upwelling penetrates farther to the west increasing SSS in the western-central Pacific, and the SPCZ heavy precipitation regime moves farther towards the south, decreasing SSS along the SPCZ mean position.

Aside from quantifying the ENSO signature on SSS, various studies have shown the important role of salinity in ocean dynamics in the tropical Pacific (e.g., Vialard and Delecluse, 1998; Vialard *et al.*, 2002). Salinity stratification in the upper ocean drives the

mixed layer and barrier layer depths in the western tropical Pacific Ocean, and therefore can modulate air-sea interactions involved in ENSO dynamics (Lukas and Linstrom, 1991). Maes *et al.* (2006) used a coupled model to show the importance of the barrier layer to set up the ocean state prior to an El Niño event. While the barrier layer thickness cannot directly be measured by satellite, there is evidence of a link between barrier layer thickness, SST anomalies and SSS horizontal gradient in the western Pacific warm pool (e.g. McPhaden and Delcroix, 2002; Bosc and Delcroix, 2008).

Following a strong El Niño phase in 2009, the tropical Pacific Ocean rapidly turned into a strong La Niña phase in early 2010 (Kim *et al.*, 2011). This La Niña phase has lasted for about two years with however two periods of maximum negative equatorial SST anomalies, occurring during the boreal falls of 2010 and 2011, nearly in phase with the mean seasonal SST cooling (Fig. 1). The Soil Moisture / Ocean Salinity (SMOS) satellite provides for the first time observations of sea surface salinity (SSS) of the World Ocean(Kerr *et al.*, 2010; Font *et al.*, 2010), and thus basin-wide observations of SSS of the tropical Pacific Ocean in its La Niña phase. Taking advantage of such unprecedented satellite dataset, but also combining *in situ* and model datasets, this paper aims at describing and analysing the 2010-2011 La Niña signature in SSS.



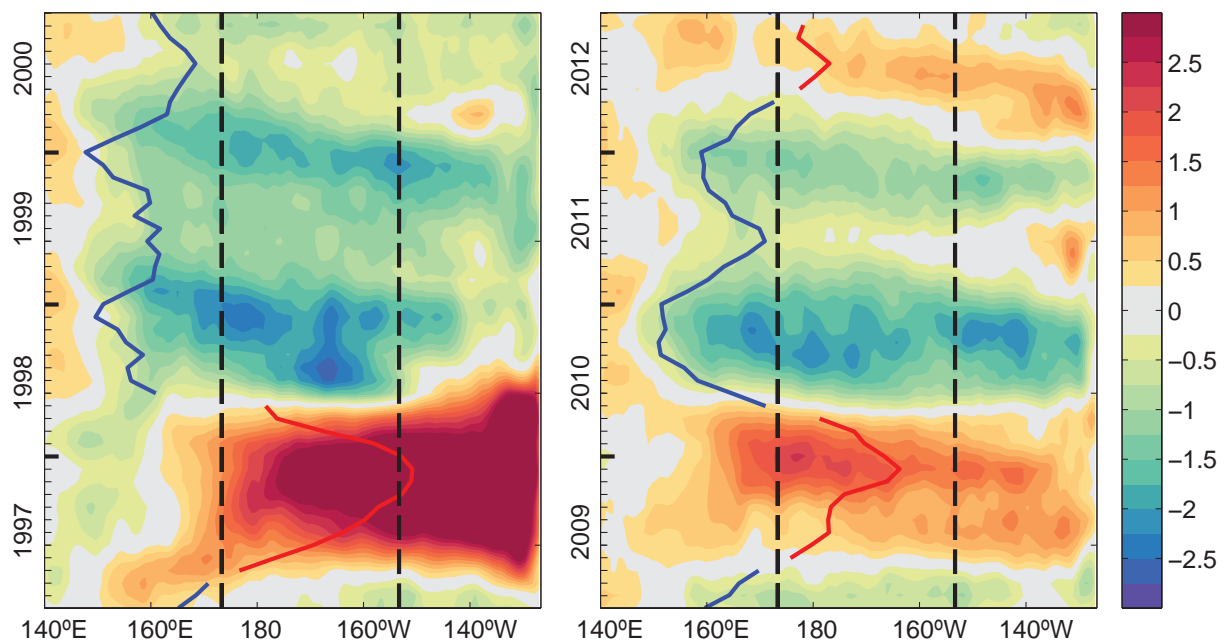Figure 1. Longitude-time plot of the monthly SST anomaly (ºC) averaged between 2ºS-2ºN from 1997 to 2000 (a) and from 2009 to 2012 (b), SST anomalies are relative to 1982-2012. The solid line represents the Niño 3.4 SSTA (ENSO index) centered on 170ºW

(20 degrees of longitude correspond to 1°C in SSTA). When blue, the line represents negative SSTA (La Niña phase) and when red, positive SSTA (El Niño phase). The dashed lines represents the longitudinal zone in which the NINO 3.4 index is computed.

This paper is organized as follows. Data and methodology are described in section 2. We then discuss the SMOS, *in situ* and model datasets, through their cross-comparison. The 2010-2011 La Niña event is then described in section 3 in terms of SSS, based on all datasets. The SSS variability and related mechanisms are assessed in section 4, using the model outputs to identify processes behind the observed SSS changes. A comparisonwitho the historical 1998-1999 La Niña is done in section 5; discussion and conclusions are given in the last section.

## II. Data and Methods

### II.1. Data description

Our analysis is carried out using complementary SMOS, *in situ* (Argo and TSG data), and model-derived near-surface salinity data sets. SMOS was launched in November 2009 and started delivering data a few months later. Three different SSS products are available (at the time of writing) at different time and space resolutions and with different correction approaches. The SMOS SSS data comes from the CATDS CEC-LOCEAN v2013 product built using ascending and descending SMOS passes. This product is created without any adjust to climatology and thus preserves the actual SSS interannual variability measured from the satellite. The SSS data are averaged over 100x100km$^2$ and oversampled on a 0.25°x0.25° grid, every 10 days or month, from January 2010 to December 2012. Data during the commissioning phase (January to June 2010) must be interpreted with care as the calibration control parameters of the instrument were quite variable, which is not the case since June 2010.

Thermosalinograph (TSG) measurements have been obtained from 1991 till present from the Voluntary Observing Ships (VOS) programs of the French SSS Observations Service. We will especially focus on data collected along the shipping routes from New Caledonia to Kiribati and Japan, as they cross the region of maximum ENSO-related SSS variability (see below). They correspond to three different VOS: Coral Islander 2, Pacific Islander 2, and Tropical Islander. SSS are measured every 15s and median values over 5min are stored. Because of the ships' draught and average speed (20 knots), the measurements are

though to represent an average of the first 10 meters depth and have a 3 km average resolution along track. In this work, the horizontal resolution is degraded to 30 km (i.e. averaging over 10-11 data points) to allow for better comparison with other datasets. The SSS is processed by a quality-control algorithm involving comparison with climatology, daily bucket samples collected on board and collocated near-surface Argo data. The accuracy of SSS values (of the order of 0.02) is a function of the linear-fit adjustment between TSG versus bucket samples and collocated Argo measurements (see Alory *et al.*, 2013, for details). Only "Good" and "Probably Good" flagged data were kept for our study.

The Argo network of profiling floats is being deployed to sample the World Ocean since about 2002 (Roemmich and Owens, 2000). The ISAS (In-Situ Analysis System) uni-variate objective analysis (OA) is based on the data provided by Argo and, to a lesser extent, on complementary data such as TAO-TRITON moorings in the tropical Pacific. We use here the 6$^{th}$ version of ISAS on a global ½°x½° horizontal mesh (77°S-66.5°N). The Argo temperature and salinity profiles are first interpolated to standard depths. The OA method is then used to spatially interpolate temperature and salinity fields at each horizontal and temporal grid point. Around each grid point, only data included in a three-dimensional ellipsoid defined by $L_x$=600 km of longitude, $L_y$=300 km of latitude and $L_t$=3 weeks are kept in the analysis. Covariance scales are 300 km wide in longitude, proportional to the Rossby radius of deformation in latitude, and 3 weeks long in time. The accuracy of the objectively analysed T and S gridded values thus depends on the number of nearby data. If there is no data within the ellipsoid then data corresponds to a first guess climatological seasonal cycle. Temperature and salinity are available from the surface to a depth of 2000 m. We average the first 4 vertical levels within 0-10 m to represent SSS. A new product was released in early 2013 with monthly data from 2002 to 2011. Only data with associated error below 80% were kept in our study. Details can be found in Gaillard *et al.* (2009).

The SST fields used here are derived from an optimal interpolation of both *in situ* and satellite data (Reynolds *et al.*, 2002). This SST produced by the National Oceanic and Atmospheric Admistration (NOAA) is available weekly from Novembre 1981 to present on a 1° x1° grid.

The numerical simulation was run by the DRAKKAR group based on the 3.2.1 version of the NEMO ocean general circulation model code (Madec *et al.*, 2008) in version 3.2.1. Our specific model run (ORCA025.L75-MRD911) has been forced by a modified ERA-interim reanalysis to prevent direct SSS restoring (Hasson *et al.*, 2013). The simulation is available from 1990 to 2011 on a 0.25°x0.25° horizontal resolution and with 75 vertical z-

coordinate levels. The time step of the model is 960s. There are 8 levels between the sea-air interface and 10 meters depth. Their average will be referred to as *surface* data. The model output, as well as each term of the mixed layer salinity (hereafter called SSS) budget equation, are archived every 5 simulated days. The model data are routinely evaluated against dedicated metrics by the DRAKKAR group, and outputs within the salinity mixed layer have been further assessed in Hasson *et al.* (2013a, b). Comparisons against *in situ* observations have highlighted the model ability to reproduce near surface salinity variability at various timescales. The model showed a particularly good representation of the fresh pool zonal displacements during ENSO events in the equatorial band and enables us to quantify all terms involved in the mixed-layer salinity budget equation.

### II.2.Data assessment

In this section, all products described above are assessed through their mutual comparison, bearing in mind their different horizontal and time resolutions, as well as the optimal interpolation methods. Moreover, one should notice that the term "SSS" does not account for the same layer depth in all datasets. SSS refers to the average salinity in the approximate 10 first meters for all datasets but the satellite based ones. The SSS derived from SMOS data corresponds to the ocean top first centimetre. Dissimilarities have been observed between near-surface salinity values corresponding to different depths during localised heavy rain events (Hénocq *et al.*, 2010; Boutin *et al.*, 2013). However our study focuses on large-scale dynamics and on longer timescales. With the exception of regions of heavy precipitation (such as the fresh pool or the intertropical convergence zones), errors due to this approximation are expected to be negligible.

The large-scale average and standard deviation of the monthly-averaged SSS over the 2010-2011 period are shown in Figures 2a-f for the model, ISAS and SMOS restricting here our investigation to the western half (140°E-140°W) of the tropical Pacific where the SSS maximum variability is observed. The modelled values (Fig. 2ad) compare rather well with ISAS (Fig. 2be) and SMOS (Fig. 2cf). The spatial correlation coefficients is 0.97 between SSS from the numerical simulation and ISAS, and 0.87 between ISAS and SMOS values (corresponding values for the standard deviations are 0.66 and 0.56, respectively). All datasets portray the "low SSS – high variability" region, roughly west of 170ºW, linked to the SPCZ and fresh pool positions, and the "high SSS – low variability" to the east of 170ºW in the southern hemisphere. Even though the overall mean patterns are well reproduced the model simulates lower-than-observed SSS in the low SSS regions and higher-than-observed

in the high SSS regions (see Hasson *et al.*, 2013ab for details). Still, the model overestimates the SSS variability in the high variability region compared to SMOS and ISAS. It is however hard to say to what extent these differences are due to the model or to the objective analysis expected smoothed variability in the observed fields.
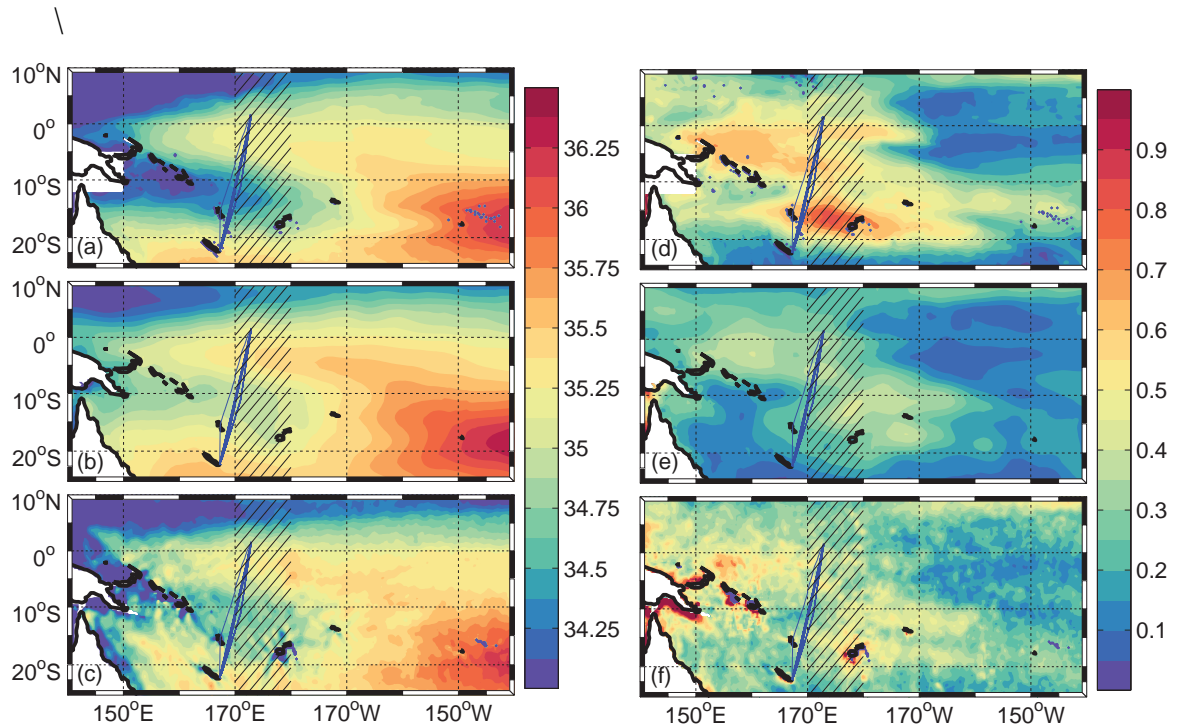


Figure 2. 2010-2011 averaged Sea Surface Salinity (pss) in the western tropical Pacific from the model (a), ISAS (b) and SMOS (c) and their respective standard deviations (d,e and f). Blue lines represents the VOS routes and the 170°E-180° hatched zones the computation area of Figures 5 to 9.

The modelled, SMOS and ISAS SSS datasets are also compared with the high-resolution (30 km) TSG values. To do so, the model output, the SMOS SSS averaged in a 100 km radius centered on each TSG data point, and ISAS datasets were collocated to the TSG data using a 10-day, 9-day and 1-month window, respectively, and all within a 50 km radius. (Recall that the original model and ISAS time resolutions are 5 days and 1 month respectively and that the near-repeat cycle of SMOS is 18 days). Colocations with less than 30 SMOS measurements are discarded. A total of 16 VOS tracks crossing the SSS high-variability region while sailing between New Caledonia and Kiribati have been selected for the comparison (blue lines in Fig. 2).
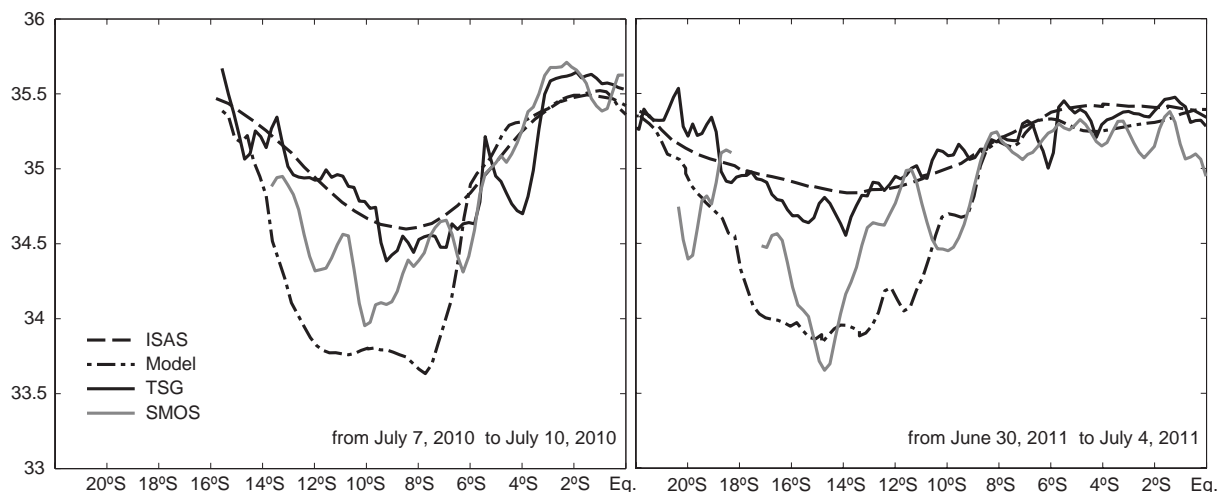
Figure 3. VOS-TSG Sea Surface Salinity (solid black) and collocated ISAS (dashed), SMOS (solid grey) and model (dot-dashed) SSS in July 2010 (left panel) and July 2011 (right panel). All in pss.

Figure 3 shows TSG SSS along two representative tracks in July 2010 and 2011 and collocated SSS from the three other datasets. All datasets compare rather well with the *in situ* VOS measurements for these two tracks. They all show a shift of the relative SSS minima from about 8°-10°S in July 2010 to 14°-16°S in July 2011. We found a mean difference from the TSG data of 0.16 for both SMOS and the model respectively. As stated above, lower than observed (*in situ*) SSS derived from SMOS in the SPCZ region could be explained by the effect of heavy precipitations on the satellite salinity retrieval (Boutin *et al.*, 2013). Also, the best comparison is obtained between the two *in situ* products (TSG and ISAS). One must however keep in mind that the Argo data used for ISAS was partly considered during the TSG quality control procedures. TSG and ISAS are thus not strictly independent products. As expected, the 1-month resolution ISAS product is much smoother than the instantaneous TSG transects. Statistics for all tracks are comparable and found in Table 1. Regarding SMOS and ISAS, it is interesting to note that our statistics compare well with what was found when comparing SMOS with Argo data (last row of Table 1) in the Pacific ITCZ region (Boutin *et al.*, 2013).

| Datasets to be compared | Mean differences | Standard deviation of the differences | RMSE | N |
|---|---|---|---|---|
| **TSG - SMOS** | 0.22 | 0.32 | 0.35 | 1416 |
| **TSG - ISAS** | -0.01 | 0.18 | 0.18 | 1698 |
| **TSG - Model** | 0.28 | 0.36 | 0.46 | 1698 |
| **SMOS & Argo** | 0.23 | 0.35 | 0.42 | 692 |

Table 1. Comparison of along track TSG SSS with collocated SMOS, ISAS, modelled SSS. Last row is a comparison of SMOS SSS and collocated Argo SSS in the ITCZ region (5-15ºN; 180-110ºW) from Boutin *et al.*, 2013; note that the latter uses a temporal radius of colocation of 10 days that leads to a slightly higher RMSE than in the present study.

## III.   The 2010-2011 ENSO Signature in SSS

An annual monthly SSS climatology was built from ISAS data after extracting the original 10-year long (2002-2011) monthly time series with a 25-month Hanning filter to screen out the main ENSO influence (as in Hasson *et al.*, 2013a). This reference monthly climatology was then subtracted from the *in situ* (ISAS), satellite based and modelled gridded SSS products to derive SSS anomalies.

Figure 4 shows the July 2010 and July 2011 SSS anomalies for the three gridded products (The month of July has been chosen as it is the month with the greatest anomaly signal after the SMOS commissioning phase, see below). Spatio-temporal variability structures observed on the three products are in good agreement with one another, similarly as in Figures 2 and 3. In July 2010, negative SSS anomalies of the order of -0.5 stretch from the Solomon to French Polynesia islands within about 5°S and 15ºS. They are bracketed by positive anomalies of the order of +0.5 to the north between 5°S and 5°N and to the south between 25ºS and 15ºS (Fig. 4abc).  Most of these SSS anomalies have drastically reversed signs one year later, in July 2011 (Fig 4def). These changes are consistent with the location of maximum standard deviation in Figure 2 (right panels) as well as with the southward 5-10° latitude shift of the minimum SSS values between July 2010 and July 2011 in Figure 3.
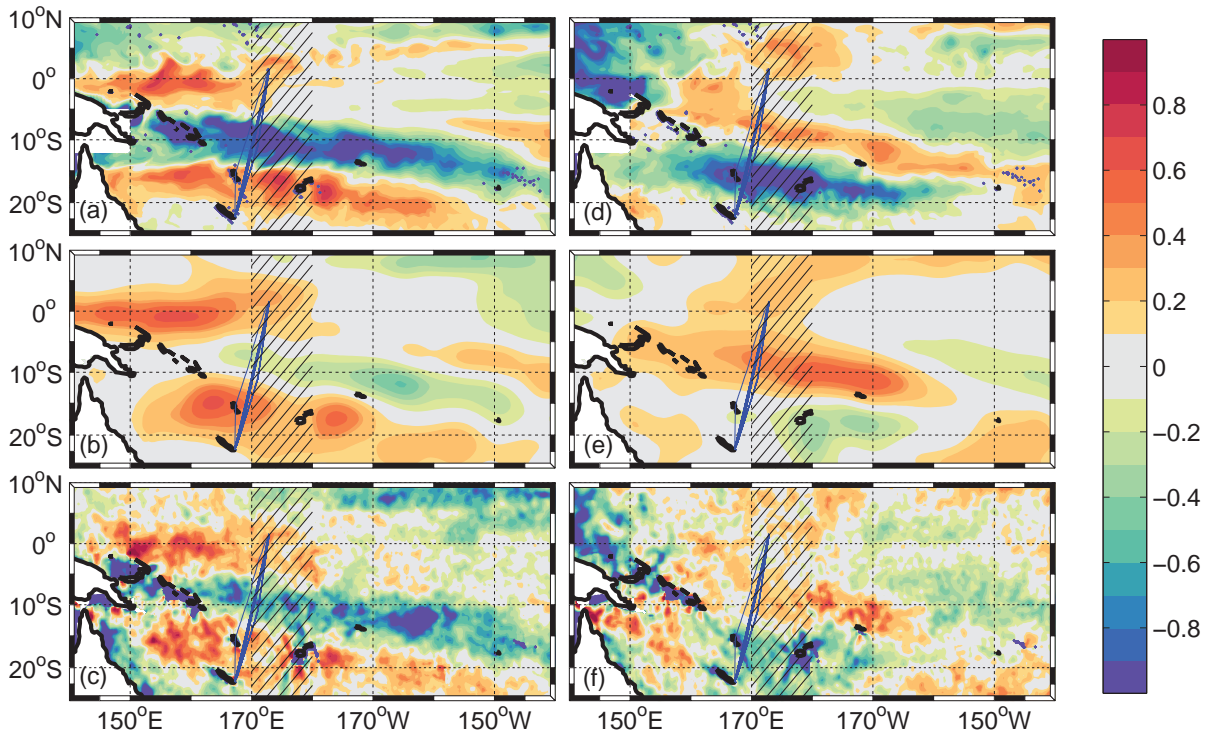
Figure 4. Sea Surface Salinity anomalies relative to the 2002-2011 ISAS monthly climatology (pss) in July 2010 (left panels) and July 2011 (right panels) for the model (a, d), ISAS (b, e) and SMOS (d, f). Hatched zones and blue lines are identical to Figure 2.

The latitude-time plots of the SSS anomaly derived from the three SSS products averaged within the 170º-180ºE band centred on the maximum anomaly patterns (hatched area on Figure 4) are shown in Figure 5abc. One can observe the concurrent timing and latitudinal shift of the reversing positive and negative SSS anomalies. These anomalies seem to be following the NINO3.4 SST index (solid red and blue lines in Figure 5). In early 2010, during the 2009-2010 El Niño wrap-up, a strong negative SSS anomaly (over -0.8) spans from 5ºS to 10ºN, and a positive SSS anomaly (over +0.8) appears south of about 10ºS. During the following La Niña episode, by the end of 2010, the various datasets show a strong triplet of anomalies, positive north of 10°S, negative within about 10ºS and 20ºS, and then positive south of 20ºS. In 2011, the negative anomaly shifts southward and becomes stronger similarly to the northern positive anomaly. This ENSO evolution is consistent with the analysis of Delcroix and Hénin (1991) based on the 1969-1988 VOS bucket data available at that time. Authors underlined the co-occurrence of regional changes in SSS and in precipitations due to the ENSO effect on the Walker circulation. They however recall their earlier study (Delcroix and Hénin, 1989) that stated the possible important role of mixing and advection upon the 1982-1983 ENSO SSS changes in the SPCZ region.
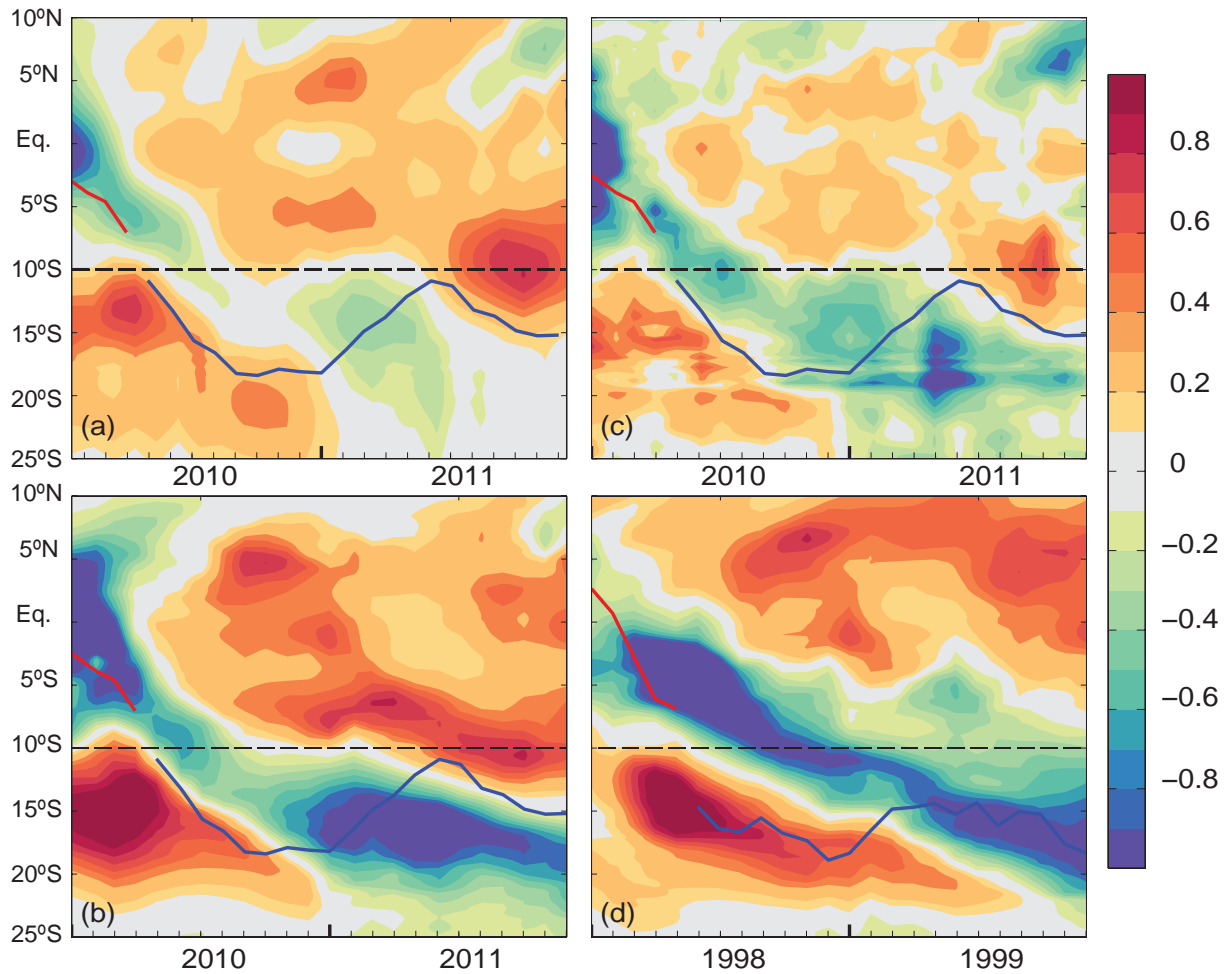
Figure 5. 2010-2011 latitude-time plot of the 170ºE-180ºE averaged sea surface salinity anomalies (pss) from ISAS (a), SMOS (b) and the model (c). Analogous plot from model data over the 1998-1999 period (d). The solid line is the Niño 3.4 SSTA (equivalent to Figure 1 but centred on 10ºS (with 20 degrees of latitude corresponding to 1°C in SSTA).

# IV. Mechanisms associated with the 2010-2011 SSS Anomalies

In order to understand the 2010-2011 variations in SSS, we investigate the processes that modify salinity within the mixed layer (hereafter still called SSS), using the model outputs as in Hasson *et al.* (2013a).

The equation of the SSS budget may be written as

$$\underbrace{\partial_t \langle S \rangle}_{I} = \underbrace{\frac{(E-P-R)}{H} \cdot \langle S \rangle}_{II} \underbrace{- \langle \vec{u}_h \cdot \vec{\nabla}_h S \rangle}_{III} + \underbrace{\frac{(w_e + d_t H) \cdot \delta S}{H}}_{IV} \underbrace{- \langle \vec{\nabla}_h \left( K_h \cdot \vec{\nabla}_h S \right) \rangle}_{V} + \underbrace{\frac{\partial_z \left( K_z \cdot \delta S \right)}{H}}_{VI} \tag{1}$$

Where $\langle X \rangle = \frac{1}{H} \int_{-H}^{0} X(z) dz$ corresponds to the parameter X averaged within the mixed layer of depth H. The other parameters are referred to as follows: E for the evaporation, P for precipitation, R for the river runoff (~0 in our study domain), $u_h$ for the horizontal velocity (including both zonal u and meridional v), $w_e$ for the entrainment velocity and K for the diffusion coefficient (horizontal h and vertical z). Moreover, δS denotes the salinity jump at the base of the mixed layer. Term (I) will be referred to as the SSS tendency, term (II) as the surface forcing, terms (III) and (V) together as the horizontal advection, and terms (IV) and (VI) together as the subsurface forcing.

As described above, the numerical simulation computes at every model time step all terms of the equation but the entrainment, which is rather insignificant (not shown). Figures 6a-d show the latitude-time plots of the SSS tendency and of the three forcing terms averaged within 170°E-180°E (as in Figure 5). The data shown in Figure 6 are the anomalies from the respective monthly climatology of the various budget components, computed from the model outputs using the same filter and over the same period as the one based on ISAS.
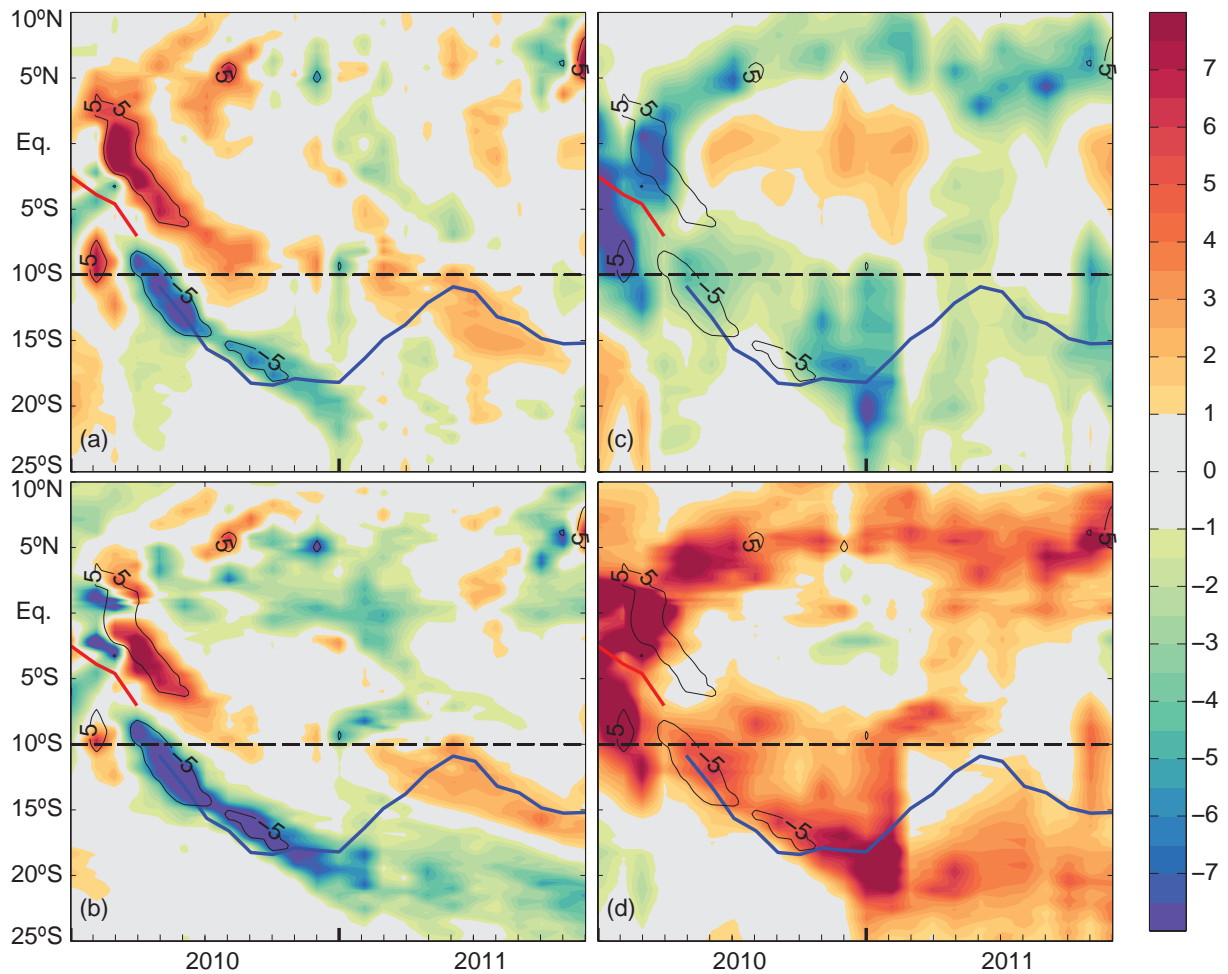
Figure 6. 2010-2011 latitude-time plot of the 170ºE-180ºE averaged SSS trend (a), horizontal SSS advection (b), surface (c) and subsurface (d) forcing. The solid line is identical to the one on Figure 5. Unit is pss yr$^{-1}$.

A positive anomaly in SSS tendency of the order of +5 pss yr$^{-1}$ stretches from about 5°N in early 2010 to 8°S in mid-2010 (Fig. 6a), and a negative anomaly of similar amplitude spans from about March to December 2010 between 7°S and 20ºS. As expected, these two events are consistent with the SSS changes portrayed by Figure 5. During these two events, the horizontal advection (Fig. 6b) seems to be the main driver of SSS changes. To better analyse this term, the respective contribution of the zonal (u) and meridonal (v) currents and off-line computed SSS gradients ($S_x$ and $S_y$; Fig. 7a-d) is investigated. Strong changes in zonal current occur in early 2010 in the form of three anomalies with alternating signs centred around the equator, 8ºS and 13ºS (Fig. 7b). They are linked to the westward intensification of the equatorial and southern branches of the SEC as well as to the eastward intensification of the SECC already documented during La Niña events in the area (Delcroix and Picaut, 1998).

The anomalies of the zonal SSS gradient ($S_x$) are however not always concomitant with the current anomalies (Fig. 7a). Therefore the zonal advection term (off-line computed $u.S_x$) holds a minor role in the SSS changes everywhere but near the equator in early 2010. In contrast, Figures 7cd indicate that the positive and negative SSS tendencies described above for Figure 6b are chiefly due to changes in the meridional SSS gradient (Fig. 7c), as there is virtually no change in meridional velocity (Fig. 7d). The displacement of the warm/fresh pool due to ENSO does modify the meridional SSS gradients in our study domain. During La Niña, starting in boreal spring 2010, the fresh pool shifts back to the western equatorial Pacific and the equatorial upwelling penetrates farther to the west. This results in an increase of both the equatorial SSS (Fig. 5a) and the meridional SSS gradient (Fig. 7b). As a consequence, there is by mid-2010 an important bipolar meridional gradient anomaly shifting south with time, positive between the equator and 8ºS and negative from 8ºS to 17ºS. The combination of this bipolar anomaly and almost-steady southward current generates significant changes in the SSS.
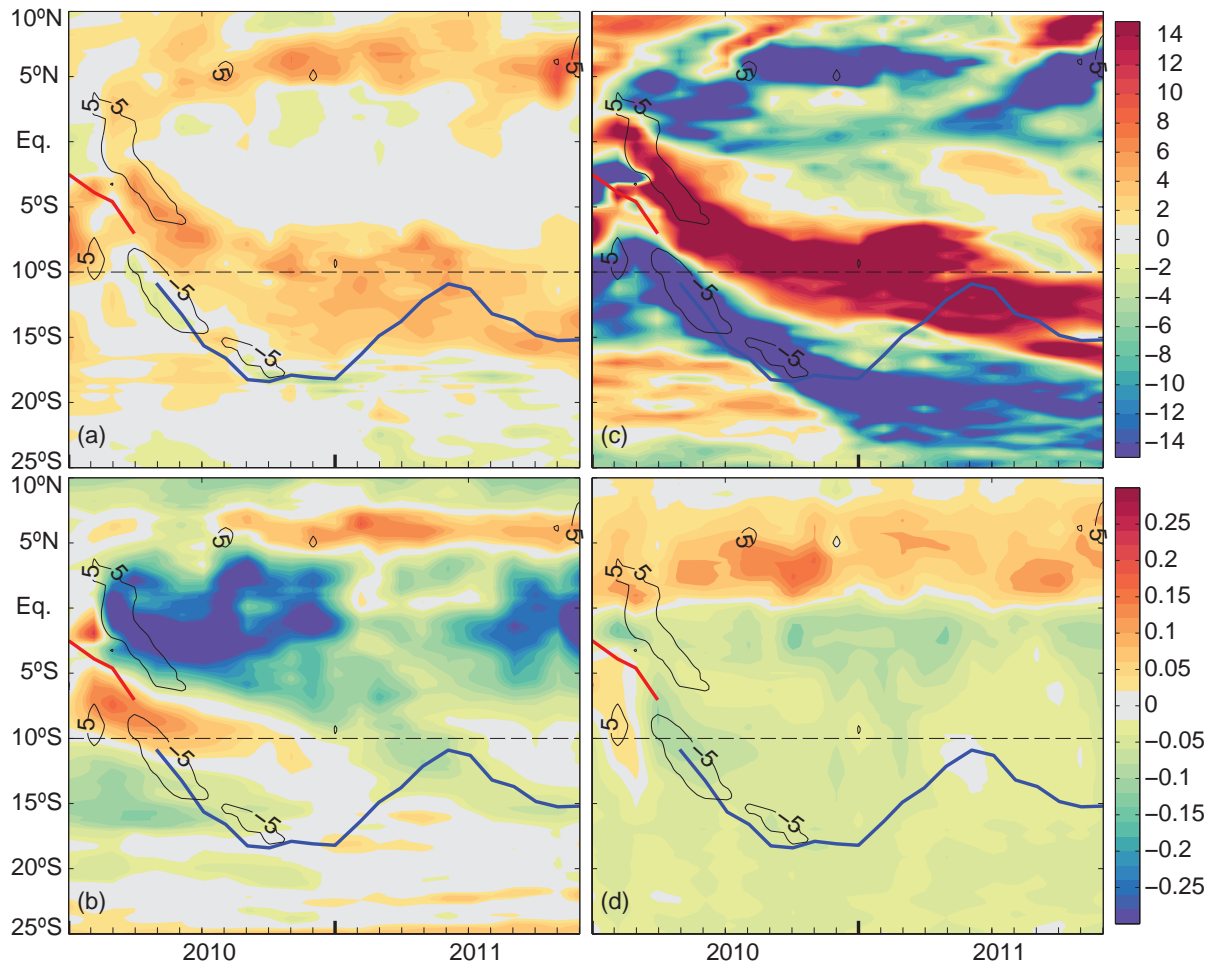
Figure 7: 2010-2011 latitude-time plot of the 170ºE-180ºE averaged zonal and meridonal SSS gradients (pss per degree longitude and latitude, respectively; a, c) and zonal and meridonal currents (m/s; b, d). The solid line is identical to the one on Figure 5.

Figure 6c shows a negative anomaly of surface forcing between 5ºN and 10ºS in early 2010, with values below -7 pss yr$^{-1}$ enhancing the negative SSS tendency. Examination of the off-line P and E modelled fields indicates that this surface forcing term is mainly modulated by P (not shown). By mid-2010, the La Niña phase develops and the equatorial surface forcing anomaly changes from negative to positive. A north-south dipole of surface forcing is in place from mid-2010 to mid-2011. The positive anomaly of surface forcing around the equator faces a negative anomaly south of 10ºS. The positive anomaly (decrease of P) is linked to the La Niña induced westward shift out of our domain of the ascending branch of the Walker circulation. The negative anomaly south of about 10°S (i.e., increase of P) is due to the enhanced activity of the SPCZ during La Niña. As described in Hasson *et al.* (2013) for a different time period, the subsurface forcing has a damping effect on SSS changes by enhancing mixing through the strengthening of the vertical S gradient (Fig. 6d). Subsurface forcing also damps the effect of horizontal advection away from the equatorial band but to a lesser extent.

## V. Comparison with the 1998-1999 La Niña

This section underlines similarities and dissimilarities between the 1998-1999 and 2010-2011 La Niña events in terms of SSS changes and driving mechanisms. The 1998-1999 La Niña event followed an extremely strong El Niño event that lasted from early 1997 to mid-1998 (Fig. 1). Observations and models indicate that the 1997 El Niño event was characterized by equatorial waters fresher than 35 pss extending unusually from the fresh pool as far as to the American coast, chiefly driven by horizontal advection to the west of 160ºW and surface forcing to the east (Vialard et al, 2002; Hasson *et al.*, 2013a). By mid-1998, easterlies resume in the eastern Pacific increasing equatorial SSS. These SSS changes are caused by the uplift of high-salinity water from below (equatorial upwelling) and the rainfall diminution as the ITCZ moves back north to its original position. The horizontal advection shifts the fresh-pool (SSS<35 pss) back to the western part of the basin (west of 170ºE).

94

Figure 5d shows the latitude-time plots of the modelled SSS anomalies (relative to the 2002-2011 period) averaged within 170°E-180°W longitudes, i.e. where the greatest anomalies occurred during 1998-1999. The ISAS product does not cover the 1998-99 La Niña period and could therefore not be used to assess the model. The modelled SSS was however compared to the gridded SSS product described in Delcroix et al (2010) and showed very good agreement (not presented here). From Figure 5ad, observed SSS anomalies are rather similar in 1998-1999 and 2010-2011. However the low-salinity waters (say, SSSA<-0.5 pss) appear later in the equatorial band and move further south in 2010-2011. Figures 8a-d show the latitude-time plots of the SSS tendency and of the three forcing terms for 1998-1999 period. The zonal processes at work in the 1998-1999 La Niña (Fig. 8b) are very similar to the ones in the 2010-2011 one (Fig. 6b). They force SSS to decrease around the equator as the zonal SSS gradient is weakly positive in 1998-1999 (Fig 9a) and the zonal current is always westward. One can also find during the first half of 1998 the alternating positive and negative anomalous zonal current from north to south, as seen in 2010-2011 (Fig. 7b and 9b). It is responsible for the positive SSS advection anomaly around 13ºS together with a gradient anomaly. Dissimilarities between the two La Niña events appear in the meridional advection and more precisely in the meridional SSS gradient, as the meridional current is rather steady: southward (northward) in the southern (northern) hemisphere.
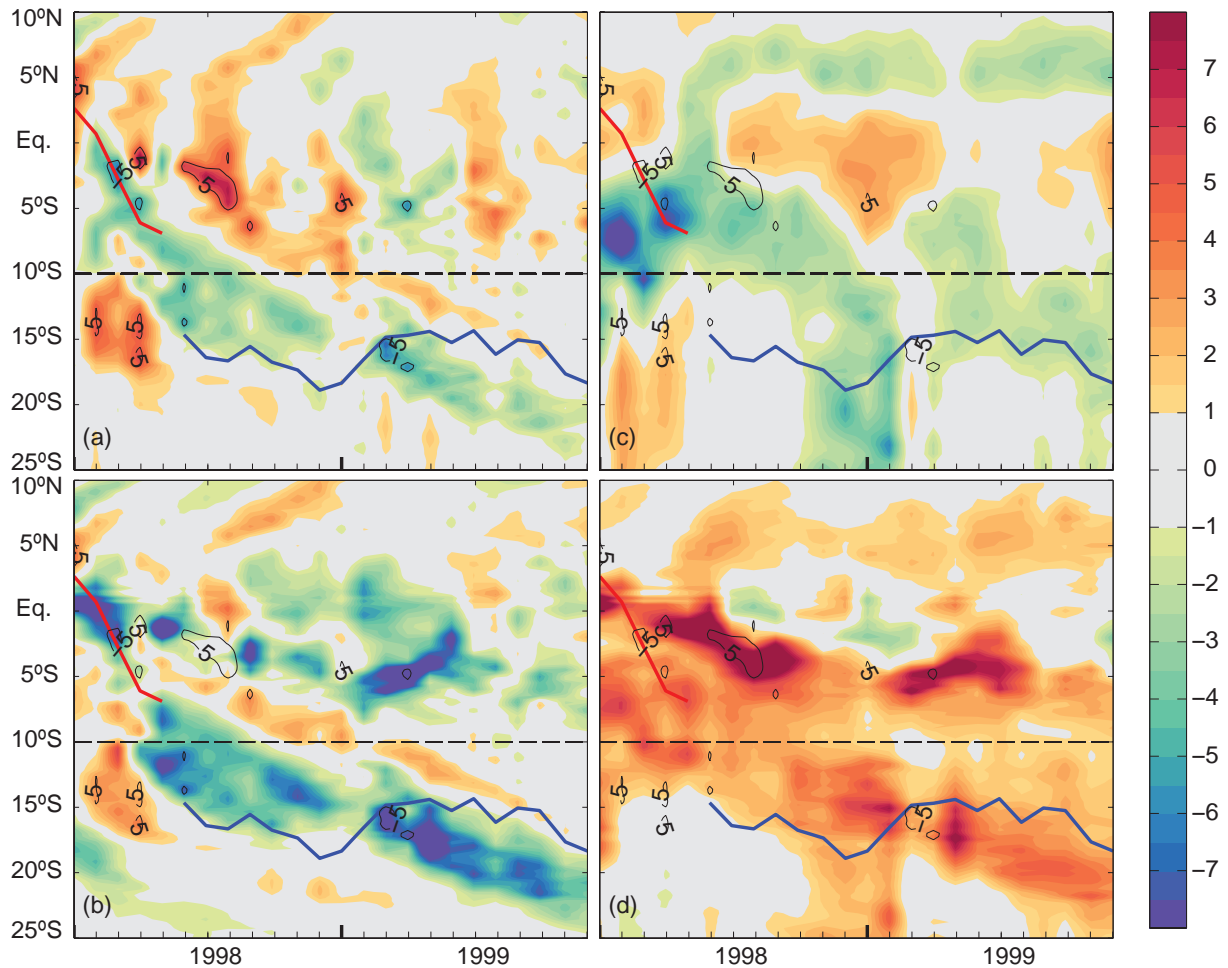
Figure 8: Same as Figure 6 but over 1998-1999.

The surface forcing is consistent with what was described in previous studies and between the two events (Figure 6c and 8c). During the last months of the preceding El Niño events, very strong precipitations (negative salinity surface forcing) occur from the equator to about 10ºS, and the opposite poleward. Delcroix and Hénin (1991) observed similar patterns from bucket SSS measurements (~165ºE) for the ENSO events of the 1969-1988 period. As in 2010, the 0-10ºS negative anomaly decreases and eventually becomes positive in early 1999 establishing the North-South dipole described earlier. The SPCZ that was not active south of 10ºS in 1998 becomes vigorous in early 1999.

Once again, the subsurface forcing acts as a strong inhibiter of SSS changes, which increase the vertical gradient and enhance the subsurface forcing efficiency (Fig. 8d). From January 1998, the meridional SSS gradient between the equator and 5ºS is much stronger that the one observed in 2010-2011. The produced anomalous negative advection is fully damped by subsurface forcing. The effect of strong precipitation events lasting for a few months around January 1998 and 1999 is also greatly diminished by the subsurface counter effect.
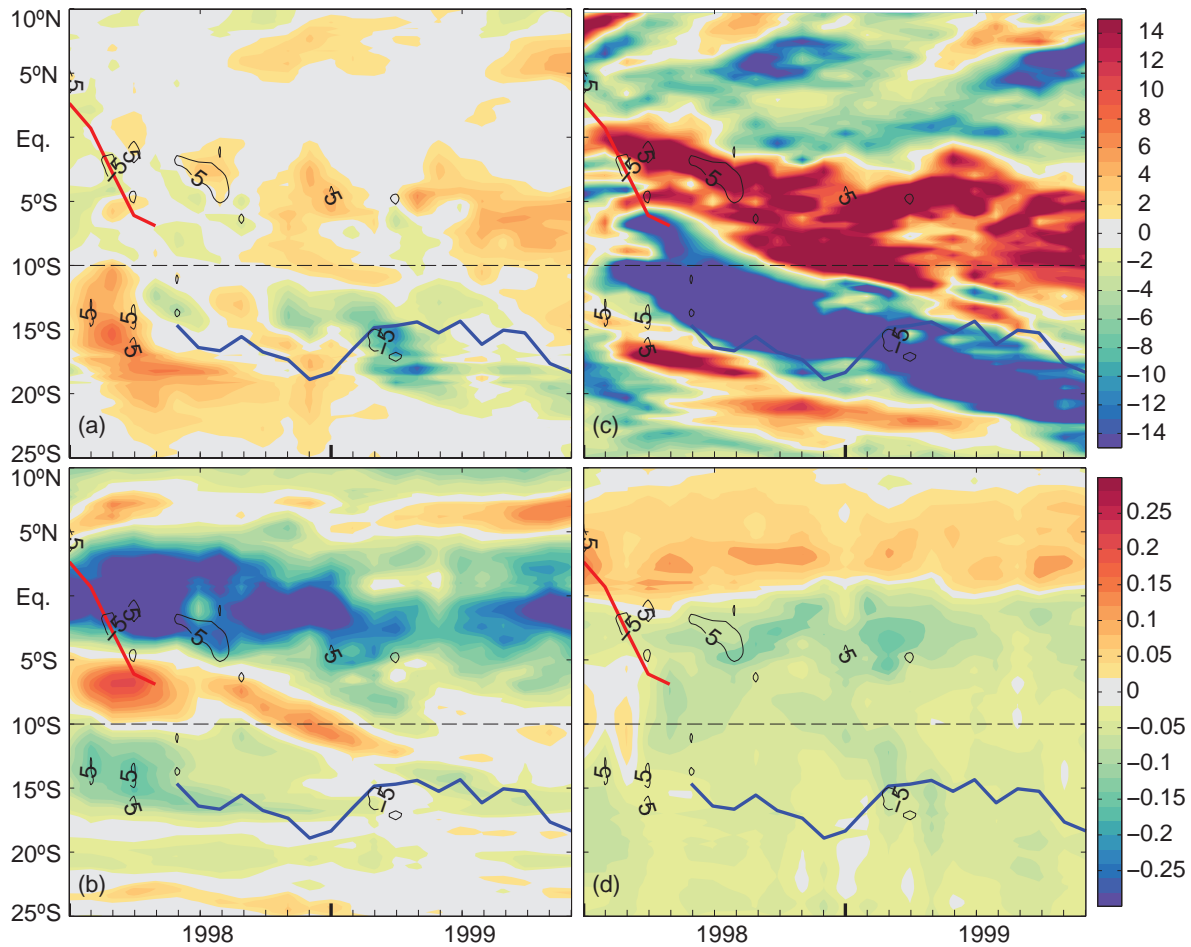
Figure 9: Same as Figure 7 but over 1998-1999.

## VI. Summary and Conclusion

The ENSO cycle is the largest interannual variation of the Earth's climate, and includes a warm El Niño phase and less-documented cold La Niña phase. In this study, we compare and investigate the SSS anomalies captured by different *in situ* observations and for the first time by satellite-derived (SMOS) observations during 2010-2011. During this period the tropical Pacific was in a long La Niña phase following a strong El Niño in 2009. We further quantify the responsible mechanisms using a validated DRAKKAR model simulation.

By the end of the 2009 El Niño, all our SSS datasets show a strong bipolar anomaly in the western half of the tropical Pacific, with a negative anomaly in the equatorial band (< -0.8 pss) and a positive anomaly south of about 8ºS (> + 0.8 pss), in agreement with El Niño previous studies (Delcroix, 1998; Singh *et al.*, 2011). From mid-2010, during La Niña, a

positive anomaly sits north of 10ºS, a negative northwest-southeast SSS anomaly lies between 10ºS and 20ºS and a positive one south of 20ºS. In 2011, anomalies shift south and amplify except from the one south of 20ºS reaching again an intensity above 0.8 pss.

The processes associated with these SSS changes were studied from the DRAKKAR simulation output, which also provides the various terms of the SSS budget but the entrainment. The analysis of the salinity tendency terms indicates that horizontal advection is the main driver of the modelled SSS changes. Looking at each horizontal advection components, it has been found that the meridional component dominates. Even though important changes in zonal velocity occur at the beginning of 2010, this term does not have such a great impact on SSS changes since the strong zonal SSS gradient anomalies are rarely concomitant. Meridional advection was mainly governed by changes in the meridional SSS gradient, as the meridional velocity was rather constant in 2010-2011. In turn, changes in the meridional gradient resulted from the ENSO-related displacements of the fresh waters of the warm pool and SPCZ. In early 2010, the fresh pool actually moves back to its westernmost position and the SPCZ shifts back south.

The modelled SSS was also affected by the surface forcing, mainly due to precipitations which are very much modulated during ENSO. A north-south dipole of surface forcing was in place from mid-2010 to mid-2011. During La Niña the ascending branch of the Walker circulation is at its western-most position causing the suppression of precipitations in the western-central equatorial Pacific (positive E-P anomaly). The high precipitations brought by the very active SPCZ shift back south of 8ºS (negative E-P anomaly). The subsurface forcing mainly has a damping effect on SSS changes induced mostly by surface forcing but also on horizontal advection.

Similarities and dissimilarities of the 2010-2011 and 1998-1999 La Niña signal in SSS and linked processes have also been discussed. The zonal processes in the western-central Pacific are very similar for the two La Niña events. This is not the case for the meridional advection. The main difference is the position of the fresh waters from the warm pool and SPCZ area which is governed by the preceding El Niño. Surface forcing is consistent for the two events but shifted south by a few degrees in 1998-1999. The subsurface forcing plays the same role during the two events and inhibits changes which increase the vertical gradient and enhance the subsurface forcing efficiency.

The use of complementary datasets such as the ones described in the present study is critical to document the ocean state and its variability such as ENSO at the basin-wide scale. The ground breaking satellite-based SSS data derived from SMOS (and also Aquarius/SAC-D, although not examined here) provides a global new source of information to study the ocean. However, such new stream of data require proper calibration and validation, in which high resolution *in situ* data play a key role. The *in situ* measurements are furthermore essential to study SSS at high resolution and before the satellite launch, as well as for assessing the realism of model simulations. Modelling is essential not only to examine and quantify processes behind the observed SSS variability but also to study changes at time scale longer than interannual as for instance, decadal variability and global change. An optimal combination of all these datasets into a merged product, maybe through the use of data assimilation, would definitely be of use.

## Aknowledgements

## References

All references can be found at the end of this manuscript.

# Chapter 5. Formation and Variability of the South Pacific Sea Surface Salinity Maximum in Recent Decades

## Foreword

Most studies on salinity in all basins have investigated variability either on the global scale or in regions of high variability. These regions correspond to precipitation-dominated regimes. In the present chapter, motivated by the scientific rational detailed in the Introduction section of the following accepted article, the maximum salinity core in the south tropical Pacific Ocean is depicted on the mean, seasonal and longer time-scales using two objectively analysed observation-based datasets, the forced model as well as ground-breaking SMOS data. We also investigate in details the mechanisms behind the surface salinity variability using the model only.

## Article

The following article has been accepted for publication in the Journal of Geophysical Research on the 22nd of August 2013.

Hasson, A. E. A., T. Delcroix, and J. Boutin, Formation and Variability of the South Pacific Sea Surface Salinity Maximum in Recent Decades, *Journal of Geophysical Research, accepted.*

## Abstract

This study investigates causes for the formation and the variability of the Sea Surface Salinity maximum (SSS>36) centred near 18°S-124°W in the South Pacific Ocean over the 1990-2011 period at the seasonal timescale and above. We use two monthly gridded products of SSS based on in-situ measurements, high-resolution along-track Voluntary Observing Ships thermosalinograph data, new SMOS satellite data, and a validated ocean general circulation model with no direct SSS relaxation. All products reveal a seasonal cycle of the location of the 36-isohaline barycentre of about +/- 400 km in longitude in response to changes in the South Pacific Convergence Zone location and Easterly winds intensity. They

also show a low frequency westward shift of the barycentre of 1400 km from the mid 1990's to the early 2010's that could not be linked to the El Nino Southern Oscillation phenomena. In the model, the processes maintaining the 22-year equilibrium of the high salinity in the mixed layer are the surface forcing ($\sim+0.7$ pss yr$^{-1}$), the horizontal salinity advection ($\sim-0.35$ pss yr$^{-1}$) and processes occurring at the mixed layer base ($\sim-0.36$ pss yr$^{-1}$).

# I.  Introduction

The global distribution of mean Sea Surface Salinity (SSS) shows the existence of one large-scale high-salinity core centred within about 15-30° latitude in each hemisphere of the Atlantic and Pacific oceans (e.g., Levitus, 1986). Analyses of observations and model outputs have indicated that these cores mainly owe their existence to the positive Evaporation minus Precipitation (E-P) budget and wind-driven Ekman salt transport, the latter accounting for the 5 to 10° latitude poleward shift of the SSS maxima relative to the E-P maxima (e.g., Delcroix and Hénin, 1991; Foltz and McPhaden, 2008; Qu *et al.*, 2011).

The climatic relevance of these high-salinity cores has been discussed in many articles. At seasonal to decadal time scales, salinity (and so density) changes in these cores affect the source branches of Shallow Tropical-subtropical overturning Cells (STCs) and the generation of spiciness anomalies (McCreary and Lu, 1994; Gu and Philander, 1997; O'Conner *et al.*, 2002; Nonaka and Sazaki, 2007; Kolodziejczyk and Gaillard, 2012). These, in turn, are thought to influence the mean background temperature distribution in the equatorial band and hence could modulate low-frequency tropical variability (Schneider *et al.*, 1999; McPhaden, and Zhang, 2004; Laurian *et al.*, 2009). At the multi-decadal time scale, the observations of positive salinity trends in these cores have been interpreted as the likely signature of global change (Cravatte *et al.*, 2009; Durack and Wijffels, 2010; Terray *et al.*, 2012). To the first order, these trends result from the E-P forcing increase in positive E-P regions, as expected by the Clausius Clapeyron relationship in a warming world (Held and Soden, 2006; Seager *et al.*, 2010). Recent model studies further suggest that not only the amplitude but also the location of the maximum E-P forcing may change in future climate in response to global warming (Seager *et al.*, 2010; Scheff and Frierson, 2012). It is thus crucial to monitor SSS changes in these cores in order to better understand their relation to climate change. Besides, these large spatial areas of rather constant SSS with different SST, wind

stress and E-P conditions are ideal for the calibration and validation of SSS estimates from SMOS and Aquarius satellites.

Studies of high-salinity cores have so far mostly focused on the northern hemisphere structures. Little work has been done for the southern hemisphere, mostly due to the lack of sufficient observations. The goal of this paper is therefore to analyse causes for the formation and variability of the poorly documented south Pacific high-salinity core, relying on multi decadal *in situ* SSS data collection, recent SMOS-derived measurements, and a validated OGCM simulation. As shown in Figure 1a, the mean core stretches as an ellipse-type surface in the eastern half of the south tropical Pacific around 25°S-10°S and 150°W-100°W. The SSS values are always higher than 36 pss over a mean surface of 5.2 x 10$^6$ km$^2$ that is about 2/3 of the Australian continent size.
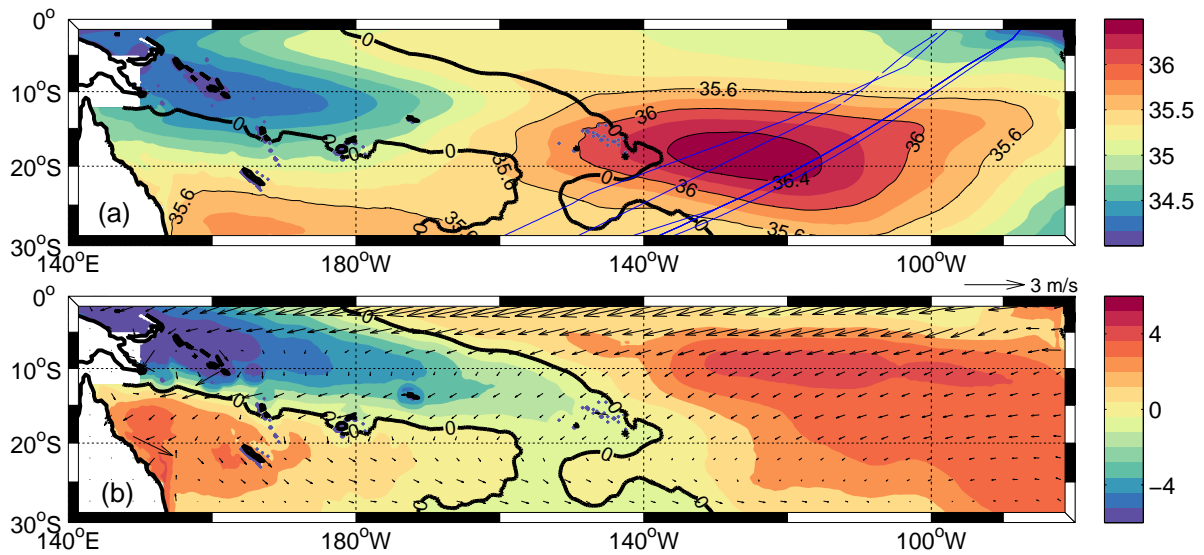


Figure 1 (a) Mean 1990-2011 modelled mixed-layer salinity. The blue lines represent the Matisse Ship routes of 2010 and 2011 discussed in the main text. (b) Mean Evaporation – Precipitation (E-P) based on ERAi; units are mm/day. Overplotted as arrows are the mean modelled surface currents. The 0 isohyet is shown on both panels with a bold black solid line.

The paper is organized as follows. Section 2 describes the *in situ*, SMOS and model derived SSS, and compares these complementary SSS products; section 3 focuses on causes of the core formation looking at its mean salinity budget; and section 4 analyses its seasonal and interannual variability and 'long-term' trend. Summary and conclusion appear in the last section.

## II. Data Description and Assessment

We use the Pacific Ocean gridded SSS product from Delcroix *et al.* (2011) which is available monthly on a 1° longitude by 1° latitude spatial grid, within the 30°N-30°S, 120°E-70°W domain from 1950 to 2008. This product, recently extended to 2009, is an objective analysis of *in situ* observations collected within 0-10 meter from Voluntary Observing Ships (VOS), TAO/TRITON moorings, Argo buoys and CTD casts. Following Hasson *et al.* (2013, hereafter HDD13), only gridded values with normalized errors less than 0.7 will be considered, restricting our confidence to values located in western half of the high-salinity core before the Argo era (see HDD13). As a complement, especially for studying the recent interannual changes, we also use the 6th version of a monthly, ½° by ½° global (77ºS-66.5ºN) gridded SSS product. The SSS values are there derived from an objective analysis of Argo data using the In Situ Analysis System (ISAS) tool not including VOS measurements (See Gaillard et al., 2009). This product covers the 2002-2012 years, but only data with an associated error below 80% were kept. Consequently, most data from 2002-2003 are discarded because of the poor data coverage in our studied region. Argo data between 0 and 10 meters was averaged to represent SSS.

We also use the original high-resolution along-track *in situ* SSS data collected from VOS crossing the high-salinity core along two different routes during their southward and northward voyages between Europe and New Zealand via the Panama channel (see Fig. 1a, blue lines). The French SSS Observation Service has installed thermo-salinographs (TSG) on VOS as early as 1992. Median SSS values assumed to represent 0-10 meter are recorded every 5mn (i.e., every 3 km at 20 knots) from prescribed 15s sample rate (Hénin and Grelet, 1996). The data quality was estimated from different tests involving comparisons with climatology, daily bucket samples collected on board and collocated near-surface Argo data. Only "Good" and "Probably Good" flagged data were kept for our study (see Alory *et al.*, 2013).

We further use the outputs of an OGCM ran by the DRAKKAR group using the NEMO z-coordinate model (Madec *et al.* 2008) in its version 3.2.1. The model configuration (ORCA025.L75-MRD911) has been presented in details by HDD13. The run was extended by 2 years and now covers the 1990-2011 period. The simulation was forced by a globally corrected ERA-interim reanalysis to prevent direct SSS restoring. Each term of the salt conservation equation (see Eq. 1 below) was computed at each simulation time step (960

seconds). The simulation output is archived every 5 days, on its original global 0.25° latitude by 0.25° longitude grid mesh with 75 vertical levels. Salinity values within the upper 9.8 m were averaged to represent SSS.

SMOS satellite was launched in November 2009 and retrieved SSS data is available from January 2010 to present. We use the ESA level 2 data (v5 reprocessing) weighted averages produced by the LOCEAN team in Paris as described in Boutin *et al.* (2013). It does not include strong relaxation to the climatology and thus preserves interannual variability (Reul *et al.*, 2013). SSS maps are made of SSS (assumed to represent the 0-10 cm) averaged over 10 days or one month and over 1°x1° and are oversampled on a 0.25° latitude by 0.25° longitude grid. As noted above, high-salinity core regions are ideal for satellite SSS retrieval as SST is warm (above 20°C), wind is moderate, and in the particular case of the South Pacific Ocean the core is also far from land and far from Radio Frequency Interferences (RFI) sources. In addition, in the SMOS/ESA processing, a large part of the south-east Pacific region (45°S-5°S-95°W-140°W) is taken as a reference for calibrating SMOS data every two weeks, thus optimizing seasonal biases correction in our region.

The model outputs are routinely evaluated by the DRAKKAR team against various metrics, and it was further carefully evaluated within the tropical Pacific Ocean (30ºN-30ºS) in HDD13. The model outputs were compared to the 1950-2009 gridded SSS products described above and to the TAO-TRITON near-surface currents. The assessment showed, in particular, a good representation of the mean, seasonal and interannual (ENSO) variability in SSS. HDD13 further underlined the model ability to quantify all terms of the mixed-layer salinity (MLS) budget that can only be qualitatively computed or inferred as a residual from observations.

Boutin *et al.* (2013) evaluated SMOS SSS against the previously-noted ISAS product in various regions of the global ocean with a 5-day and 50 km colocation radius. In the northern subtropical Atlantic salinity maximum, they found a standard deviation of the difference of 0.28 and a mean bias of -0.13. In this study, we extend the colocation radius to 9 days, in order to cover the 18-day SMOS repeat sub-cycle. For the same region, this reduces the standard deviation of the differences by 18%.

The model and SMOS ability to reproduce small-scale *in situ* SSS was assessed for our studied region using 8 high-resolution VOS TSG transects. A representative example of a voyage across the high SSS core in February 2011 is shown in Figure 2. For a collocation radius of 9 days and 50 km (and averaging the along-track *in situ* SSS data over 20-30 km, i.e. close to model and SMOS grid sizes), the standard deviations of the differences between

SMOS and in-situ SSS and modelled SSS and in-situ SSS are 0.20 and 0.26, and the mean biases are -0.08 and 0.07, respectively (statistics computed over 1,502 data points).



Figure 2 Comparison between near-surface salinity data derived from (black line) the TSG instrument installed on board M/V Matisse and the collocated SSS: (dashed line) modelled and (dotted line) SMOS values. The Matisse salinity values were obtained during 20-27 February 2011 along the northern shipping line shown in Figure 1a.

Having gained reasonable confidence in the model and SMOS data, the remaining part of this paper relies mostly on the model outputs enabling us to properly quantify terms of the salinity budget; whenever available, the gridded *in situ* and/or SMOS SSS data will be used to reinforce our conclusions.

## III.    Causes of the high-salinity core formation

The mean modelled SSS, surface current and E-P forcing fields for the south tropical Pacific are shown in Figure 1 to set the context. (See Figure 1a from HDD13 for an analogous observed SSS map). As stated above, there is a clear southwest shift between the location of the SSS maxima (SSS > 36 pss) and the E-P maxima (> 2 mm/day), consistent with the mean

surface current direction. Not shown here, the location of mean E-P maxima coincides with the location of maximum wind speed that governs the strength of E process. To quantify causes of the high-salinity core formation, we looked at the MLS budget. Following HDD13, the MLS balance may be written as:

$$\underbrace{\partial_t \langle S \rangle}_{I} = \underbrace{\frac{(E-P)}{H} \cdot \langle S \rangle}_{II} - \underbrace{\langle \vec{u}_h \cdot \vec{\nabla}_h S \rangle}_{III} + \underbrace{\frac{(w_e + d_t H) \cdot \delta S}{H}}_{IV} + \underbrace{\langle \vec{\nabla}_h (K_h \cdot \vec{\nabla}_h S) \rangle}_{V} + \underbrace{\frac{\partial_z (K_z \cdot \delta S)}{H}}_{VI} \qquad (1)$$

where $\langle X \rangle = \frac{1}{H} \int_{-H}^{0} X(z) dz$, S denotes salinity within the mixed layer of depth H, (E-P) the Evaporation and Precipitation difference (defined positive out of the ocean), $u_h$ the horizontal velocity vector averaged within the mixed layer (having (u) and (v) components defined positive eastward (x) and northward (y), respectively), $w_e$ the entrainment velocity at the base of the mixed layer, $\delta S$ the salinity jump at the base of the mixed layer, and $K_h$ and $K_v$ the horizontal and vertical diffusion coefficients respectively. We consider influence of river runoffs as negligible in the southeast tropical Pacific. The term (I) in Equation (1) is referred to as the MLS tendency, term (II) as the surface forcing, terms (III) and (V) together as the horizontal advection, and terms (IV) and (VI) together as the subsurface forcing.

Figure 3 shows the 1990-2011 averaged contributions of the surface and subsurface forcing and horizontal advection terms for high-salinity regions delimited by three different isohalines. Where SSS is 36.0 pss or saltier, the 1990-2011 MLS tendency is +0.02 pss/year (not shown). The surface forcing is the dominant (positive) term, removing fresh water from the ocean, with a mean contribution of about +0.73 pss/year. On average the off-line calculation based on the model output suggests that E and P respectively account for about +4/3 and -1/3 of the surface forcing term. Horizontal advection makes a negative contribution to the salt budget, bringing low-salinity waters from the northeast (see Fig. 1a), with a mean contribution of -0.36 pss/year (i.e., -0.08, -0.15 and -0.12 pss/year for zonal and meridional advections (term III) and horizontal diffusion (term V), respectively). About half of the surface forcing is thus balanced by horizontal advection, the other half (-0.35 pss/year) being due to the subsurface forcing, by mixing high-salinity waters with waters below the near-surface layer. Figure 3 also quantifies the mean salinity budget in regions delimited by the 35.6 and 36.4 isohalines. Overall, the surface forcing remains rather constant for any chosen high-salinity regions, while the horizontal advection decreases and the subsurface forcing increases as the isohalines grow. This is due to a reduction of the horizontal salinity gradients

and to an increase of the vertical salinity gradients (not shown here) from the 35.6 to the 36.4 pss and saltier regions.
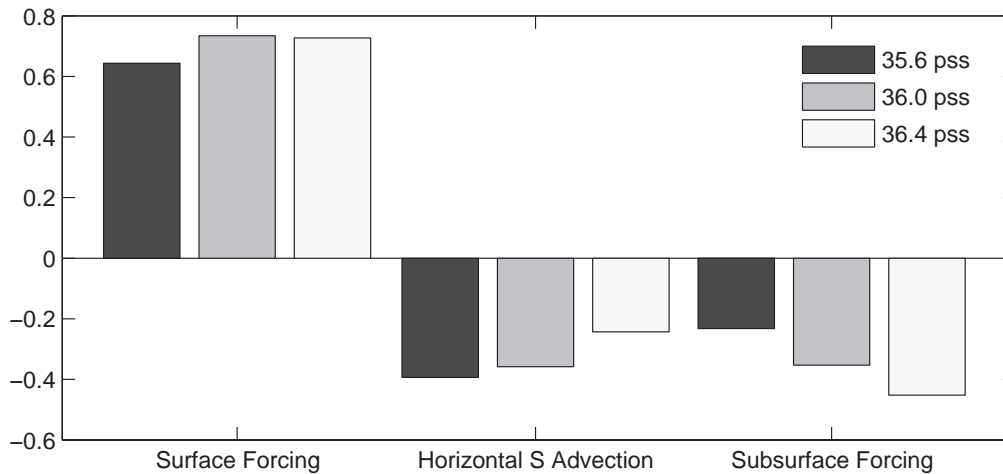


Figure 3 Mean modelled mixed-layer salinity budgets in the high-salinity regions bounded by the 35.6, 36 and 36.4 isohalines shown in Figure 1a.

## IV.    Variability of the high-salinity core

### IV.1.    Seasonal variability

To analyse the seasonal variability of the high salinity region, we constructed a MLS mean monthly year from both the 1990-2011 modelled and the 1990-2009 observed data, and for each of the terms in Eq. (1). The monthly climatologies were calculated after filtering the possible influence of interannual (ENSO) changes, as detailed in HDD13. As only two years (2010-2011) of data were available for SMOS, the corresponding mean year in MLS was constructed without filtering.

The modelled high-salinity region (SSS > 36 pss) shows virtually no seasonal variability in its absolute maximum SSS values and size (not shown) but does in its location as indicated by the horizontal displacements of the monthly 36 isohaline contours in Figure 4a. The 36 isohaline extends as far as 155°W to the west during austral summer and 100°W to the east in winter with weak meridional displacement. The mean 36-isohaline barycentre is located at 18.4°S - 123.8°W. It reaches its easternmost position in March (120.3°W) and westernmost position in September (127.7°W), driving a zonal cycle with around 400 km amplitude (see the coloured dots on Fig. 4a and black dots on Fig. 5a). The seasonal meridional cycle of the barycentre is relatively negligible. The SMOS-derived zonal barycentre cycle (stars on Fig. 5a) is close to being in temporal phase with the modelled one.

There are however a couple of degrees of latitude shift possibly reflecting issues in SMOS SSS retrieval and/or the different considered time periods and ENSO filtering. The same comparison cannot be directly applied to the Delcroix et al. (2011) gridded SSS product as the eastern half of the high salinity region lacks of *in situ* data and thus holds a mean normalized error above 0.7 (see HDD13). As an alternative, the barycentre displacement was compared for data west of 120ºW only from both the model and the gridded product (grey dots and diamonds on Fig. 5a). Again, the observed and modelled barycentre seasonal displacements do agree. Hence, observations both from SMOS and the gridded product show seasonal zonal displacements consistent with the one reproduced by the model, giving more confidence in the model ability to reproduce this real feature.
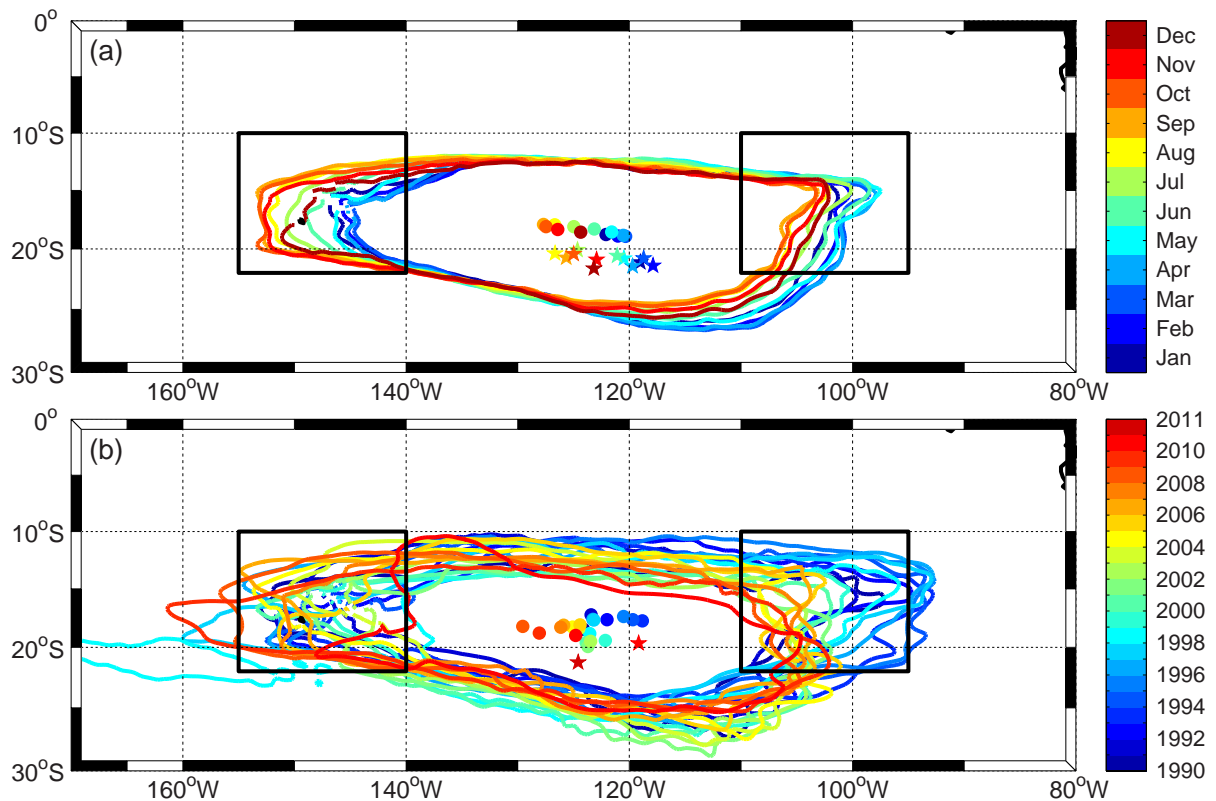


Figure 4. (a) Monthly and (b) annual mean positions of the modelled 36-isohaline. On both panels the coloured dots and stars show respectively the barycentre of the modelled and SMOS-derived 36 isohalines. The two rectangles denote the *east-* and *west-boxes* discussed in Section 4.

The model offers a mean to understand the mechanisms behind this zonal cycle as each term of the MLS budget can be examined. Two zones (black boxes on Fig. 4a) on the western (10°S-22°S, 155°W-140°W, *west-box*) and on the eastern (10°S-22°S, 110°W-95ºW, *east-box*) sides of the high MLS core have been designed to capture its movements. Because

of its displacement, the MLS variations in the two boxes are in anti-phase (Fig. 5b). The MLS tendency and three main processes (Fig. 6) have a seasonal cycle in anti-phase from east to west. The examination of each term of the MLS budget shows the prevailing role of the surface forcing in both zones, the horizontal advection and subsurface forcing being much weaker.



Figure 5. (a) Mean seasonal variability of the longitudinal location of the barycentre of high-salinity (S>36 pss) waters based on the model (black dots) and SMOS (stars) datasets, and with data only west of 120°W for the model (grey dots) and the VOS-derived SSS gridded product (GSSS, diamond). (b) Mean seasonal SSS anomaly in the *east-box* (Model – solid line) and in the *west-box* (model and gridded product – dashed lines).

The analysis of the surface forcing field indicates that the seasonal displacements of the high salinity region are mainly due to the synchronous variation in the intensity and position of the South Pacific Convergence Zone (SPCZ) and of the Easterly winds. In austral summer (DJF), the SPCZ is very active, its eastern portion reaches the *west-box*, and P is high (see Vincent, 1994), decreasing SSS in the *west-box* (Fig. 5b). The surface forcing is damped by the opposite effect of subsurface processes, which is more efficient as the surface freshening increases the vertical salinity gradient. In the *east-box*, the Easterlies are stronger than average, increasing evaporation and SSS. Subsurface processes are less efficient since it lies in a region of subduction (Nonaka and Sazaki, 2007) where vertical salinity gradient

across the mixed layer base is weak. From these combined effects, the high-salinity region and its barycentre reach their eastern-most position in March. Following the SPCZ seasonal cycle, the reverse mechanism takes place in austral winter (JJA). The SPCZ and the associated heavy P move towards the equator and Easterlies are weaker than average. As a consequence, SSS increases in the *west-box* and decreases in the *east-box*, forcing the high-salinity region and its barycentre to move back to the west.
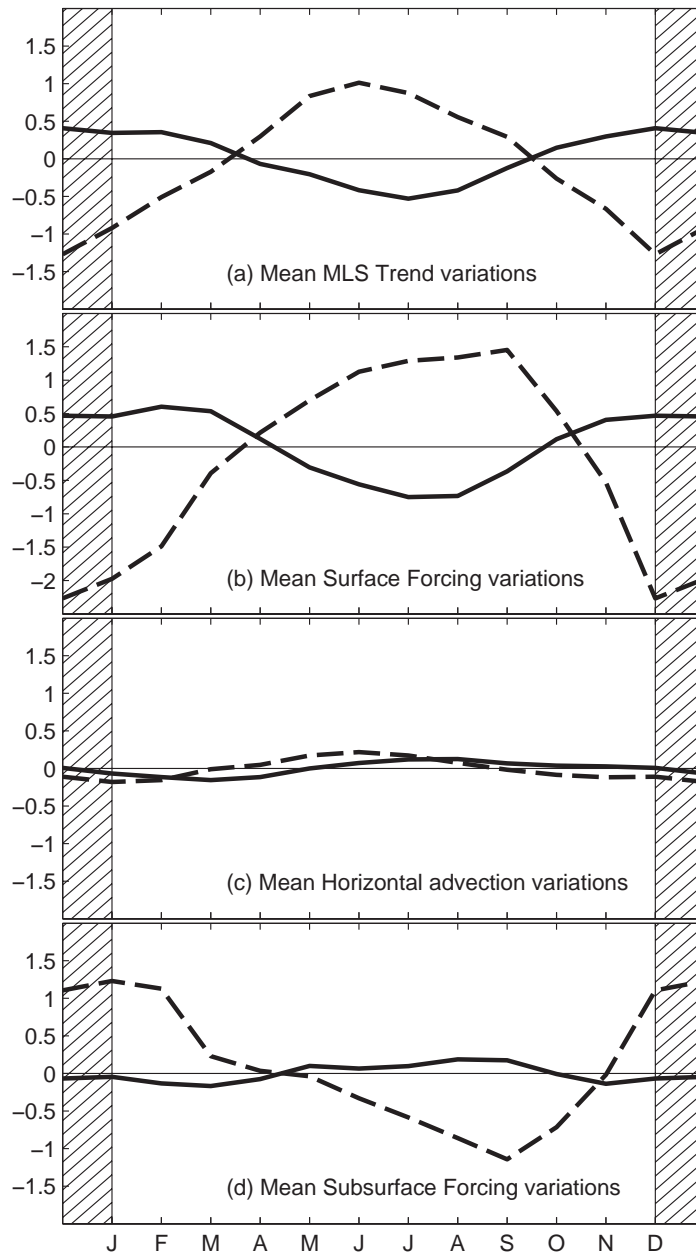


Figure 6. Mean seasonal variations of the model-derived (a) mixed-layer salinity (MLS) tendency and contributions of (b) the surface forcing, (c) the horizontal advection and (d) the subsurface forcing within the *east-* (solid lines) and *west-boxes* (dashed lines) shown in Figure 4. Units are pss per year.

## IV.2. Interannual Variability

The evolution of the SSS maximum region is further investigated on timescales greater than annual, using model and observed data. Following HDD13, the low frequency signal is extracted by filtering with a 13-month Hanning filter the difference between the original timeseries and the mean year described above (except for SMOS data).
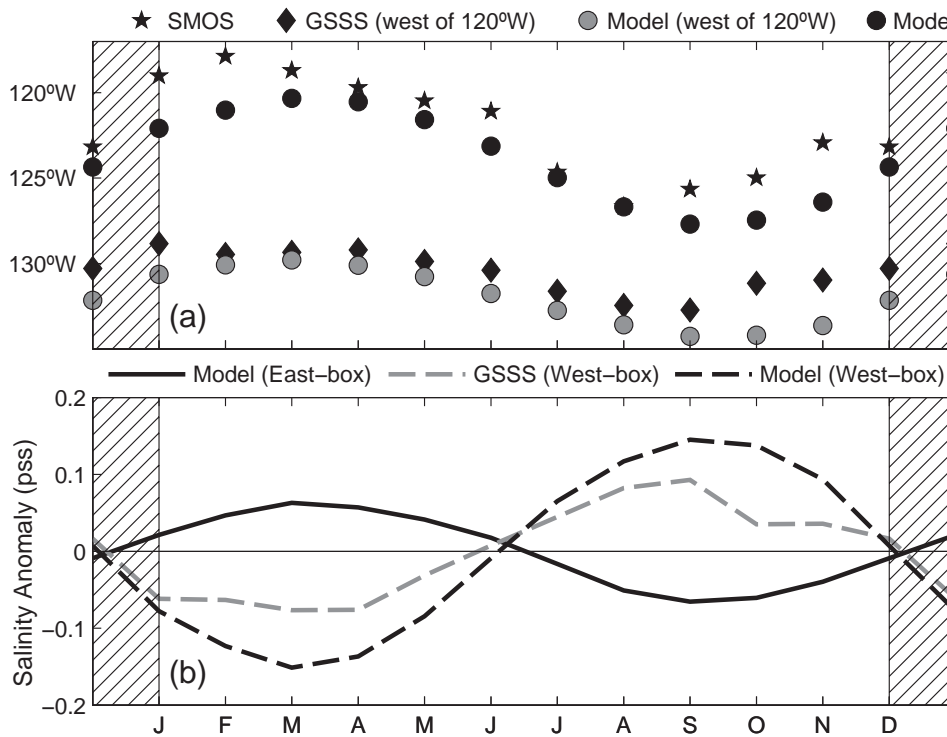


Figure 7. (a) Interannual variability of the longitudinal location of the barycentre of high-salinity (S>36 pss) waters based on the model (black dots, left axis) and SMOS (stars in 2010, left axis) datasets. Interannual sea surface temperature anomaly in the Nino3.4 region (dotted line, right axis). (b) Modelled interannual mixed-layer salinity (solid black line), VOS-derived SSS (dashed line), and ARGO-derived SSS (solid grey line) in the *east-box* shown in Figure 4. (c) same as (b) for the *west-box*. The horizontal thin lines in (b) and (c) represent the 1990-2011 averaged modelled MLS in the east- and west-box, respectively. Averaged SSS from observational products are shown only when at least half of the data within the boxes is above the error criterion described in Section 2.

The high salinity core shows very weak variability in its barycentre meridional displacement (280 km peak to peak) but significant zonal displacements over the 22-year simulation (Fig. 4b). The easternmost position of the mid-year (July) 36 isohaline contours

shift gradually westward by about 1000 km from about 95°W in the early 1990's to about 105°W in the late 2000's. The position of the contours westernmost edge does not show such a steady shift during the same time period. The annual barycentre positions have an essentially zonal displacement, with a quasi-steady westward shift of the order of 1400 km during 1990-2011 (Fig. 4b and Fig. 7a). Even though no certain conclusion can be drawn from the short SMOS time series, the westward shift of the barycentre does appear in 2010-2011, with a magnitude comparable to the modelled shift (stars in Fig. 4b and 7a). From 2004, the region includes a sufficient number of VOS-TSG data and Argo measurements so that the two derived in situ gridded products can be compared to the model output. Despite a mean difference of the order of 5-degree of longitude with the model, both in situ datasets show a westward displacement of the barycentre location (Figure 8), in agreement with the modelled shift.
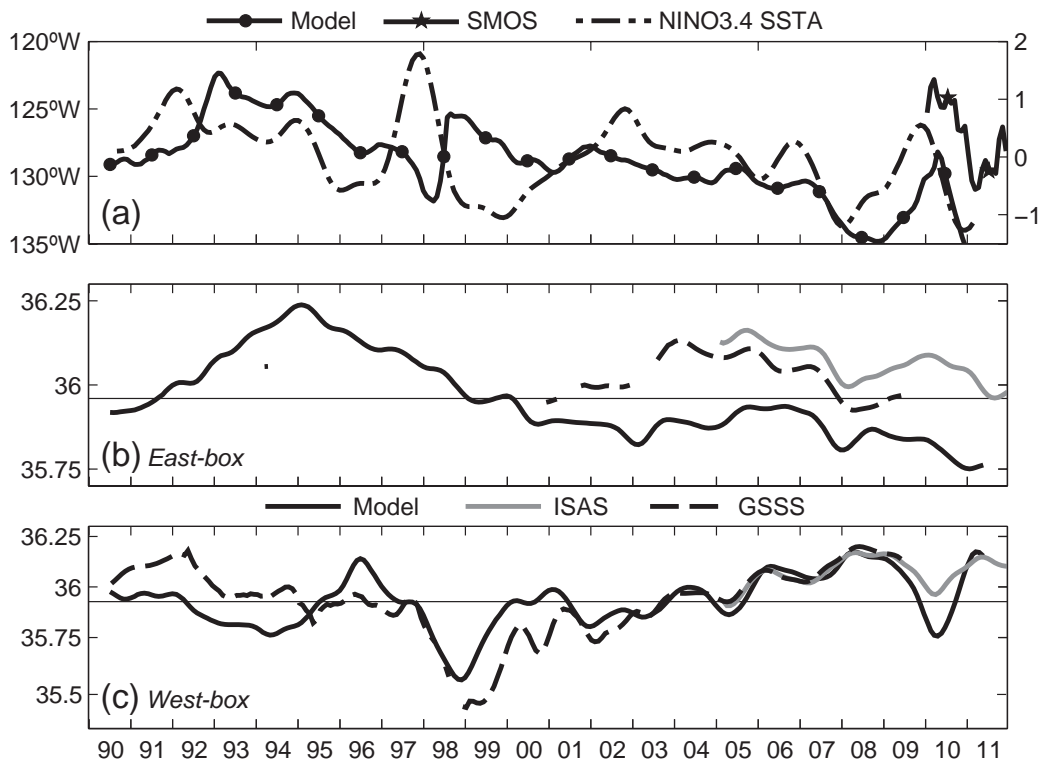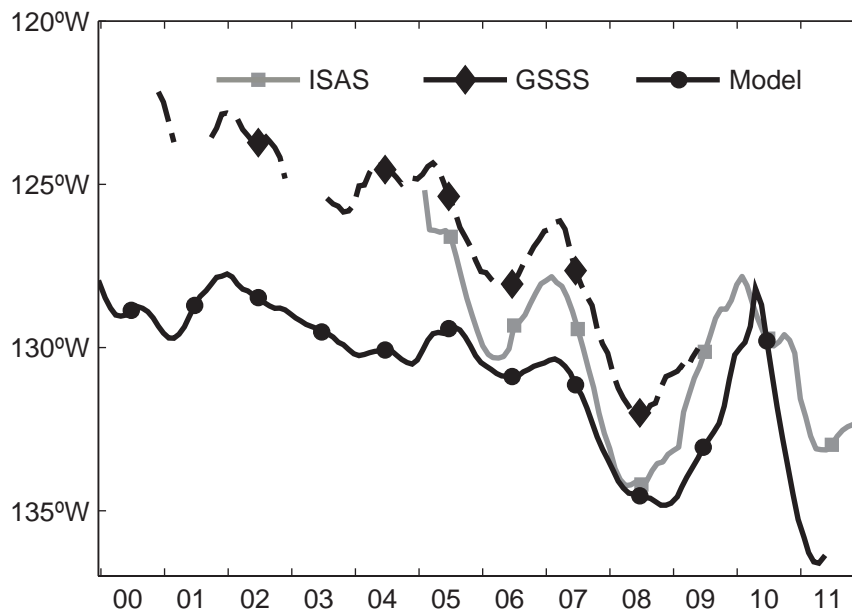


Figure 8. Interannual variability of the longitudinal location of the barycentre of high-salinity (S>36 pss) waters based on the model (black dots), the VOS-derived (black diamonds) and ARGO-derived (grey squares) gridded SSS product datasets. Barycentre locations are shown for the observations only when at least half of the data within the east-box is above the error criterion described in Section 2.

Changes in modelled MLS within the east and west boxes are also investigated to better understand the 36 isohaline interannual zonal movement. Figures 7bc indicate good agreement between the modelled MLS and the corresponding changes in observed SSS, when

available. Unlike the seasonal variations, the two MLS time series are not in anti-phase. The *west-box* MLS shows strong interannual variability, anti-correlated (R=-0.6) with a 9-month lag to the modelled NINO3.4 SST (Fig. 7a) used as an ENSO index. This anti-correlation however mostly reflects the MLS decreases during the 1998-99 La Nina event, in agreement with the observational results of Gouriou and Delcroix (2002). The link between the *west-box* MLS variability and the remaining La Nina and El Nino events is not that clear, if any. The lack of well-marked El Nino signature is not surprizing during the Central Pacific El Niño types in 1992-95, 2002-05, and 2009-10, as they were shown to have a weak regional impact on observed SSS (Singh *et al.*, 2011). In contrast, the *east-box* MLS does not exhibit interannual changes, even during 1998-99. Figure 7bc further shows that at the decadal time scale, the *west-box* MLS increases from the late 1990's to the early 2010's, whereas the *east-box* MLS freshens almost linearly from the mid-1990's to the early 2010's. This is consistent with the quasi-linear westward shift of the 36-isohaline barycentre position. Except when we have sufficient observations, conclusions should be drawn with care. One should keep in mind that such a westward shift cannot be checked over two complete decades with observations in the eastern half of the high-salinity core.

All terms of the MLS budget in the eastern and western boxes were also investigated in order to understand mechanisms responsible for the low-frequency displacement of the high-salinity core. In agreement with the analysis above, all terms are found to be statistically uncorrelated to the modelled NINO3.4 SST (or other ENSO indices), preventing us to derive conclusions regarding possible ENSO effects. At the decadal time scale, Table 1 indicates that the long-term mean salinity tendency over 1994-2011 is about +0.3 and -0.3 in the *west-* and *east- boxes* respectively. These MLS changes reflect the contribution of the surface forcing, subsurface forcing and horizontal advection terms, which are mostly of analogous importance, nearly compensating each other. They also are one order of magnitude larger than the resulting MLS tendency. As a consequence, it is difficult to identify the true origin(s) of the modelled westward shift (that does exist in nature), which is mainly due to a small decrease of the east box salinity and to a small increase of the west box salinity. Both salinity changes are small residual of large changes in the corresponding MLS terms.

|  | West Box | East Box |
|---|---|---|
| Advection | -5.1 | -13.5 |
| Subsurface | +18.2 | -12.7 |
| Surface | -12.8 | + 25.9 |
| Total | +0.3 | -0.3 |

Table 1 Long-term (1994-2011) averaged contribution of the different terms of the MLS budget for the so-called east and west boxes (see Figure 4). Advection denotes the terms III + IV, Subsurface the terms IV + VI, and Surface the terms II in Equation (1). Units are pss per 18 years.

## V. Summary and conclusions

This study examines causes for the formation and variability of the salinity maximum waters (SSS > 36) located in the south eastern tropical Pacific (centred at 18.4°S and 123.8°W) and covering a region of about 5.2 x 10$^6$ km$^2$ over the 1990-2011 period. This work relies on situ and SMOS-derived SSS data to document the main features, and on a validated DRAKKAR simulation to quantify mechanisms at play. This work is motivated by the need to improve our understanding of maximum salinity waters, in line with the interpretation of climate and hydrological cycle changes at different time scales.

From the model output, waters with salinity above 36 pss result from a balance between the surface forcing (E-P) that increases the MLS by about 0.73 pss/year, and the compensating horizontal advection and subsurface forcing. Each of these two processes decreases the salinity by about half of the surface forcing. The ratio between the three processes is consistent with what was found by Qu *et al.* (2011) in the North Atlantic Salinity Maximum. The modelled salinity maximum waters have their 20 year average salinity increasing by 0.02 pss/year which is qualitatively consistent with the "dry get dryer" paradigm although stronger than estimated from different observation datasets and time periods by Terray *et al.* (2012) and Durack and Wijffels (2010). The observations and the model both show high-salinity waters variability at the seasonal and longer time scales. At the seasonal time scale, salinity maximum waters shift eastward in austral summer and westward in austral winter, with an amplitude of 400 km. This is the consequence of the changing intensity of the SPCZ and easterly winds that modulate P and E, respectively. At longer time

scales, the salinity maximum waters barycentre was found to move westward by about 1400 km during 1990-2011, with no clear relationship with the occurrence of individual El Nino / La Nina events.

While we have assessed processes responsible for the formation and seasonal variability of the maximum salinity waters, using different types of data, we have not clearly identified causes for the low-frequency variability. The westward shift of the salinity maximum waters remains puzzling, and is worth to be further investigated. The shift is not noticeably linked to ENSO, though it corresponds to a tendency for more La Nina than El Nino events (see the cooling trend of NINO3.4 SST in Fig. 7a). It also corresponds to a tendency for more Central than Eastern Pacific El Nino types during 1990-2011, suggesting a plausible association with ENSO. Interestingly, our findings are consistent with the expected effects of the westward shift of the eastern edge of the SPCZ (and related regional P decrease) in future climate projections (Brown *et al.*, 2013). It however somewhat differs from the poleward (and not westward) shift of the south-eastern Pacific dry zone and south-westward extension of the high-salinity waters predicted by general circulation models in a warming world (Seager *et al.*, 2010; Scheff and Frierson, 2012; Ganachaud *et al.*, 2013). The question about the westward shift is likewise of interest for biological studies, bearing in mind that salinity maximum waters in the studied region partly overlap with oligotrophic waters that have been shown to expand both northward and southward in recent years (Polovina *et al.*, 2008). Also, the impact of changes in the location of the high SSS core could impact the STC as noted in the Introduction. It is clearly another interesting issue through its potential impact on the downstream salinity fields, and possibly the mean background state of the equatorial band.

The degree of confidence we can have in the model outputs and/or its ERA-interim forcing sets from which we derived part of our results is obviously a central question. The DRAKKAR model basic variables have been carefully validated in earlier studies (e.g., Barnier et al., 2006; Hasson et al., 2013). In particular, it was shown that the model captures well the observed mean, seasonal and interannual SSS changes of the tropical Pacific. Furthermore, it provided a good representation of the observed surface zonal currents obtained from the TAO-TRITON moorings at 110°W, 140°W, 165°E and 156°E (i.e., the only long time series of direct current observations). The model outputs (and/or its ERA-interim forcing sets) are however obviously not perfect. We know, for instance, that the modelled equatorial zonal current variability tends to be underestimated by about 75%, and that the modelled MLD is on average 21% shallower than the observed MLD (Hasson et al.,

2013). The roles of such biases on the present results are not clear and admittedly need to be examined in details in further studies. Moreover, Hasson et al. (2013) have shown the present difficulty, not to say impossibility, to rigorously evaluate terms involved in the MLS balance using low-resolution gridded observational data only, such as gridded SSS products and surface currents estimated from altimetry and Ekman drifts. In other words, we cannot be 100% sure that the model reproduces the observed features for the good reasons. Notwithstanding, when observations are available, the systematic good correspondence between the observed and modelled mean and variability of the South Pacific SSS maximum indicates the likeliness of our results to be realistic. Based on about two decades of data only, it would be of great interest to extend our investigation with longer MLS time series, such as future *in situ* and remotely sensed observations, other validated model simulations, and/or climate model projections.

## Acknowledgements

## References

All references can be found at the end of this manuscript.

# Chapter 6. Conclusions and Perspectives

Salinity is one of the three fundamental physical variables the ocean dynamics together with temperature and pressure, as they control density. Salinity has been regarded for years as one of the Essential Climate Variables (ECV) within the Global Climate Observing System (GCOS). Most climate-related studies focus however on sea temperature and processes linked to salinity remain largely under-explored. This is explained by the difference in the number of observation data between temperature and salinity.

This final chapter of my PhD encloses 2 sections: conclusions and perspectives. The history of salinity measurement and its evolution through time are briefly recalled (as well as present-day available salinity datasets). It is followed by a short literature review on the near-surface salinity studies led in the tropical Pacific Ocean at all time and space scales. All articles from which these results come from are not cited here for conciseness but can all be found in the preceding chapters. The main results of the studies embodied in Chapter 3 to 5 are then summarized. The perspectives are divided into two sub-sections: one addressing rather technically oriented issues and the other discussing various scientific perspectives.

## I.  Conclusions

Theoretically, salinity is the "Total amount of dissolved material in grams in one kilogram of sea water" (Sverdrup et al, 1942). Over the last 100 years, research has improved our knowledge on salinity and its measurement leading to various evolutions of its practical definition. Nowadays salinity is mainly derived from the conductivity ratio of the water sample compared to a known solution. This definition is the official « Practical Salinity Scale 1978 » (Unesco, 1981); it is the format into which salinity observations are archived in international databases. Recently, new spaceborne measurements of ocean emissivity from SMOS and Aquarius/SAC-D satellites have enabled scientist to retrieve surface salinity.

Via the seawater Equation of State, salinity influences density and impacts the ocean dynamics and in particular geostrophic currents, deep-waters formation, and mixed layer depths. Moreover, salinity has no feedback on the atmosphere and therefore is an essential tool to track water masses, oceanic fronts and even the marine freshwater cycle. This underlines the importance of better understanding the mechanisms associated with salinity changes and why scientists attach an increasing importance to their study.

The growing understanding of salinity goes together with more observational datasets made available for all. Before the 1970s, salinity measurements were sparse in the tropics. Salinity observations have expanded greatly since the TOGA decade (1985-1994) with an increased number of systematic measurements from VOS and TAO-TRITON, PIRATA and RAMA moorings, drifting buoys, Argo profilers and, to a lesser extent, XCTD probes. Objective analyses and models have also been developed in the recent decades giving complete (though not necessarily accurate) 3D and sometimes 4D pictures of ocean salinity.

The Global Ocean <u>mean</u> near-surface salinity patterns are well known with inter-basins differences. The Atlantic and Pacific Oceans present similar patterns with low salinity areas in the tropical band near the atmospheric convergence zones (SPCZ and ITCZ), near large river mouths (e.g. Amazon, Niger) and at high latitudes. High salinity cores are found near each subtropical gyre. The Indian Ocean has a very peculiar salinity distribution with strong spatial variations.

The mixed layer salinity budget is maintained by the equilibrium of three forcing terms, at the surface (evaporation and precipitation), horizontally (advection, mixing and diffusion) and vertically through the base (entrainment, advection, mixing and diffusion). Only the surface and horizontal forcing terms can be inferred directly from observations and the vertical component can be estimated with their difference. All studies show, on the global scale, the role of all terms with equal importance.

My PhD study focuses on the near-surface salinity of the <u>tropical Pacific Ocean, whose mean spatial distribution is</u> characterised by two high salinity cores (one in each hemisphere) and large areas of low salinity. The western tropical Pacific is home to the so-called warm/fresh pool associated with specific vertical haline stratification, the barrier layer, which controls the density mixed layer depth. The fresh waters areas also present the largest variability and most studies have focused on these regions at (almost) all time scales.

The smallest (under a month and a few kilometres) and largest (pluri-decadal and above, global) scales studies are highly tributary to the temporal and spatial observations sampling. However it has been shown that small-scale salinity variability in space (less than 1° in longitude and latitude) and time (less than 1 month) can reach values of the order of 0.4 pss, illustrating the difficulties when interpreting sparse in situ data measurements. At time scales around a month and just above the TIWs generate variability in the surface salinity field within 10º off the equator. The recently launched Aquarius/SAC-D satellite has observed TIWs patterns in surface salinity. The seasonal variability is one of the strongest signals in

surface salinity and is located in the low salinity regions. It is mainly caused by the seasonal cycle of the precipitation associated with the ITCZ and SPCZ.

At the interannual time scale ENSO is the principal variability mode. ENSO is a well-known atmosphere ocean coupled phenomena with a periodicity ranging from 2 to 8 years, leading to strong salinity modifications in the western half of the equatorial band and along the mean SPCZ position mainly. ENSO alters the fresh pool horizontal and vertical haline distribution associated with currents, precipitation and temperature changes. The PDO is thought to be the main decadal signal over the Pacific Ocean with an oscillatory pattern affecting salinity and other oceanic parameters. The strongest signal in salinity is found in the warm-pool and SPCZ, which is consistent with the heavy precipitation band displacement with the PDO. Above the pluri-decadal time scale, climate shifts, trends and climate change can affect salinity. However, only a few extensive timeseries, for instance along regular VOS lines and from coral-derived paleo-salinity records, together with validated model simulation can be of use for long-term analyses. Observations show a freshening of the low salinity region over the last few decades. Analogous changes are found in climate projections linked with an intensification of freshwater cycle.

During the course of my PhD, I used complementary in-situ data sets, in-situ based gridded products and a numerical simulation to assess all terms of the mixed layer salinity budget equation (see Eq. II.1 in chapter X). The analysed observational datasets encompass surface salinity from VOS bucket samples, VOS-TSG, precipitation, evaporation, near-surface currents and mixed-layer depth. The gridded salinity products are derived from the objective analysis of different salinity datasets such as Argo profiles, VOS- and TAO/TRITON-TSG, drifters, etc. The innovative surface salinity derived from SMOS satellite was also used. The DRAKKAR model simulation was run from 1990 to 2011 and forced by a corrected ERAi reanalysis. All terms of Equation II.1 but the entrainment were computed at the native model time-step and averaged and archived every 5 days in order to preserve the maximum small-scale variability. All data were treated using the MatLab software and most were filtered using a three-step Hanning filter approach to distinguish the seasonal signal from the interannual and above.

In the first study (Chapter 3), a broad description of the Tropical Pacific Ocean mixed layer salinity budget was given using both observations and the model simulation over two decades (1990-2010). Only the mixed layer salinity tendency and horizontal advection terms

were computed from gridded observations. The remaining forcing terms (subsurface forcing, horizontal mixing and diffusion) were inferred all together a residual. The model reliability was assessed by direct comparison with in-situ data and by "reproducing" the observed mixed layer salinity budget. In order to do so, a third modelled dataset called "ObsLike" was built to mirror the observations temporal and spatial grid resolutions. The differences between the original and "ObsLike" modelled budget underline the relatively poor ability of observational data to catch the full MLS variability. Indeed, only the original dataset includes diffusion/mixing, vertical advection and entrainment at the ML base, non-linear terms, as well as high-frequency (< 1 month) and small-scale (< 100 km) variability.

The observation based, ObsLike and original modelled budgets present analogous patterns in surface forcing outlining heavy precipitation in the atmospheric convergence zones (negative tendency) and string evaporation in subtropical areas (positive tendency). They also show corresponding patterns in horizontal advection with transport of low-salinity by the NECC and SECC (negative tendency) and of high salinity waters by the NEC and SEC (positive tendency). The eastern equatorial salinity advection signal, particularly strong in the full-resolution model output, displays high-frequency (<1 month) variability that cannot be accounted for with low-resolution observations. Even though patterns are opposite and of the same magnitude the surface forcing and horizontal advection do not balance each other, pointing out the importance of all terms to close the mean MLS budget.

The tropical Pacific Ocean mixed layer salinity variability is analysed with the original model output at seasonal and interannual timescales. The study focuses on processes associated with salinity changes in the high variability regions.

In accordance with the literature, the strongest seasonal signal was found along the ITCZ, SPCZ, in the western equatorial Pacific, in the northern part of the Coral Sea and off Central America. Processes in the ITCZ and SPCZ were found to be slightly different with a stronger influence from horizontal advection in the ITCZ as surface forcing principally drives salinity in the SCPZ.

At the interannual timescale, ENSO modulates salinity patterns primarily around the equator and in the SPCZ region. Salinity changes are mainly driven by horizontal advection in the western equatorial Pacific, as shown in past studies. Near atmospheric convergence zones, surface contribution is strongly linked to the heavy precipitation bands migration. In the SPCZ, changes are largely due to horizontal MLS advection. In all regions, subsurface processes modulate both the other contributors, damping variability.

ENSO events are unlike one from another and salinity changes were further analysed for the contrasted 1997-98 EP and 2002-03 CP El Niño events. During the first months of both events, the fresh pool eastward displacement leads to the presence of low salinity waters in the equatorial western-central basin from horizontal advection. Only for the 1997-98 EP El Nino event, low salinity waters reach the eastern basin because of the persistence of negative MLS horizontal advection and enhanced negative surface forcing linked to the ITCZ shift. For both events, the subsurface forcing has a clear tendency to increase the MLS.

To sum up, this first study presents the processes responsible for the surface salinity mean distribution in the Tropical Pacific Ocean. It focuses on regions of high variability at seasonal and interannual timescales and underlines the different processes at the equator associated to the two El Nino flavours. The following study focuses on salinity changes in the SPCZ and warm-pool during the most recent 2010-2011 La Nina event. They are particularly well observed with the recent development of autonomous in situ and satellite-based instruments.

In the second study (Chapter 5), the SSS anomalies captured by the SMOS satellite during 2010-2011 when the tropical Pacific was in a long La Niña phase are described and compared to an in-situ based analysis. Moreover, we gave a possible explanation for it using the validated DRAKKAR model simulation.

All datasets present a strong bipolar anomaly in the western tropical Pacific by the end of the 2009 El Nino in agreement with observations of historical El Niño events. La Nina is in place from mid-2010 with positive surface salinity anomalies north of 10ºS and south of 20ºS and negative anomaly in between. During the second year of La Nina (2011), anomalies amplify and shift southward.

The associated processes are studied and the numerical simulation unveils the key role of the horizontal salt advection in the salinity changes. Horizontal salt advection is mainly governed by the meridional salinity gradient modulated by ENSO. In fact, in early 2010 under La Nina conditions the fresh pool moves back to its westernmost position and the SPCZ shifts back south. Surface salinity is also driven by the ENSO modified surface forcing patterns. During the 2010-2011 La Nina the ascending branch of the Walker circulation follows the fresh pool to the west and the SPCZ shifts back south to its pre-El Nino position. Both atmospheric systems are enhanced during La Nina and bring heavier than normal precipitations. Salinity changes are damped by the subsurface forcing which is however more sensitive to surface forcing.

Salinity changes and linked processes of the 2010-2011 La Nina are compared with the historical also quite-strong 1998-1999 La Nina event. Even though horizontal advection patterns are similar, the preceding El Nino modulates them via the salinity anomalies distribution. The same impact is observed on the subsurface forcing. The Walker circulation and SPCZ alterations are consistent for the two events leading to comparable surface forcing.

Studies regarding the subtropical low salinity variability regions, also known as maximum salinity regions, are limited even though they have been shown to be of importance for the interpretation of climate and hydrological cycle changes at different time scales. Moreover, these regions are strategic calibration spots for the salinity measuring satellites.

In the third study (chapter 4), the emphasis is put on the South Pacific SSS maximum region. This study aims at understanding the causes for the formation and variability of the salinity maximum waters (SSS > 36) located in the south-eastern tropical Pacific (centred at 18.4°S and 123.8°W). The region is first described with surface salinity observations and processes generating the maximum salinity core variability are quantified using the same validated forced model.

As was found in the North Atlantic, the salinity budget is a balance between the evaporation dominated surface forcing and the equally compensating horizontal advection and subsurface forcing. The modelled average salinity within the core increases by 0.02 pss/year over the 1990-2011 period. This is consistent with the dry-get-drier paradigm, but stronger than what as previously estimated from other studies based on different observations and/or time periods.

Seasonal and longer time scales variability of the high salinity core were revealed from the model and the observation datasets. The salinity core has a seasonal zonal displacement cycle with an amplitude of 400 km due to the seasonal surface forcing cycle. Moreover, a surprizing 1400 km westward shift of that core occurred during 1990-2011, with no clear relationship with the occurrence of individual El Nino / La Nina events. This real, though still-unexplained, shift is further discussed below

## II. Perspectives

### II.1. Technical issues

I've shown that the use of complementary datasets is critical to analyse the SSS variability and budget. On the one hand, when studying surface salinity variability from one type of in-situ observations solely, errors are difficult to identify - and thus to quantify - whether they directly originate from measurements (i.e. from the instruments), from sampling and/or averaging procedures because of the lack of sufficient data, and from the impossibility to measure terms of the MLS budget (in absence of suitable instrumentation). On the other hand, studying surface salinity variability from models only relies on tuned parameterisations, forcing datasets and all the implied errors. From a technical point of view, confronting results obtained from different datasets such as VOS, Argo, model and SMOS is thus crucial as it enables us to reinforce our conclusions whenever consistent.

Regarding observations, irregular sampling and averaging is an error source for the salinity budget. Delcroix *et al.* (2005) have underlined this effect on surface salinity estimates. I have presented in Chapter 3 the original and altered versions of the modelled salinity budget terms to illustrate the impact of sampling and averaging. The "ObsLike" dataset represents the observations sampling of data from which the budget is computed. The main difference was found in the eastern Pacific trapped closely to the equator and revealed the plausible important role of intraseasonal frequency (<1 month) MLS changes in closing the budget. This strong variability seems to be associated with TIWs.

As presented above at various time and space scales, the mixed layer salinity budget is not only the balance between sea surface forcing and horizontal advection but also between processes taking place at the mixed layer base. However, no observational dataset is available to study the impact of vertical velocity, mixing and small-scale variability on the budget on a global scale. Only a few studies have been carried out based on observations with dedicated instruments (see Lueck *et al.*, 2002, for a review).

Recently, the SPURS (Salinity Processes in the Upper Ocean Regional Study) experiment has been taking place to address the essential role of the ocean in the global water cycle. To do so, researchers study large-scale salinity changes in the North Atlantic salinity maximum core, simultaneously with those happening within the first meters depth. Most

notably, the 20-day Strasse campaign has sampled throughout a 100x100 km$^2$ region in order to follow very small-scale variability over a few days. Various instruments were deployed such as modified profiling floats and Lagrangian drifters, autonomous surface and underwater vehicles to measure near-surface salinity. Drifters have also been deployed to enable the evaluation of meso-scale and above variability. First results indicate high temporal variability associated with vertical mixing and horizontal meso-scale structures (as presented by Boutin et al. during the 2012 Fall AGU meeting). Further analyses from SPURS observations should help to better understand all terms of the surface salinity budget, especially at meso scales, and better apprehend the quality of surface salinity data from space and simulations.

I noted above that confronting results obtained from different data sets is crucial. This was actually done in the course of my study, for the in situ, satellite and model data, but not among the different SSS satellite products. Several SMOS and Aquarius datasets are presently available, some of which are described in Chapter 2 and more are to come. They all present advantages and disadvantages which, to be frank and given time constraints, I did not fully investigate. It would thus be interesting to test the sensitivity of the analyses presented in this manuscript using all of them, firstly to re-assess our results and possibly also to help improve SMOS data processing procedures.

Numerical simulations can provide the global field subsurface terms to close the salinity budget. However, mixing is parameterised in the model and only sporadic in-situ data presented above can be used to validate the output. It is therefore important to ask ourselves if the model properly reproduces the mixed layer salinity variability, and if it simulates the budget terms for the correct reasons?

Even though observations are primordial to study the salinity budget, modelling is a remarkable tool. Models provide hints concerning variability; which cannot be observed globally with the present datasets, such as the intraseasonal time-scale and below as well as the decadal time-scale and above. However, sensitivity testing should also be done on modelled based results with independent model (from NEMO and ERAi) like for instance HYCOM (Gordon et al., 2000) or ECCO (Wunsh et al., 2007). Moreover, most model simulations still need a surface salinity relaxation term to prevent large salinity drifts. Reasons for this un-stabilised salinity content within the ocean in models are not clear but they could be related to an inexact representation of the freshwater cycle.

To conclude, firstly, I believe that a better understanding of the observed horizontal and vertical meso-scale variability is clearly desirable *per s*e, especially in key regions, and to improve model simulations. I expect that progresses will be made in this direction, based

partly on the SPURS experiment. Secondly, I did not have time to test the sensitivity of my results by using other model simulations and other satellite-derived SSS products. This is clearly a technical issue, which would have been useful to address. Thirdly, I do realize that an optimal combination of all salinity datasets into a merged product would be quite useful to estimate salinity at various depths in order to reproduce the "best" variability at all scales. Again, I assume this will be done in the near future. Many products of this kind have been developed for other variables, for instance for sea surface temperature (Reynold *et al.* 2002) and sea level height (Ducet *et al.*, 2000), and the acquired experience would benefit the development of 'reliable' surface and sub-surface salinity fields, to the advantage of research studies and operational oceanography.

## II.2. Scientific perspectives

The salinity budget studies presented in this manuscript reveal various mechanisms underlying changes at intraseasonal to interannual timescales using a large pool of complementary datasets. The mean structure was documented and significant changes have been identified at these scales, either on the global or regional scale.

### II.2.1. Formation of the South Pacific SSS maximum

Despite knowing the mechanisms maintaining the south Pacific maximum salinity core (presented in Chapter 5), the reasons behind the precise geographical location of the core itself are not yet fully explained. Simple (or coupled) models could be used to study the build up of salinity cores at the global scale. A simulation from the ocean at rest with constant average salinity (e;g. fixed at 35 pss) could be set into motion with climatological forcing at the surface boundary to understand why the cores are in place. I sense this will further help us to understand the responsible mechanisms.

### II.2.2. TIW and surface salinity budget

As stated before, the TIW imprints the surface salinity field on the equatorial eastern Pacific Ocean. Lee *et al.* (2012) showed that high-resolution satellite SSS seems to be ideal to study the 17-day TIW. The likely role of TIW on the salt budget in the equatorial Pacific is still an open question which must be addressed using, for example, a similar methodology presented by Menkes *et al.* (2006) for the mixed layer temperature budget. They were able to rebuild each term of the mixed layer temperature budget (equivalent to Equation II.1) with daily output (with less than 1% error). Menkes *et al.* (2006) subsequently separated variability below 60 days with a boxcar filter and evaluated the effect of TIWs on the mixed layer heat budget. We have tried to reconstruct each term of Equation II.1 as shown in Figure III.5

(Hasson et al., 2013a, their Figure 5). This cannot be done with the monthly averages and 5-day archive presented in the studies above but should be tested for salinity with 1-day outputs.

*II.2.3.  The Barrier Layer and ENSO*

The role of the peculiar vertical stratification of the warm pool during ENSO events was not assessed in my PhD work. Vialard *et al.* (2002) have quantified the impact of haline stratification and horizontal gradient on the mixed layer depth, currents and SST in the equatorial band using a control and a modified simulation experiment (i.e. considering the salinity as constant for vertical mixing and horizontal pressure gradients computation). Both simulations are forced by observations at the surface boundary. Even though salinity was found to only weakly affect the mean state, it has no impact on the 1997-1998 El Nino development. Various studies have underlined the salinity likely role on the ocean prior to an El Nino but, to my knowledge, only one coupled model suggested that the BL is crucial for its development  (Maes *et al.*, 2002, 2011). This particular study compared control runs to modified simulations where the salinity had either no impact on the vertical mixing scheme or no impact on the horizontal pressure gradient force within the warm-pool. Differences appeared in the mean climatology and the low frequency variability. The fading of the barrier layer deepens the mixed layer and thus decreases the sensitivity of the coupling between SST, winds and atmospheric deep convection. This weakened coupling induces a sharp decrease in the amplitude of ENSO and even forces the ocean back to the mean seasonal cycle of the model.

As noted above, the barrier layer is though to play a key role in the El Nino development but, to my knowledge, no study has yet been conducted for differentiating its potential role behind the two types of El Nino: EP and CP. This could have been done during the course of my PhD, assuming I had enough time. The first step would be to assess the model ability to reproduce the barrier layer and its variability. It would then be interesting to analyse its role in the El Nino differentiation.

Besides, still regarding ENSO, causes for the interannual variability of the maximum salinity core are not clearly identified. Even though its position seem to be connected to ENSO with net changes in the 1997-1999 period (during very strong La Nina event), no evidence of such a link could be established outside this period.

### *II.2.4. Trend in salinity*

The westward shift of the salinity maximum waters also remains puzzling, and should be further investigated. The two salinity gridded products and the model output revealed the shift. We hypothesised on the possible link between this shift and the tendency for more Central than Eastern Pacific El Nino types during 1990-2011, suggesting a plausible association with ENSO. Based on around two decades of data only, it would be of great interest to extend our investigation with longer time series, such as future in situ and remotely sensed observations, other validated model simulations, a combined product as suggested above and/or climate model projections.

Several papers using observations and modelling have looked at long-term surface salinity changes. Various results are shown in Figure II.1 for the tropical Pacific only. They all show a consistent freshening of the warm pool and SPCZ region and, in agreement with our study, an increased salinity in the subtropical gyres (when data is sufficient).



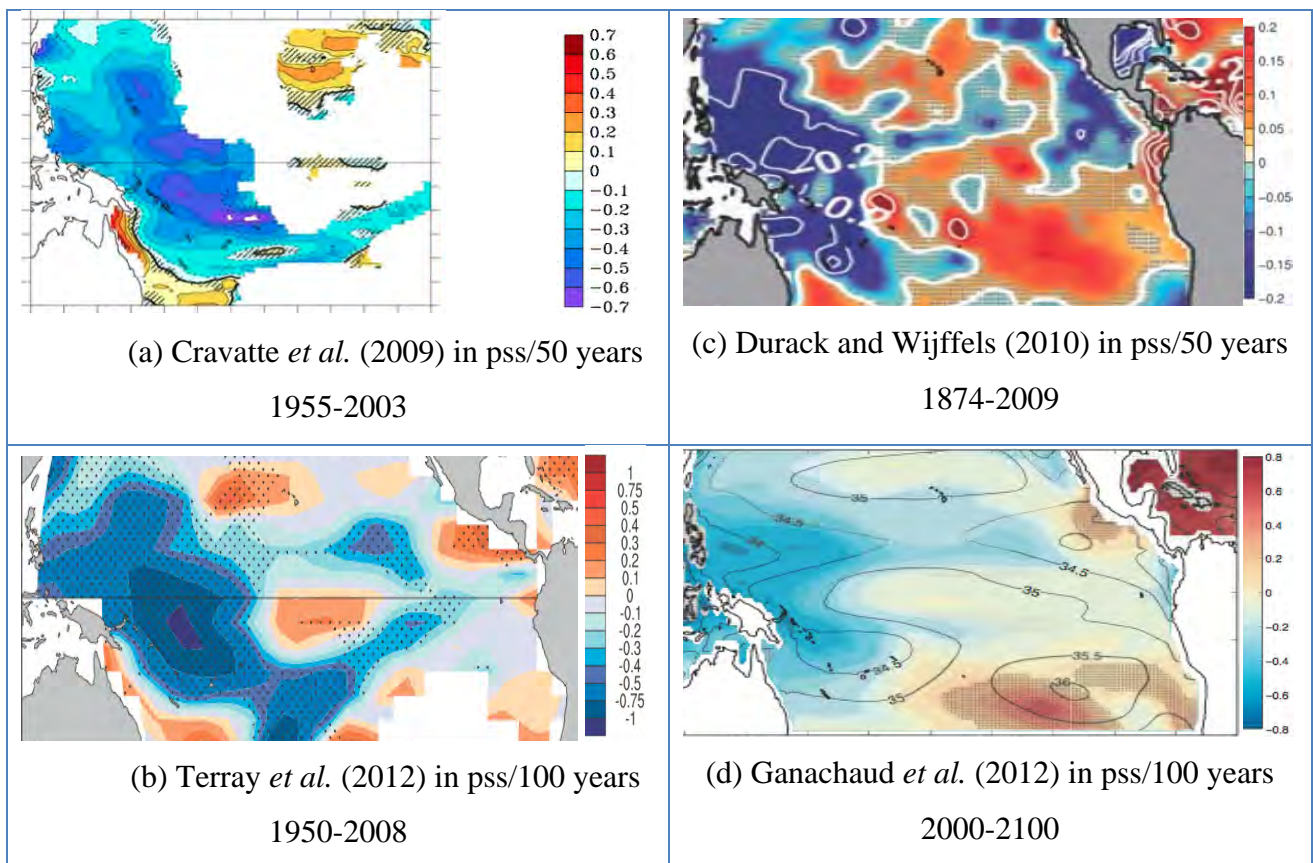|     |     |
| --- | --- |
| (a) Cravatte *et al.* (2009) in pss/50 years 1955-2003 | (c) Durack and Wijffels (2010) in pss/50 years 1874-2009 |
| (b) Terray *et al.* (2012) in pss/100 years 1950-2008 | (d) Ganachaud *et al.* (2012) in pss/100 years 2000-2100 |

Figure II.1 Changes in surface salinity in the tropical Pacific Ocean from Delcroix *et al.* (2011) gridded product described in Chapter II over different time periods (a) and (b), vertical profiles (mainly historical casts and Argo)(c) and multi-model mean 21$^{st}$ century projection under global warming (d).

It would be interesting to better understand these changes, which could be attributed to a change in evaporation, precipitation or ocean dynamics changes (i.e. any term of Equation II.I). Several studies have identified changes in precipitations in the SPCZ (e.g. Brown *et al.*, 2013), in the Walker circulation (Power and Smith, 2007) and on the global scale in climate projections (Seager *et al.*, 2010; Scheff and Frierson, 2012).

Changes in surface salinity on the long term can affect various biological and dynamical systems. Oligotrophic waters located in the subtropical gyre have indeed expanded both northward and southward in recent years (Polovina *et al.*, 2008). Moreover, changes in salinity affect the water mass density and may alter the STC and/or change properties of the waters exported to the equatorial band. This last hypothesis could be checked and analysed using a Lagrangian tracking tool such as ARIANE (Blanke and Raynaud, 1997).

Also, Cravatte et al. (2009) showed an eastward displacement of the SPCZ low salinity waters, and we showed a westward displacement of the salinity maximum core. Altogether, these changes should thus result in a strengthening of the SPCZ zonal salinity front, which might be interesting (and rather easy) to document and analyse with observational and modelling data sets.

## II.3. Inferring the marine fresh water cycle

Using salinity to improve our understanding of the global hydrological cycle variability at all timescales has a lot to offer when dealing with water management in region of water scarcity. Indeed, freshwater has often been called the « blue gold » as more and more people are under water stress. "Fierce competition for fresh water may well become a source of conflict and wars in the future" (Kofi Annan, 2001).

Several studies (some of which are cited in chapter I) have tried to derive atmospheric forcing (evaporation minus precipitation) from surface salinity changes and the reverse. However, this has proved to be difficult, even impossible in certain regions given all the oceanic processes involved (e.g. Vinogardova *et al.*, 2013). In order to do so, surface salinity changes and all near-surface oceanic processes must be known:

(1) The new surface salinity products from satellites enable researchers to capture salinity changes. Optimal combination of satellite and observation fields would be, as mentioned above, of great interest for a most accurate monitoring of surface salinity.

(2) Horizontal salt advection can be obtained from near-surface currents and salinity field. We showed in Chapter 3 the need for high temporal and spatial resolution to reproduce

the intraseasonal variability of the horizontal salinity advection. The observed currents dataset (OSCAR) presented in this thesis could not account for this variability. The production of high-resolution daily datasets is needed for this purpose either based on observations or on assessed models.

(3) Subsurface processes are shown in this thesis to be of prime importance to close the MLS budget. However they are not well monitored in the Global Ocean implying that large-scale analyses cannot be based on observations and models cannot be assessed. I think this is the key parameter that should be considered to be able one day to improve knowledge of the freshwater cycle using surface salinity observations.

Because evaporation and precipitation are difficult to estimate globally with accuracy, salinity has been thought to provide an alternative in quantifying freshwater fluxes. Two satellite missions have been developed in this context. However, to my knowledge, no study has yet been published regarding the use of observed (satellite and *in situ*) SSS to improve the representation of E-P. In the recent decades, tremendous improvements have been made in the observation and understanding of salinity at various time-scales but there is still a long way to go before using remotely sensed salinity data as a reliable inversed rain gauge.

*References*

# References

Adler, R. F., and Co-authors, 2003: The version-2 global precipitation climatology project (GPCP) monthly precipitation analysis (1979-present). *Journal of Hydrometeorology*, 4, 1147-1167.

Alory, G., C. Maes, T. Delcroix, N. Reul, and S. Illig, 2012: Seasonal dynamics of sea surface salinity off Panama: The far Eastern Pacific Fresh Pool. *Journal of Geophysical Research: Oceans*, 117, C04028.

Alory, G., et al., 2013: A global voluntary observing ships sea surface salinity network: data collection and quality control.

Ando, K., and M. J. McPhaden, 1997: Variability of surface layer hydrography in the tropical Pacific Ocean. *Journal of Geophysical Research-Oceans*, 102, 23063-23078.

Ashok, K., S. K. Behera, S. A. Rao, H. Weng, and T. Yamagata, 2007: El Nino Modoki and its possible teleconnection. *Journal of Geophysical Research-Oceans*, 112.

Ballabrera-Poy, J., R. Murtugudde, and A. J. Busalacchi, 2002: On the potential impact of sea surface salinity observations on ENSO predictions. *Journal of Geophysical Research-Oceans*, 107.

Barnier, B., R. Dussin, and J. M. Molines, 2011: Scientific Validation Report (ScVR) for V1 Reprocessed Analysis and Reanalysis: GLORYS2V1. MyOcean FP7-SPACE-2007-1 project, report MYO-WP04-ScCV-rea-CNRS.

Barnier, B., and Coauthors, 2006: Impact of partial steps and momentum advection schemes in a global ocean circulation model at eddy-permitting resolution. *Ocean Dynamics*, 56, 543-567.

Bingham, F. M., G. R. Foltz, and M. J. McPhaden, 2010: Seasonal cycles of surface layer salinity in the Pacific Ocean. *Ocean Science*, 6, 775-787.

Blanke, B., and P. Delecluse, 1993: Variability of the tropical Atlantic Ocean simulated by a General Circulaiton Model with 2 different mixed-layer physics. *Journal of Physical Oceanography*, 23, 1363-1388.

Bonjean, F., and G. S. E. Lagerloef, 2002: Diagnostic model and analysis of the surface currents in the tropical Pacific Ocean. *Journal of Physical Oceanography*, 32, 2938-2954.

## References

Bosc, C., and T. Delcroix, 2008: Observed equatorial Rossby waves and ENSO-related warm water volume changes in the equatorial Pacific Ocean. *Journal of Geophysical Research-Oceans*, 113.

Bosc, C., T. Delcroix, and C. Maes, 2009: Barrier layer variability in the western Pacific warm pool from 2000 to 2007. *Journal of Geophysical Research-Oceans*, 114.

Boulanger, J. P., and C. Menkes, 1999: Long equatorial wave reflection in the Pacific Ocean from TOPEX/POSEIDON data during the 1992-1998 period. *Climate Dynamics*, 15, 205-225.

Boutin, J., N. Martin, G. Reverdin, X. Yin, and F. Gaillard, 2013: Sea surface freshening inferred from SMOS and ARGO salinity: impact of rain. *Ocean Science*, 9, 183-192.

Boutin, J., N. Martin, X. Yin, J. Font, N. Reul, and P. Spurgeon, 2012: First Assessment of SMOS Data Over Open Ocean: Part II-Sea Surface Salinity. *Ieee Transactions on Geoscience and Remote Sensing*, 50, 1662-1675.

Boyer, T. P., S. Levitus, J. I. Antonov, R. A. Locarnini, and H. E. Garcia, 2005: Linear trends in salinity for the World Ocean, 1955-1998. *Geophysical Research Letters*, 32.

Brown, J., A. Moise, and R. Colman, 2012: The South Pacific Convergence Zone in CMIP5 simulations of historical and future climate. *Climate Dynamics*, 1-19.

Chou, C., and J. D. Neelin, 2004: Mechanisms of global warming impacts on regional tropical precipitation. *Journal of Climate*, 17, 2688-2701.

Chou, C., J. D. Neelin, C.-A. Chen, and J.-Y. Tu, 2009: Evaluating the "Rich-Get-Richer" Mechanism in Tropical Precipitation Change under Global Warming. *Journal of Climate*, 22, 1982-2005.

Clarke, A. J., 2008: *An Introduction to the Dynamics of El Nino & the Southern Oscillation.* Elsevier Science.

Cole, J. E., J. T. Overpeck, and E. R. Cook, 2002: Multiyear La Nina events and persistent drought in the contiguous United States. *Geophysical Research Letters*, 29.

Cooper, N. S., 1988: The Effect of Salinity on Tropical Ocean Models. *Journal of Physical Oceanography*, 18, 697-707.

Cox, R. A., F. Culkin, and J. P. Riley, 1967: The electrical conductivity/chlorinity relationship in natural sea water. *Deep Sea Research and Oceanographic Abstracts*, 14, 203-220.

Cravatte, S., T. Delcroix, D. Zhang, M. McPhaden, and J. Leloup, 2009: Observed freshening and warming of the western Pacific Warm Pool. *Climate Dynamics*, 33, 565-589.

Cronin, M. F., and M. J. McPhaden, 1998: Upper ocean salinity balance in the western equatorial Pacific. *Journal of Geophysical Research-Oceans*, 103, 27567-27587.

——, 2002: Barrier layer formation during westerly wind bursts. *Journal of Geophysical Research-Oceans*, 107.

Dai, A., T. Qian, K. E. Trenberth, and J. D. Milliman, 2009: Changes in Continental Freshwater Discharge from 1948 to 2004. *Journal of Climate*, 22, 2773-2792.

Delcroix, T., 1998: Observed surface oceanic and atmospheric variability in the tropical Pacific at seasonal and ENSO timescales: A tentative overview. *Journal of Geophysical Research-Oceans*, 103, 18611-18633.

Delcroix, T., and C. Henin, 1989: Mechanisms of subsurface thermal structure and sea-surface thermohaline variabilities in the southwestern tropical Pacific during 1975-85. *Journal of Marine Research*, 47, 777-812.

——, 1991: Seasonal and interannual Variations of Sea Surface Salinity in the Tropical Pacific Ocean. *Journal of Geophysical Research-Oceans*, 96, 22135-22150.

Delcroix, T., and J. Picaut, 1998: Zonal displacement of the western equatorial Pacific "fresh pool". *Journal of Geophysical Research-Oceans*, 103, 1087-1098.

Delcroix, T., and M. McPhaden, 2002: Interannual sea surface salinity and temperature changes in the western Pacific warm pool during 1992-2000. *Journal of Geophysical Research-Oceans*, 107.

Delcroix, T., G. Eldin, and C. Henin, 1987: Upper Ocean Water Masses and Transports in the Western Tropical Pacific (165ºE). *Journal of Physical Oceanography*, 17, 2248-2262.

Delcroix, T., L. Gourdeau, and C. Henin, 1998: Sea surface salinity changes along the Fiji-Japan shipping track during the 1996 La Nina and 1997 El Nino period. *Geophysical Research Letters*, 25, 3169-3172.

Delcroix, T., S. Cravatte, and M. J. McPhaden, 2007: Decadal variations and trends in tropical Pacific sea surface salinity since 1970. *Journal of Geophysical Research-Oceans*, 112.

Delcroix, T., C. Henin, V. Porte, and P. Arkin, 1996: Precipitation and sea-surface salinity in the tropical Pacific Ocean. *Deep-Sea Research Part I-Oceanographic Research Papers*, 43, 1123-1141.

Delcroix, T., M. J. McPhaden, A. Dessier, and Y. Gouriou, 2005: Time and space scales for sea surface salinity in the tropical oceans. *Deep-Sea Research Part I-Oceanographic Research Papers*, 52, 787-813.

*References*

Delcroix, T., B. Dewitte, Y. duPenhoat, F. Masia, and J. Picaut, 2000: Equatorial waves and warm pool displacements during the 1992-1998 El Nino Southern Oscillation events: Observation and modeling. *Journal of Geophysical Research-Oceans*, 105, 26045-26062.

Delcroix, T., G. Alory, S. Cravatte, T. Correge, and M. J. McPhaden, 2011: A gridded sea surface salinity data set for the tropical Pacific with sample applications (1950-2008). *Deep-Sea Research Part I-Oceanographic Research Papers*, 58, 38-48.

Demey, P., and Y. Menard, 1989: Synoptic Analysis and Dynamical Adjustment of GEOS-3 and SEASAT Atlimeter Eddy fields in the Northwest Atlantic. *Journal of Geophysical Research-Oceans*, 94, 6221-6230.

Deser, C., A. S. Phillips, and J. W. Hurrell, 2004: Pacific interdecadal climate variability: Linkages between the tropics and the North Pacific during boreal winter since 1900. *Journal of Climate*, 17, 3109-3124.

Dessier, A., and J. R. Donguy, 1994: The Sea Surface Salinity in the Tropical Atlantic between 10 degS and 30 degN Seasonal and Interannual Variations (1997-1989). *Deep-Sea Research Part I-Oceanographic Research Papers*, 41, 81-100.

Dewitte, B., J. Choi, S. I. An, and S. Thual, 2012: Vertical structure variability and equatorial waves during central Pacific and eastern Pacific El Nios in a coupled general circulation model. *Climate Dynamics*, 38, 2275-2289.

Dickson, B., I. Yashayaev, J. Meincke, B. Turrell, S. Dye, and J. Holfort, 2002: Rapid freshening of the deep North Atlantic Ocean over the past four decades. *Nature*, 416, 832-837.

Dittmar, W., 1884: *Composition of Ocean-water.* Eyre & Spottiswood.

Donguy, J. R., and C. Henin, 1976: Anomalous Navifacial Salinities in the Tropical Pacific Ocean. *Journal of Marine Research*, 34, 355-364.

——, 1980: Surface conditions in the Eastern Equatorail Pacific Related to the Intertropical Convergence Zone of Winds. *Deep-Sea Research Part a-Oceanographic Research Papers*, 27, 693-714.

Donguy, J. R., and G. Meyers, 1996: Seasonal variations of sea-surface salinity and temperature in the tropical Indian Ocean. *Deep-Sea Research Part I-Oceanographic Research Papers*, 43, 117-138.

Durack, P. J., and S. E. Wijffels, 2010: Fifty-Year Trends in Global Ocean Salinities and Their Relationship to Broad-Scale Warming. *Journal of Climate*, 23, 4342-4362.

Durand, F., L. Gourdeau, T. Delcroix, and J. Verron, 2002: Assimilation of sea surface salinity in a tropical Oceanic General Circulation Model (OGCM): A twin experiment approach. *Journal of Geophysical Research-Oceans*, 107.

Emery, W. J., 1976: Role of Vertical Motion in Heat Budget of Upper Noretheastern Pacific Ocean. *Journal of Physical Oceanography*, 6, 299-305.

Ferry, N., L. Parent, G. Garric, M. Drevillon, C. Desportes, C. Bricaut, and F. Hernandez, 2011: Scientific Validation Report (ScVR) for V1 Reprocessed Analysis and Reanalysis : GLORYS2V1. MyOcean FP7-SPACE-2007-1 project, report MYO-WP04-ScCV-rea-MERCATOR_V1.

Fieux, M., and C. Andrié, 2010: *L'océan planétaire.* Les Presses de l'ENSTA.

Folland, C. K., and Coauthors, 2001: Global temperature change and its uncertainties since 1861. *Geophysical Research Letters*, 28, 2621-2624.

Foltz, G. R., and M. J. McPhaden, 2008: Seasonal mixed layer salinity balance of the tropical North Atlantic Ocean. *Journal of Geophysical Research-Oceans*, 113.

Font, J., and Coauthors, 2010: SMOS: The Challenging Sea Surface Salinity Measurement From Space. *Proceedings of the Ieee*, 98, 649-665.

Gaillard, F., E. Autret, V. Thierry, P. Galaup, C. Coatanoan, and T. Loubrieu, 2009: Quality Control of Large Argo Datasets. *Journal of Atmospheric and Oceanic Technology*, 26, 337-351.

Ganachaud, A., A. Sen Gupta, J. Brown, K. Evans, C. Maes, L. Muir, and F. Graham, 2012: Projected changes in the tropical Pacific Ocean of importance to tuna fisheries. *Climatic Change*, 1-17.

Gill, A. E., 1982: *Atmosphere-Ocean Dynamics.* Vol. Volume 30, Academic Press, 1-662 pp.

Gouriou, Y., and T. Delcroix, 2002: Seasonal and ENSO variations of sea surface salinity and temperature in the South Pacific Convergence Zone during 1976-2000. *Journal of Geophysical Research-Oceans*, 107.

Grodsky, S. A., J. A. Carton, and F. M. Bingham, 2006: Low frequency variation of sea surface salinity in the tropical Atlantic. *Geophysical Research Letters*, 33.

Gu, D. F., and S. G. H. Philander, 1997: Interdecadal climate fluctuations that depend on exchanges between the tropics and extratropics. *Science*, 275, 805-807.

Gu, D. F., S. G. H. Philander, and M. J. McPhaden, 1997: The seasonal cycle and its modulation in the eastern tropical Pacific Ocean. *Journal of Physical Oceanography*, 27, 2209-2218.

## References

Gu, G., and R. Adler, 2013: Interdecadal variability/long-term changes in global precipitation patterns during the past three decades: global warming and/or pacific decadal variability? *Climate Dynamics*, 40, 3009-3022.

Hackert, E., J. Ballabrera-Poy, A. J. Busalacchi, R.-H. Zhang, and R. Murtugudde, 2011: Impact of sea surface salinity assimilation on coupled forecasts in the tropical Pacific. *Journal of Geophysical Research: Oceans*, 116, C05009.

Halpern, D., R. A. Knox, and D. S. Luther, 1988: Observations of 20-Day Period Meridional Current Oscillations in the Upper Ocean along the Pacific Equator. *Journal of Physical Oceanography*, 18, 1514-1534.

Hare, S. R., 1996: Low frequency climate variability and salmon production, University of Washington, 306 pp.

Hasson, A. E. A., T. Delcroix, and R. Dussin, 2013a: An assessment of the mixed layer salinity budget in the tropical Pacific Ocean. Observations and modelling (1990-2009). *Ocean Dynamics*, 63, 179-194.

Hasson, A. E. A., T. Delcroix, and J. Boutin, 2013b: Formation and Variability of the South Pacific Sea Surface Salinity Maximum in Recent Decades *Submitted to JGR*.

Held, I. M., and B. J. Soden, 2006: Robust responses of the hydrological cycle to global warming. *Journal of Climate*, 19, 5686-5699.

Henin, C., and J. Grelet, 1996: A merchant ship thermo-salinograph network in the Pacific Ocean. *Deep-Sea Research Part I-Oceanographic Research Papers*, 43, 1833-1855.

Henocq, C., J. Boutin, F. Petitcolin, G. Reverdin, S. Arnault, and P. Lattes, 2010: Vertical Variability of Near-Surface Salinity in the Tropics: Consequences for L-Band Radiometer Calibration and Validation. *Journal of Atmospheric and Oceanic Technology*, 27, 192-209.

Hires, R. I., and R. Montgomery, 1972: Navifacial temperature and salinity along the track from Samoa to Hawaii, 1957–1965. *J. Mar. Res*, 30, 177-200.

Johnson, E. S., G. S. E. Lagerloef, J. T. Gunn, and F. Bonjean, 2002: Surface salinity advection in the tropical oceans compared with atmospheric freshwater forcing: A trial balance. *Journal of Geophysical Research-Oceans*, 107.

Juillet-Leclerc, A., S. Thiria, P. Naveau, T. Delcroix, N. Le Bec, D. Blamart, and T. Correge, 2006: SPCZ migration and ENSO events during the 20th century as revealed by climate proxies from a Fiji coral. *Geophysical Research Letters*, 33.

Kerr, Y., 1998: The SMOS Mission: MIRAS on RAMSES. A proposal to the call for Earth Explorer Opportunity Mission. CESBIO, 50.

Kerr, Y. H., P. Waldteufel, J. P. Wigneron, J. M. Martinuzzi, J. Font, and M. Berger, 2001: Soil moisture retrieval from space: The Soil Moisture and Ocean Salinity (SMOS) mission. *Ieee Transactions on Geoscience and Remote Sensing*, 39, 1729-1735.

Kerr, Y. H., and Coauthors, 2010: The SMOS Mission: New Tool for Monitoring Key Elements of the Global Water Cycle. *Proceedings of the Ieee*, 98, 666-687.

Kessler, W. S., 2006: The circulation of the eastern tropical Pacific: A review. *Progress in Oceanography*, 69, 181-217.

Kessler, W. S., and B. A. Taft, 1987: Dynamic Heights and Zonal Geostrophic Transports in the Central Tropical Pacific during 1979–84. *Journal of Physical Oceanography*, 17, 97-122.

Kessler, W. S., M. C. Spillane, M. J. McPhaden, and D. E. Harrison, 1996: Scales of variability in the equatorial Pacific inferred from the tropical atmosphere-ocean buoy array. *Journal of Climate*, 9, 2999-3024.

Kim, W., S.-W. Yeh, J.-H. Kim, J.-S. Kug, and M. Kwon, 2011: The unique 2009-2010 El Nino event: A fast phase transition of warm pool El Nino to La Nina. *Geophysical Research Letters*, 38.

Knudsen, M., 1903: *On the Standard-Water Used in the Hydrographical Research Until July 1903*.

Kolodziejczyk, N., and F. Gaillard, 2012: Observation of spiciness interannual variability in the Pacific pycnocline. *Journal of Geophysical Research-Oceans*, 117.

Kripalani, R. H., and A. Kulkarni, 1997: Rainfall variability over South-east Asia - Connections with Indian monsoon and enso extremes: New perspectives. *International Journal of Climatology*, 17, 1155-1168.

Lagerloef, G., and T. Delcroix, 2001: Sea surface salinity : a regional case study for the tropical Pacific. In: Observing the Ocean in the 21st Century, 137-148 pp.

Lagerloef, G., R. Schmitt, J. Schanze, and H.-Y. Kao, 2010: The Ocean and the Global Water Cycle. *Oceanography*, 23, 82-93.

Lagerloef, G., and Coauthors, 2008: The AQUARIUS/SAC-D Mission: Designed to Meet the Salinity Remote-sensing Challenge. *Oceanography*, 21, 68-81.

Lagerloef, G. S. E., G. T. Mitchum, R. B. Lukas, and P. P. Niiler, 1999: Tropical Pacific near-surface currents estimated from altimeter, wind, and drifter data. *Journal of Geophysical Research-Oceans*, 104, 23313-23326.

## References

Large, W. G., and S. G. Yeager, 2004: Diurnal to decadal global forcing for ocean and sea-ice models: The data sets and flux climatologies.

Laurian, A., A. Lazar, and G. Reverdin, 2009: Generation Mechanism of Spiciness Anomalies: An OGCM Analysis in the North Atlantic Subtropical Gyre. *Journal of Physical Oceanography*, 39, 1003-1018.

Le Menn, M., J. L. d. B. de la Tocnaye, P. Grosso, L. Delauney, C. Podeur, P. Brault, and O. Guillerme, 2011: Advances in measuring ocean salinity with an optical sensor. *Measurement Science & Technology*, 22.

Lee, T., G. Lagerloef, M. M. Gierach, H.-Y. Kao, S. Yueh, and K. Dohan, 2012: Aquarius reveals salinity structure of tropical instability waves. *Geophys. Res. Lett.*, 39, L12610-L12610.

Legeckis, R., 1977: Long Waves in Eastern Equatorial Pacific Ocean - View from a Geostationary Satellite. *Science*, 197, 1179-1181.

Levitus, S., 1986: Annual Cycle of Salinity and Salt Storage in the World Ocean. *Journal of Physical Oceanography*, 16, 322-343.

Levitus, S., and U. S. N. O. a. A. Administration, 1982: *Climatological Atlas of the World Ocean.* U.S. Department of Commerce, National Oceanic and Atmospheric Administration.

Lukas, R., and E. Lindstrom, 1991: The Mixed Layer of the Western Equatorial Pacific Ocean. *Journal of Geophysical Research-Oceans*, 96, 3343-3357.

Lyman, J. M., G. C. Johnson, and W. S. Kessler, 2007: Distinct 17-and 33-day tropical instability waves in subsurface observations. *Journal of Physical Oceanography*, 37, 855-872.

Madec, G., 2008: *NEMO ocean engine*. 300.

Maes, C., J. Picaut, and S. Belamari, 2002: Salinity barrier layer and onset of El Nino in a Pacific coupled model. *Geophysical Research Letters*, 29.

Maes, C., K. Ando, T. Delcroix, W. S. Kessler, M. J. McPhaden, and D. Roemmich, 2006: Observed correlation of surface salinity, temperature and barrier layer at the eastern edge of the western Pacific warm pool. *Geophysical Research Letters*, 33.

Manabe, S., and R. J. Stouffer, 1995: Simulation of Abrupt Climate-change Induced by Fresh-water Input to the North Atlantic Ocean. *Nature*, 378, 165-167.

Mann, M. E., and J. Park, 1994: Global-scale Modes of Surface Temperature Variability on Interannual to Century Timescales. *Journal of Geophysical Research-Atmospheres*, 99, 25819-25833.

Mantua, N. J., and S. R. Hare, 2002: The Pacific decadal oscillation. *Journal of Oceanography*, 58, 35-44.

Mantua, N. J., S. R. Hare, Y. Zhang, J. M. Wallace, and R. C. Francis, 1997: A Pacific interdecadal climate oscillation with impacts on salmon production. *Bulletin of the American Meteorological Society*, 78, 1069-1079.

Marshall, J., and F. Schott, 1999: Open-ocean convection: Observations, theory, and models. *Reviews of Geophysics*, 37, 1-64.

McCreary, J. P., and P. Lu, 1994: Interaction between the Subtropical and Equatorial Ocean Circulations - The Subtropical Cell. *Journal of Physical Oceanography*, 24, 466-497.

McPhaden, M. J., and S. P. Hayes, 1990: Variability in the Eastern Equatorial Pacific Ocean During 1986-1988. *Journal of Geophysical Research-Oceans*, 95, 13195-&.

McPhaden, M. J., and X. Yu, 1999: Equatorial waves and the 1997-98 El Nino. *Geophysical Research Letters*, 26, 2961-2964.

McPhaden, M. J., and D. X. Zhang, 2002: Slowdown of the meridional overturning circulation in the upper Pacific Ocean. *Nature*, 415, 603-608.

——, 2004: Pacific Ocean circulation rebounds. *Geophysical Research Letters*, 31.

Meehl, G. A., 1987: The Annual Cycle and Interannual Variability in the Tropical Pacific and Indian Ocean Regions. *Monthly Weather Review*, 115, 27-50.

Meehl, G. A., A. Hu, and B. D. Santer, 2009: The Mid-1970s Climate Shift in the Pacific and the Relative Roles of Forced versus Inherent Decadal Variability. *Journal of Climate*, 22, 780-792.

Menkes, C., J. P. Boulanger, and A. J. Busalacchi, 1995: Evaluation of TOPEX and basin-wide tropical ocean and global atmosphere-tropical atmosphere ocean sea surface topographies and derived geostrophic currents. *Journal of Geophysical Research-Oceans*, 100, 25087-25099.

Miller, J. R., 1976: Salinity Effect in a Mixed Layer Ocean Model. *Journal of Physical Oceanography*, 6, 29-35.

Millero, F. J., 2010: HISTORY OF THE Equation of State of Seawater. *Oceanography*, 23, 18-33.

Millero, F. J., R. Feistel, D. G. Wright, and T. J. McDougall, 2008: The composition of Standard Seawater and the definition of the Reference-Composition Salinity Scale. *Deep-Sea Research Part I-Oceanographic Research Papers*, 55, 50-72.

*References*

Minobe, S., 1997: A 50-70 year climatic oscillation over the North Pacific and North America. *Geophysical Research Letters*, 24, 683-686.

Montegut, C. D., G. Madec, A. S. Fischer, A. Lazar, and D. Iudicone, 2004: Mixed layer depth over the global ocean: An examination of profile data and a profile-based climatology. *Journal of Geophysical Research-Oceans*, 109.

Montegut, C. d. B., J. Mignot, A. Lazar, and S. Cravatte, 2007: Control of salinity on the mixed layer depth in the world ocean: 1. General description. *Journal of Geophysical Research-Oceans*, 112.

Nicholson, S. E., and J. C. Selato, 2000: The influence of La Nina on African rainfall. *International Journal of Climatology*, 20, 1761-1776.

Nonaka, M., and H. Sasaki, 2007: Formation mechanism for isopycnal temperature-salinity anomalies propagating from the eastern South Pacific to the equatorial region. *Journal of Climate*, 20, 1305-1315.

O'Connor, B. M., R. A. Fine, K. A. Maillet, and D. B. Olson, 2002: Formation rates of subtropical underwater in the Pacific Ocean. *Deep-Sea Research Part I-Oceanographic Research Papers*, 49, 1571-1590.

Pawlowicz, R., 2013: Key Physical Variables in the Ocean: Temperature, Salinity, and Density. *Nature Education Knowledge*.

Penduff, T., and Coauthors, 2010: Impact of global ocean model resolution on sea-level variability with emphasis on interannual time scales. *Ocean Science*, 6, 269-284.

Philander, S. G., J. R. Holton, and R. Dmowska, 1989: *El Nino, La Nina, and the Southern Oscillation.* Elsevier Science.

Philander, S. G. H., 1985: El Nino and La Nina. *Journal of the Atmospheric Sciences*, 42, 2652-2662.

Picaut, J., M. Ioualalen, C. Menkes, T. Delcroix, and M. J. McPhaden, 1996: Mechanism of the zonal displacements of the Pacific warm pool: Implications for ENSO. *Science*, 274, 1486-1489.

Picaut, J., M. Ioualalen, T. Delcroix, F. Masia, R. Murtugudde, and J. Vialard, 2001: The oceanic zone of convergence on the eastern edge of the Pacific warm pool: A synthesis of results and implications for El Nino-Southern Oscillation and biogeochemical phenomena. *Journal of Geophysical Research-Oceans*, 106, 2363-2386.

Polovina, J. J., E. A. Howell, and M. Abecassis, 2008: Ocean's least productive waters are expanding. *Geophysical Research Letters*, 35.

Power, S., T. Casey, C. Folland, A. Colman, and V. Mehta, 1999: Inter-decadal modulation of the impact of ENSO on Australia. *Climate Dynamics*, 15, 319-324.

Qiu, B., R. B. Scott, and S. Chen, 2008: Length scales of eddy generation and nonlinear evolution of the seasonally modulated South Pacific Subtropical Countercurrent. *Journal of Physical Oceanography*, 38, 1515-1528.

Qu, T., S. Gao, and I. Fukumori, 2011: What governs the North Atlantic salinity maximum in a global GCM? *Geophysical Research Letters*, 38.

Rahmstorf, S., 1995: Bifurcations of the Atlantic Thermohaline Circulation in Response to changes in the Hydrological Cycle. *Nature*, 378, 145-149.

Rasmusson, E. M., and T. H. Carpenter, 1982: Variations in the tropical sea-surface temperature and surface wind fields associated with the southern oscillation El Nino. *Monthly Weather Review*, 110, 354-384.

Reul, N., and Coauthors, 2013: Sea Surface Salinity Observations from Space with the SMOS Satellite: A New Means to Monitor the Marine Branch of the Water Cycle. *Surveys in Geophysics*, 1-42.

Reverdin, G., D. Cayan, H. D. Dooley, D. J. Ellett, S. Levitus, Y. Dupenhoat, and A. Dessier, 1994: Surface Salinity of the North-Atlantic - Can We Reconstruct its Fluctuations over the Last 100 Years? *Progress in Oceanography*, 33, 303-346.

Reynolds, R. W., M. Ji, and A. Leetmaa, 1998: Use of salinity to improve ocean modeling. *Physics and Chemistry of the Earth*, 23, 543-553.

Rodier, M., G. Eldin, and R. Le Borgne, 2000: The Western Boundary of the Equatorial Pacific Upwelling: Some Consequences of Climatic Variability on Hydrological and Planktonic Properties. *Journal of Oceanography*, 56, 463-471.

Roemmich, D., and W. B. Owens, 2000: The Argo Project: Global ocean observations for understanding and prediction of climate variability. *Oceanography*, 13, 45–50.

Roemmich, D., and Coauthors, 1999: ARGO: The Global Array of Profiling Floats. *Exchanges*, 7788-7901.

Ropelewski, C. F., and M. S. Halpert, 1996: Quantifying Southern Oscillation - Precipitation relationships. *Journal of Climate*, 9, 1043-1059.

Salinger, M. J., J. A. Renwick, and A. B. Mullan, 2001: Interdecadal Pacific Oscillation and South Pacific climate. *International Journal of Climatology*, 21, 1705-1721.

Sarachik, E. S., and Mark A. Cane., 2010: *The El Niño-Southern Oscillation Phenomenon.* Cambridge University Press.

*References*

Schanze, J. J., R. W. Schmitt, and L. L. Yu, 2010: The global oceanic freshwater cycle: A state-of-the-art quantification. *Journal of Marine Research*, 68, 569-595.

Scheff, J., and D. M. W. Frierson, 2012: Robust future precipitation declines in CMIP5 largely reflect the poleward expansion of model subtropical dry zones. *Geophysical Research Letters*, 39.

Schmitt, R. W., 1995: The Ocean Component of the Global Water Cycle. *Reviews of Geophysics*, 33, 1395-1409.

——, 2008: Salinity and the Global Water Cycle. *Oceanography*, 21, 12-19.

Schneider, N., A. J. Miller, M. A. Alexander, and C. Deser, 1999: Subduction of decadal North Pacific temperature anomalies: Observations and dynamics. *Journal of Physical Oceanography*, 29, 1056-1070.

Seager, R., N. Naik, and G. A. Vecchi, 2010: Thermodynamic and Dynamic Mechanisms for Large-Scale Changes in the Hydrological Cycle in Response to Global Warming. *Journal of Climate*, 23, 4651-4668.

Singh, A., and T. Delcroix, 2011: Estimating the effects of ENSO upon the observed freshening trends of the western tropical Pacific Ocean. *Geophysical Research Letters*, 38.

Singh, A., T. Delcroix, and S. Cravatte, 2011: Contrasting the flavors of El Nino-Southern Oscillation using sea surface salinity observations. *Journal of Geophysical Research-Oceans*, 116.

Spall, M. A., and R. S. Pickart, 2001: Where does dense water sink? A subpolar gyre example. *Journal of Physical Oceanography*, 31, 810-826.

Sprintall, J., and D. Roemmich, 1999: Characterizing the structure of the surface layer in the Pacific Ocean. *Journal of Geophysical Research-Oceans*, 104, 23297-23311.

Sudre, J., and R. A. Morrow, 2008: Global surface currents: a high-resolution product for investigating ocean dynamics. *Ocean Dynamics*, 58, 101-118.

Sverdrup, H. U., 1943: On the Ratio between Heat Conduction from the Sea Surface and Heat Used for Evaporation. *Annals of the New York Academy of Sciences*, 44, 81-88.

Sverdrup, H. U., M. W. Johnson, and R. H. Fleming, 1942: *The Oceans: Their Physics, Chemistry, and General Biology.* Asia Publishing House.

Terray, L., L. Corre, S. Cravatte, T. Delcroix, G. Reverdin, and A. Ribes, 2012: Near-Surface Salinity as Nature's Rain Gauge to Detect Human Influence on the Tropical Water Cycle. *Journal of Climate*, 25, 958-977.

Thomas, B. D., T. G. Thompson, and C. L. Utterback, 1934: *The Electrical Conductivity of Sea Water.* University of Washington.

Tomczak, M., 1999: Some historical, theoretical and applied aspects of quantitative water mass analysis. *Journal of Marine Research*, 57, 275-303.

Tranchant, B., C. E. Testut, N. Ferry, L. Renault, E. Obligis, C. Boone, and G. Larnicol, 2008: Data assimilation of simulated SSS SMOS products in an ocean forecasting system. *Journal of Operational Oceanography*, 1, 19-27.

Trenberth, K. E., 1990: Recent Observed Interdecadal Climate Changes in the Northern Hemisphere. *Bulletin of the American Meteorological Society*, 71, 988-993.

Ueki, I., K. Ando, Y. Kuroda, and K. Kutsuwada, 2002: Salinity variation and its effect on dynamic height along the 156 degrees E in the Pacific warm pool. *Geophysical Research Letters*, 29.

Unesco, C. i. d. é. européennes, I. C. o. S. U. S. C. o. O. Research, I. A. f. t. P. S. o. t. Ocean, and J. P. o. O. T. a. Standards), 1981: *Background papers and supporting data on the International equation of state of seawater 1980.* Unesco.

Vialard, J., and P. Delecluse, 1998a: An OGCM study for the TOGA decade. Part I: Role of salinity in the physics of the western Pacific fresh pool. *Journal of Physical Oceanography*, 28, 1071-1088.

——, 1998b: An OGCM study for the TOGA decade. Part II: Barrier-layer formation and variability. *Journal of Physical Oceanography*, 28, 1089-1106.

Vialard, J., P. Terray, J. P. Duvel, R. S. Nanjundiah, S. S. C. Shenoi, and D. Shankar, 2011: Factors controlling January-April rainfall over southern India and Sri Lanka. *Climate Dynamics*, 37, 493-507.

Vialard, J., C. Menkes, J. P. Boulanger, P. Delecluse, E. Guilyardi, M. J. McPhaden, and G. Madec, 2001: A model study of oceanic mechanisms affecting equatorial Pacific sea surface temperature during the 1997-98 El Nino. *Journal of Physical Oceanography*, 31, 1649-1675.

Vialard, J. M., P. Delecluse, and C. Menkes, 2002: A modeling study of salinity variability and its effects in the tropical Pacific Ocean during the 1993-1999 period. *Journal of Geophysical Research-Oceans*, 107.

Vinayachandran, P. N., and R. S. Nanjundiah, 2009: Indian Ocean sea surface salinity variations in a coupled model. *Climate Dynamics*, 33, 245-263.

Vincent, D. G., 1994: The South Pacific Convergence Zone (SPCZ) - A Review. *Monthly Weather Review*, 122, 1949-1970.

## References

Vinogradova, N. T., and R. M. Ponte, 2013: Clarifying the link between surface salinity and freshwater fluxes on monthly to interannual time scales. *Journal of Geophysical Research: Oceans*, 118, 3190-3201.

Waldteufel, P., J. Boutin, and Y. Kerr, 2003: Selecting an optimal configuration for the Soil Moisture and Ocean Salinity Mission. *Radio Science*, 38.

Weyl, P. K., 1968: The role of the oceans in climatic change: A theory of the Ice Ages. *Meteorol. Monographs*, 830.

Xiaobin, Y., J. Boutin, N. Martin, and P. Spurgeon, 2012: Optimization of L-Band Sea Surface Emissivity Models Deduced From SMOS Data. *Geoscience and Remote Sensing, IEEE Transactions on*, 50, 1414-1426.

Yaremchuk, M., 2006: Sea surface salinity constrains rainfall estimates over tropical oceans. *Geophysical Research Letters*, 33.

Yim, B. Y., S. W. Yeh, Y. Noh, B. K. Moon, and Y. G. Park, 2008: Sea surface salinity variability and its relation to El nino in a CGCM. *Asia-Pacific Journal of Atmospheric Sciences*, 44, 173-189.

Yu, L., 2011: A global relationship between the ocean water cycle and near-surface salinity. *Journal of Geophysical Research-Oceans*, 116.

Yu, L., X. Jin, and R. A. Weller, 2008: Multidecade Global Flux Datasets from  the Objectively Analyzed Air-sea Fluxes (OAFlux) Project: Latent and sensible  heat fluxes, ocean evaporation, and related surface meteorological variables., 64pp. pp.

Zhang, R. H., and S. Levitus, 1997: Structure and cycle of decadal variability of upper-ocean temperature in the North Pacific. *Journal of Climate*, 10, 710-727.